Fate and Effective Control of Superfine Powdered Activated Carbon Particles in Drinking Water Treatment Process Consisting of Coagulation-Flocculation, Sedimentation, and Sand Filtration

by
Yoshifumi Nakazawa
Hokkaido University
2021

ACKNOWLEDGEMENTS

Compiling this dissertation, I have been supported by many affectionate people. First of all, I would like to express my sincere gratitude to all of them.

I would like to express my utmost respect and gratitude to Prof. Yoshihiko Matsui (Environmental Risk Engineering Lab.) for his unfailing support and guidance throughout my research work on this dissertation. During my studies with him, I have learned a lot from him and he has demonstrated me the most sophisticated way of working in the world. I am convinced that all the experiences I have gained through my research life so far are invaluable and will become the foundation and driving force that will strongly support my life in the future.

I would like to express my sincere respect and gratitude to Associate Professor Taku Matsushita and Associate Professor Nobutaka Shirasaki of the same laboratory, for their advice on my research from various perspectives and for their guidance on how to effectively present my research. This dissertation would not have been possible without the encouragement of them.

I also would like to extend my gratitude to each committee: Prof. Satoshi Okabe, Prof. Katsuki Kimura and Prof. Hisashi Satoh, who reviewed this dissertation, for his valuable comments and helpful advice.

I would like to express my sincere respect and gratitude to Ms. Atsuko Kikuchi, who has helped me in various situations as a secretary of the laboratory. Thanks to her daily assistance, all the work related to my research could be carried out without obstacle.

I would like to express my sincere gratitude to my seniors, peers, and juniors with whom I spent time in the laboratory. In particular, I would like to express my deepest gratitude to Mr. Yusuke Hanamura and Mr. Kouki Shinno for their contributions to Chapters 2 and 3, and to Mr. Taketo Abe for his contribution

to Chapters 4 and 5.

I will never forget my friends who have been my emotional support. Without them, with whom I went on trips, enjoyed hobbies, and talked with, I would not have been able to continue my research to here.

Finally, I would like to express my deepest gratitude to my parents, Mrs. Yoriko and Mr. Takeshi Nakazawa, who did not oppose my way of life, but rather enjoyed it with me.

This work was supported by a JSPS Research Fellowship [grant number JP19J11070] from the Japan Society for the Promotion of Science.

本論文をとりまとめるにあたり，私は数多くの方々の多大なお力添えに支えられてきました．本論の展開に先立って，その方々への心からの謝意を表したいと思います．

私が本論文に関する研究に取り組む上で，労を惜しまずに終始ご指導をくださいました松井佳彦教授 (環境リスク工学研究室) には最大の敬意と感謝を申し上げます．先生のもとで研究している期間，学ぶところの多いご助言を折々にいただくとともに，世界で最も洗練された働き方をお示しくださいました．これまでの研究生活をとおして得られた全ての経験がかけがえの無いものであり，これからの私の人生を強く支える礎かつ，原動力となると確信しています．

同研究室の松下拓准教授ならびに白崎伸隆准教授に心より敬意と感謝を申し上げます．両先生方には，研究に関して多角的な視点からご助言をいただくと共に，研究発表の際の効果的な伝え方をご指導いただきました．先生方の励ましがなければこの論文は形にならなかったであろうと思います．

副査として本論文を審査していただいた岡部聡教授，木村克輝教授，佐藤久教授には貴重なご意見とアドバイスを頂きました．ここに感謝の意を表したいと思います．

同研究室の秘書として様々な場面でお力添えくださった菊地敦子さまに心から敬意と感謝を申し上げます．菊地さまから日頃のご助力をいただいたからこそ，研究に関するすべての業務が滞りなく遂行できました．

研究室でともに過ごした先輩，同輩，後輩に心から感謝いたします．特に，2 章および 3 章に多大なご貢献をいただいた花村悠佑氏，信野光貴氏，また 4 章および 5 章に多大なご貢献をいただいた阿部丈人氏に深く感謝申し上げます．

私の精神的な支えとなってくれた友人たちの存在を忘れることはありません．ともに旅行に行ったり，趣味を楽しんだり，語り合ったりした友人たちの存在無くしては，ここまで研究を続けていられなかったのではないかと思います．

最後になりますが，私の生き方に反対することなく，むしろ共に楽しんでくださった両親，中沢依子氏，中沢毅氏に深く感謝いたします．

CONTENTS

1 INTRODUCTION

1.1 Background

1.1.1 Adsorption treatment in water purification

Recent water purification plants have been suffered by taste and odor problems. A number of suffered population in Japan reached to a peak (20 million people) in 1990, and have then decreased gradually. However, a number of suffered water suppliers have still increased (The Ministry of Health Labor and Welfare 2018). Earthy-musty odor took up 90% of 31 issues referring to odor type, in 2017 (The Ministry of Health Labor and Welfare 2018). Dissolved organic compounds like geosmin and 2-MIB accounting for the earthy-musty odor are hard to be removed from water by conventional drinking water treatment consisting of coagulation-flocculation, sedimentation, and filtration. Therefore, advanced water treatment are needed.

When removing dissolved organic compounds, in particular those of low molecular size, in water treatment processes, adsorption by activated carbon (AC) has been a common practice for many years. Activated carbon is used as an adsorbent either in powdered or granular form. While granular activated carbon is used in a bed adsorber, powdered activated carbon (PAC) can be applied at any point in the treatment process if PAC is sufficiently removed before the treated water enters the distribution system.

1.1.2 Superfine powdered activated carbon

Recent developments in milling technology now enable the production of superfine powdered activated carbon particles (SPAC) down to micron and submicron dimensions. SPAC has an extremely fast rate of adsorption and higher capacity to adsorb dissolved organic contaminants compared with conventionally sized PAC (Amaral *et al.* 2016, Ando *et al.* 2010, Ando *et al.* 2011, Apul *et al.* 2017, Ateia *et al.* 2019, Bonvin *et al.* 2016, Decrey *et al.* 2020, Dunn and Knappe 2019, Jiang *et al.* 2015, Matsui *et al.* 2015, Matsui *et al.* 2013, Matsui *et al.* 2012, Murray *et al.* 2019, Partlan *et al.* 2020). To date, the majority of research dealing with SPAC has focused on its use as part of membrane filtration processes (Amaral et al. 2016, Ellerie *et al.* 2013, Heijman *et al.* 2009, Matsui *et al.* 2007). In membrane filtration processes, SPAC is used as an adsorbent for the removal of dissolved organic contaminants before the water is treated by membrane filtration, which removes the SPAC entirely. SPAC is already used in full-scale water treatment plants that use membrane filtration processes because dosage costs are lower for SPAC than for PAC (Kanaya *et al.* 2015).

SPAC may also be useful as part of conventional treatment processes that use coagulation–flocculation, sedimentation, and rapid sand filtration (CSF) as the three stages of treatment. However, it is possible that SPAC will be inefficiently removed in these conventional treatment processes compared with membrane filtration processes; that is, SPAC particles might not be adequately removed during the treatment process and could then enter the distribution system.

1.1.3 Challenges related to SPAC application

The main concern for the adsorption processes is the removal efficiencies of target adsorbate compounds to be treated, but plant operators also pay attention to avoid fine black carbon particles from remaining in treated water and entering

the distribution system. It is actually not uncommon that PAC, which is applied upstream of a separation process such as rapid sand filtration, sometimes passes through the filters and enters the distribution system, provoking black or grey water complaints from consumers (American Society of Civil Engineers and American Water Works Association 1998). Black water is usually caused by inadequate coagulation and sedimentation or high doses of PAC (Randtke and Horsley 2012). Even trace concentrations of black carbon particles remaining in treated water, which do not make the water black or grey and do not violate drinking water quality standards for turbidity, could deteriorate the quality of food, such as tofu, that is produced from the water, etc., which causes complains from food manufacturers. Plant operators pay closer attention to the turbidity or particle count in treated water when PAC is dosed than when PAC is not dosed (Bureau of Waterworks Tokyo Metropolitan Government 2014). When applying SPAC instead of PAC, however, a criterion from plant operator sites, in particular those with a safety orientation, would be that the level of carbon particles remaining in treated water when SPAC is applied should be at a similar or lower level than when PAC is applied.

If coagulation and flocculation are performed well, there should be few residual particles in the treated water. That is because proper coagulation and flocculation results in the formation of large floc particles with good settling properties and water with low turbidity after settling and filtration. Plenty of studies have been conducted for the effect of coagulants and coagulation conditions on floc formation and turbidly removal (Edzwald 2011). Several studies have focused on particle charge neutralization, the size and growth of floc particles, settling velocity, permeability, carbon particles as a ballasting agent for settling, nuclei for coagulation, or a pretreatment agent of coagulation-hindering compounds, and the reduction of turbidity after sedimentation and filtration with respect to the use of PAC. Younker and Walsh (2016) have reported that the

addition of PAC prior to the addition of a coagulant ($FeCl_3$) reduces floc size but has little impact on the final turbidity after sedimentation. Aguilar *et al.* (2003) have reported that the use of PAC decreases the number of particles remaining after coagulation-flocculation and sedimentation. In a membrane filtration study, the addition of SPAC or PAC enhanced floc formation, and at the same dose, larger, more permeable floc particles were formed with SPAC than with PAC because of the fractal effect and the increased frequency of particle–particle collisions with SPAC (Matsui *et al.* 2009). These results thus suggest that the addition of SPAC may have positive effects on the coagulation–flocculation process because the carbon particles serve as nuclei for flocculation.

However, few studies have focused on the particles remaining in treated water after sedimentation and filtration. The effects of the addition of PAC on the turbidity of treated water after CSF were reported more than 25 years ago. Some studies reported that PAC at concentrations up to 30 mg/L did not compromise the quality of the treated water in terms of particulate matter contamination (Carns and Stinson 1978, Gifford *et al.* 1989). However, in those studies the quality of the filtered water was evaluated via a naked-eye visual assessment. If the size distribution of floc particles (Hu *et al.* 2013, Sun *et al.* 2016, Zhang *et al.* 2008) is examined, it may be possible to determine the amount of residual particles. However, such residual particles are present in only very small concentrations at the very extreme ends of the size distribution, making them difficult to be determined using particle distribution data (Lee *et al.* 2009, Yu *et al.* 2015). In this context, some studies on residual particles have been carried out using microscopy.

1.1.4 Fates of particles in water purification

In drinking water treatment employing a CSF process, other kinds of particles including micro plastics (MPs) should be adequately removed as well as AC particles.

MPs have drawn attention throughout the world, since it have been revealed that MPs have widely been distributing in the ocean, freshwater, the air, and soil (Dris *et al.* 2016, Freeman *et al.* 2020, Iqbal *et al.* 2020, Iwasaki *et al.* 2017, Koelmans *et al.* 2019, Rodrigues *et al.* 2018, Wang *et al.* 2021, Wong *et al.* 2020, Wu *et al.* 2019, Zhou *et al.* 2020). MPs with a size of <10 μm have been reported their toxicity on human health (Kögel *et al.* 2020, Revel *et al.* 2018), and so their fate in drinking water treatment processes should be well understood (WHO 2019).

MPs have actually detected in finished water as well as raw water of some full-scale water treatment plants (Kosuth *et al.* 2018, Mintenig *et al.* 2019, Pivokonsky *et al.* 2018, Shen *et al.* 2020, Wang *et al.* 2020b). While MPs in treated ground water are in an extremely trace concentration (0.7 particles/m3) (Mintenig et al. 2019), those in treated river waters are in much higher concentrations. When a river water were treated by coagulation, floatation, sand filtration, and granular activated carbon (GAC), the residual PM concentration in finished water was 628 particles/L and a removal ratio of PM was 83% (Pivokonsky et al. 2018). The detected MPs had shapes like fragments and fibers and most of them had a size of <10 um. Wang et al. (2020b) have investigated an advanced water treatment plant (coagulation/flocculation, sedimentation, sand filtration and ozonation combined with GAC filtration) and indicated similar concentration and removal rate.

Quite recently, the effects of treatment conditions on the treatability of MP in water treatment have been investigated by using waters spiked MP (Ma *et al.* 2019, Rajala *et al.* 2020, Skaf *et al.* 2020, Wang *et al.* 2020c, Zhou *et al.* 2021). However, these studies uses waters spiked with MPs of unrealistically high concentrations, and it is needed that evaluating the removal performance with a trace concentration of MP reflecting actual contamination. Additionally, some of these study use fluorescent MPs with larger in specific gravity than the naked MPs or does not stipulate specific gravity of used MPs, but the change in specific gravity may affect the removal efficiencies. Zhang *et al.* (2020) use fluorescent particles at a concentration similar to that observed in practice (1800−9500 particles/L) and report the removal rate of 86.9−99.9% by a media filter. MPs with a particle size of 10−20 μm were less effectively removed than particles with other sizes. However, the authors use a specific filter combining cheesecloth and anthracite, but such a filter is not widely used in water treatments compared with a sand filtration. Moreover, it has been reported that industrially produced MP has been physically/photochemically weathered after being emitted to environment (Sun *et al.* 2020), and the weathered MP (called as secondary MP) (WHO 2019) has been changed in hydrophobicity and chemical composition (Lin *et al.* 2020, Naik *et al.* 2020, Wang *et al.* 2020a, Zhu *et al.* 2020a, Zhu *et al.* 2020b). The changes related to weathering on MP might affect its removal efficiency in water treatment.

The primary objective of CSF treatment is to reduce turbidity by removing suspended particles, fundamentally clay particles, and the turbidity reduction is well examined (Edzwald 2011). CSF has proven effective in removing such clay particles even with smaller size and higher concentrations than those of micro plastics (WHO 2019). However, the behavior of particulate matter as particles in CSF and its residual at the low concentration level found for micro plastics in filtered water are not enough discussed. Turbidity measurement does not

fundamentally have enough sensitivity for evaluating trace concentrations of particles and their high removal rates (log reduction) (Cho *et al.* 2020). On the other hand, the removals of viruses with the particle sizes ranging from 30 to 100 nm by CSF are studied by quantifying their number concentration in real-time polymerase chain reaction (PCR), and the removals at 0.8−2.5 log levels are reported (Shirasaki *et al.* 2018).

Overall, the above-mentioned studies suggest that the removal rates of particulate matters contaminated in raw water for drinking water production are very different depending on the types of particles: ~ 1 log removal for MPs of the size 0.2 μm−5 mm, 0.8−2.5 log removal for viruses of the size 30−100 nm, and sufficient removal of clay particles typically of the size 1.0 μm−1.0 mm. However, the removal efficiencies of these particles and AC particles by CSF have not been evaluated and compared at the same condition.

1.2 Objectives and components of this research

According to the background, I set objectives of the present study to reveal behavior of fine carbon particles in CSF process and to achieve efficiently removal of the particles, with following specific directions.

i. To develop a method for identifying and quantifying very low concentrations of SPAC (<1 μg/L, <1000 carbon particles/mL) in treated water, and to determine the concentration and characteristics of the carbon particles remaining after CSF.

ii. To find better coagulation conditions and find a better coagulant for the removal of SPAC. The effects of coagulation and flocculation reactor configuration on the removal of SPAC particles were also investigated.

iii. To examine the behavior of particles that cannot grow into floc particles due to insufficient charge neutralization, which were referred as stray particles, during the CSF process with respect to the amount of residual carbon particles in sand filtrate at the end of the treatment process.

iv. To reveal the fate of particles including clay particles, virus, and micro plastics as well as carbon particles in the same treatment condition.

In this dissertation, I will proceed discussions with following Chapters to achieve the objectives:

Chapter 1 summarizes recent state related to adsorption treatment in water purification, and refers SPAC application and challenges related to particle separation. In addition, the objectives of the present study are listed.

Chapter 2 aims to establish a method for identifying and quantifying very low concentrations of SPAC. This method is composed of membrane filtration and microscopic image analysis, and is validated in terms of accuracy and applicability, comparing to turbidity measurement which is conventionally used for evaluating particle removal. By using the established method, fine carbon particles remaining after CSF process are determined their size and concentration. In addition, characteristics of the particles are analyzed in terms of a charge-state and a size of particles, which are related to treatment performance.

Chapter 3 aims to find better coagulation conditions and find a better coagulant for the removal of SPAC. In this context, mixing operation conditions including mixing intensity, mixing time, and reactor configuration are examined, dividing the operation into two components of coagulation and flocculation. The effects of coagulant type and coagulant dose on the removal of SPAC are also examined, by using two commercially available poly-aluminum chlorides (PACls) and lab-made PACls prepared in our research group.

Chapter 4 aims to disclose the behavior of carbon particles during the CSF process. Particles after coagulation are supposed to be classified into two groups: particles that can grow into floc particles and those that cannot grow into floc particles. The latter particles are determined by using the microscopic method established in Chapter 2, and are examined a relationship with the residual particles remaining in finished water, taking account of a charge-state and a size of particles.

Chapter 5 aims to reveal the fates and removals of MPs, clay, AC, and virus particles during CSF. We applied counting methods for identifying and quantifying these particles including clay particles at very low concentration levels, which enabled comparative discussion for all particles with the same accuracy on the removal rate evaluation.

Chapter 6 summarizes findings of this research and states a conclusion.

1.3 Reference

Aguilar, M.I., Sáez, J., Lloréns, M., Soler, A. and Ortuño, J.F. (2003) Microscopic observation of particle reduction in slaughterhouse wastewater by coagulation–flocculation using ferric sulphate as coagulant and different coagulant aids. Water Research 37(9), 2233-2241.

Amaral, P., Partlan, E., Li, M., Lapolli, F., Mefford, O.T., Karanfil, T. and Ladner, D.A. (2016) Superfine powdered activated carbon (S-PAC) coatings on microfiltration membranes: Effects of milling time on contaminant removal and flux. Water Research 100, 429-438.

American Society of Civil Engineers and American Water Works Association, U. (1998) Water Treatment Plant Design, McGraw-Hill.

Ando, N., Matsui, Y., Kurotobi, R., Nakano, Y., Matsushita, T. and Ohno, K. (2010) Comparison of natural organic matter adsorption capacities of super-powdered activated carbon and powdered activated Carbon. Water Res 44(14), 4127-4136.

Ando, N., Matsui, Y., Matsushita, T. and Ohno, K. (2011) Direct observation of solid-phase adsorbate concentration profile in powdered activated carbon particle to elucidate mechanism of high adsorption capacity on super-powdered activated carbon. Water Research 45(2), 761-767.

Apul, O.G., Hoogesteijn von Reitzenstein, N., Schoepf, J., Ladner, D., Hristovski, K.D. and Westerhoff, P. (2017) Superfine powdered activated carbon incorporated into electrospun polystyrene fibers preserve adsorption capacity. Science of The Total Environment 592, 458-464.

Ateia, M., Erdem, C.U., Ersan, M.S., Ceccato, M. and Karanfil, T. (2019) Selective removal of bromide and iodide from natural waters using a novel AgCl-SPAC composite at environmentally relevant conditions. Water Research 156, 168-178.

Bonvin, F., Jost, L., Randin, L., Bonvin, E. and Kohn, T. (2016) Super-fine powdered activated carbon (SPAC) for efficient removal of micropollutants from wastewater treatment plant effluent. Water Research 90, 90-99.

Bureau of Waterworks Tokyo Metropolitan Government, T. (2014) Personal communication.

Carns, K.E. and Stinson, K.B. (1978) Controlling Organics: The East Bay Municipal Utility District Experience. Journal (American Water Works Association) 70(11), 637-644.

Cho, K., An, B.M., So, S., Chae, A. and Song, K.G. (2020) Simultaneous control of algal micropollutants based on ball-milled powdered activated carbon in combination with permanganate oxidation and coagulation. Water Research 185, 116263.

Decrey, L., Bonvin, F., Bonvin, C., Bonvin, E. and Kohn, T. (2020) Removal of trace organic contaminants from wastewater by superfine powdered activated carbon (SPAC) is neither affected by SPAC dispersal nor coagulation. Water Research 185, 116302.

Dris, R., Gasperi, J., Saad, M., Mirande, C. and Tassin, B. (2016) Synthetic fibers in atmospheric fallout: A source of microplastics in the environment? Marine Pollution Bulletin 104(1), 290-293.

Dunn, S.E. and Knappe, D.R.U. (2019) DBP Precursor and Micropollutant Removal by Powdered Activated Carbon.

Edzwald, J.K. (2011) WATER QUALITY & TREATMENT A Handbook on Drinking Water, American Water Works Association, American Society of Civil Engineers, McGraw-Hill.

Ellerie, J.R., Apul, O.G., Karanfil, T. and Ladner, D.A. (2013) Comparing graphene, carbon nanotubes, and superfine powdered activated carbon as adsorptive coating materials for microfiltration membranes. Journal of Hazardous Materials 261, 91-98.

Freeman, S., Booth, A.M., Sabbah, I., Tiller, R., Dierking, J., Klun, K., Rotter, A., Ben-David, E., Javidpour, J. and Angel, D.L. (2020) Between source and sea: The role of wastewater treatment in reducing marine microplastics. Journal of Environmental Management 266, 110642.

Gifford, J.S., George, D.B. and Adams, V.D. (1989) Synergistic effects of potassium permanganate and PAC in direct filtration systems for THM precursor removal. Water Research 23(10), 1305-1312.

Heijman, S.G.J., Hamad, J.Z., Kennedy, M.D., Schippers, J. and Amy, G. (2009) Submicron powdered activated carbon used as a pre-coat in ceramic micro-filtration. Desalination and Water Treatment 9(1-3), 86-91.

Hu, C.-Y., Lo, S.-L., Chang, C.-L., Chen, F.-L., Wu, Y.-D. and Ma, J.-l. (2013) Treatment of highly turbid water using chitosan and aluminum salts. Separation and Purification Technology 104, 322-326.

Iqbal, S., Xu, J., Allen, S.D., Khan, S., Nadir, S., Arif, M.S. and Yasmeen, T. (2020) Unraveling consequences of soil micro- and nano-plastic pollution on soil-plant system: Implications for nitrogen (N) cycling and soil microbial activity. Chemosphere 260, 127578.

Iwasaki, S., Isobe, A., Kako, S.i., Uchida, K. and Tokai, T. (2017) Fate of microplastics and mesoplastics carried by surface currents and wind waves: A numerical model approach in the Sea of Japan. Marine Pollution Bulletin 121(1), 85-96.

Jiang, W., Xiao, F., Wang, D.S., Wang, Z.C. and Cai, Y.H. (2015) Removal of emerging contaminants by pre-mixed PACl and carbonaceous materials. RSC Advances 5(45), 35461-35468.

Kögel, T., Bjorøy, Ø., Toto, B., Bienfait, A.M. and Sanden, M. (2020) Micro- and nanoplastic toxicity on aquatic life: Determining factors. Science of The Total Environment 709, 136050.

Kanaya, S., Kawase, Y., Mima, S., Sugiura, K., Murase, K. and Yonekawa, H. (2015) Drinking Water Treatment Using Superfine PAC (SPAC): Design and Successful Operation History in Full-scale Plant, pp. 624-631, Salt Lake City, Utah, USA.

Koelmans, A.A., Mohamed Nor, N.H., Hermsen, E., Kooi, M., Mintenig, S.M. and De France, J. (2019) Microplastics in freshwaters and drinking water: Critical review and assessment of data quality. Water Research 155, 410-422.

Kosuth, M., Mason, S.A. and Wattenberg, E.V. (2018) Anthropogenic contamination of tap water, beer, and sea salt. PLOS ONE 13(4), e0194970.

Lee, B.-B., Choo, K.-H., Chang, D. and Choi, S.-J. (2009) Optimizing the coagulant dose to control membrane fouling in combined coagulation/ultrafiltration systems for textile wastewater reclamation. Chemical Engineering Journal 155(1), 101-107.

Lin, J., Yan, D., Fu, J., Chen, Y. and Ou, H. (2020) Ultraviolet-C and vacuum ultraviolet inducing surface degradation of microplastics. Water Research 186, 116360.

Ma, B., Xue, W., Hu, C., Liu, H., Qu, J. and Li, L. (2019) Characteristics of microplastic removal via coagulation and ultrafiltration during drinking water treatment. Chemical Engineering Journal 359, 159-167.

Matsui, Y., Aizawa, T., Kanda, F., Nigorikawa, N., Mima, S. and Kawase, Y. (2007) Adsorptive removal of geosmin by ceramic membrane filtration with super-powdered activated carbon. Journal of Water Supply: Research and Technology-Aqua 56(6-7), 411-418.

Matsui, Y., Hasegawa, H., Ohno, K., Matsushita, T., Mima, S., Kawase, Y. and Aizawa, T. (2009) Effects of super-powdered activated carbon pretreatment on coagulation and trans-membrane pressure buildup during microfiltration. Water Research 43(20), 5160-5170.

Matsui, Y., Nakao, S., Sakamoto, A., Taniguchi, T., Pan, L., Matsushita, T. and Shirasaki, N. (2015) Adsorption capacities of activated carbons for geosmin and 2-methylisoborneol vary with activated carbon particle size: Effects of adsorbent and adsorbate characteristics. Water Res 85, 95-102.

Matsui, Y., Nakao, S., Taniguchi, T. and Matsushita, T. (2013) Geosmin and 2-methylisoborneol removal using superfine powdered activated carbon: shell adsorption and branched-pore kinetic model analysis and optimal particle size. Water Research 47(8), 2873-2880.

Matsui, Y., Yoshida, T., Nakao, S., Knappe, D.R. and Matsushita, T. (2012) Characteristics of competitive adsorption between 2-methylisoborneol and natural organic matter on superfine and conventionally sized powdered activated carbons. Water Res 46(15), 4741-4749.

Mintenig, S.M., Löder, M.G.J., Primpke, S. and Gerdts, G. (2019) Low numbers of microplastics detected in drinking water from ground water sources. Science of The Total Environment 648, 631-635.

Murray, C.C., Vatankhah, H., McDonough, C.A., Nickerson, A., Hedtke, T.T., Cath, T.Y., Higgins, C.P. and Bellona, C.L. (2019) Removal of per- and polyfluoroalkyl substances using super-fine powder activated carbon and ceramic membrane filtration. Journal of Hazardous Materials 366, 160-168.

Naik, R.A., Rowles, L.S., Hossain, A.I., Yen, M., Aldossary, R.M., Apul, O.G., Conkle, J. and Saleh, N.B. (2020) Microplastic particle versus fiber generation during photo-transformation in simulated seawater. Science of The Total Environment 736, 139690.

Partlan, E., Ren, Y., Apul, O.G., Ladner, D.A. and Karanfil, T. (2020) Adsorption kinetics of synthetic organic contaminants onto superfine powdered activated carbon. Chemosphere 253, 126628.

Pivokonsky, M., Cermakova, L., Novotna, K., Peer, P., Cajthaml, T. and Janda, V. (2018) Occurrence of microplastics in raw and treated drinking water. Science of The Total Environment 643, 1644-1651.

Rajala, K., Grönfors, O., Hesampour, M. and Mikola, A. (2020) Removal of microplastics from secondary wastewater treatment plant effluent by coagulation/flocculation with iron, aluminum and polyamine-based chemicals. Water Research 183, 116045.

Randtke, S.J. and Horsley, M.B. (2012) WATER TREATMENT PLANT DESIGN, FIFTH EDITION, AWWA, American Society of Civil Engineers, McGraw-Hill.

Revel, M., Châtel, A. and Mouneyrac, C. (2018) Micro(nano)plastics: A threat to human health? Current Opinion in Environmental Science & Health 1, 17-23.

Rodrigues, M.O., Abrantes, N., Gonçalves, F.J.M., Nogueira, H., Marques, J.C. and Gonçalves, A.M.M. (2018) Spatial and temporal distribution of microplastics in water and sediments of a freshwater system (Antuã River, Portugal). Science of The Total Environment 633, 1549-1559.

Shen, M., Song, B., Zhu, Y., Zeng, G., Zhang, Y., Yang, Y., Wen, X., Chen, M. and Yi, H. (2020) Removal of microplastics via drinking water treatment: Current knowledge and future directions. Chemosphere 251, 126612.

Shirasaki, N., Matsushita, T., Matsui, Y. and Yamashita, R. (2018) Evaluation of the suitability of a plant virus, pepper mild mottle virus, as a surrogate of human enteric viruses for assessment of the efficacy of coagulation–rapid sand filtration to remove those viruses. Water Research 129, 460-469.

Skaf, D.W., Punzi, V.L., Rolle, J.T. and Kleinberg, K.A. (2020) Removal of micron-sized microplastic particles from simulated drinking water via alum coagulation. Chemical Engineering Journal 386, 123807.

Sun, S., Weber-Shirk, M. and Lion, L.W. (2016) Characterization of Flocs and Floc Size Distributions Using Image Analysis. Environmental Engineering Science 33(1), 25-34.

Sun, Y., Yuan, J., Zhou, T., Zhao, Y., Yu, F. and Ma, J. (2020) Laboratory simulation of microplastics weathering and its adsorption behaviors in an aqueous environment: A systematic review. Environmental Pollution 265, 114864.

The Ministry of Health Labor and Welfare, J. (2018) State of issues in drinking water originated from accidents or offensive taste and odor. https://www.mhlw.go.jp/stf/seisakunitsuite/bunya/topics/bukyoku/kenkou/suido/kikikanri/03.html

Wang, C., Xian, Z., Jin, X., Liang, S., Chen, Z., Pan, B., Wu, B., Ok, Y.S. and Gu, C. (2020a) Photo-aging of polyvinyl chloride microplastic in the presence of natural organic acids. Water Research 183, 116082.

Wang, Y., Wang, X., Li, Y., Li, J., Liu, Y., Xia, S. and Zhao, J. (2021) Effects of exposure of polyethylene microplastics to air, water and soil on their adsorption behaviors for copper and tetracycline. Chemical Engineering Journal 404, 126412.

Wang, Z., Lin, T. and Chen, W. (2020b) Occurrence and removal of microplastics in an advanced drinking water treatment plant (ADWTP). Science of The Total Environment 700, 134520.

Wang, Z., Sedighi, M. and Lea-Langton, A. (2020c) Filtration of microplastic spheres by biochar: removal efficiency and immobilisation mechanisms. Water Research 184, 116165.

WHO (2019) Microplastics in drinking-water.

Wong, J.K.H., Lee, K.K., Tang, K.H.D. and Yap, P.-S. (2020) Microplastics in the freshwater and terrestrial environments: Prevalence, fates, impacts and sustainable solutions. Science of The Total Environment 719, 137512.

Wu, P., Huang, J., Zheng, Y., Yang, Y., Zhang, Y., He, F., Chen, H., Quan, G., Yan, J., Li, T. and Gao, B. (2019) Environmental occurrences, fate, and impacts of microplastics. Ecotoxicology and Environmental Safety 184, 109612.

Younker, J.M. and Walsh, M.E. (2016) Effect of adsorbent addition on floc formation and clarification. Water Research 98, 1-8.

Yu, W.-z., Qu, J.-h. and Gregory, J. (2015) Pre-coagulation on the submerged membrane fouling in nano-scale: Effect of sedimentation process. Chemical Engineering Journal 262, 676-682.

Zhang, P., Wu, Z., Zhang, G., Zeng, G., Zhang, H., Li, J., Song, X. and Dong, J. (2008) Coagulation characteristics of polyaluminum chlorides PAC-Al30 on humic acid removal from water. Separation and Purification Technology 63(3), 642-647.

Zhang, Y., Diehl, A., Lewandowski, A., Gopalakrishnan, K. and Baker, T. (2020) Removal efficiency of micro- and nanoplastics (180 nm–125 μm) during drinking water treatment. Science of The Total Environment 720, 137383.

Zhou, G., Wang, Q., Li, J., Li, Q., Xu, H., Ye, Q., Wang, Y., Shu, S. and Zhang, J. (2021) Removal of polystyrene and polyethylene microplastics using PAC and FeCl3 coagulation: Performance and mechanism. Science of The Total Environment 752, 141837.

Zhou, Y., Wang, J., Zou, M., Jia, Z., Zhou, S. and Li, Y. (2020) Microplastics in soils: A review of methods, occurrence, fate, transport, ecological and environmental risks. Science of The Total Environment 748, 141368.

Zhu, K., Jia, H., Sun, Y., Dai, Y., Zhang, C., Guo, X., Wang, T. and Zhu, L. (2020a) Long-term phototransformation of microplastics under simulated sunlight irradiation in aquatic environments: Roles of reactive oxygen species. Water Research 173, 115564.

Zhu, L., Zhao, S., Bittar, T.B., Stubbins, A. and Li, D. (2020b) Photochemical dissolution of buoyant microplastics to dissolved organic carbon: Rates and microbial impacts. Journal of Hazardous Materials 383, 121065.

2 IDENTIFYICAION AND CHARACTERIZATION OF SUPERFINE ACTIVATED-CARBON PARTICLES REMAINING IN SAND FILTRATE

2.1 Introduction

Adsorption treatment in drinking water treatment has used PAC for a long period, and recent nano-milling technology allows to produce further fine and effective SPAC (Amaral *et al.* 2016, Ando *et al.* 2010, Ando *et al.* 2011, Apul *et al.* 2017, Ateia *et al.* 2019, Bonvin *et al.* 2016, Decrey *et al.* 2020, Dunn and Knappe 2019, Jiang *et al.* 2015, Matsui *et al.* 2015, Matsui *et al.* 2013a, Matsui *et al.* 2012, Murray *et al.* 2019, Partlan *et al.* 2020). SPAC has a size approx. 1 μm, and such a fine particles has been hard to be identified and quantified. This has hindered SPAC application to conventional drinking water treatment composed of coagulation-flocculation, sedimentation, and sand filtration, because no one has been able to evaluate removal performance of SPAC itself (Carns and Stinson 1978, Gifford *et al.* 1989, Lee *et al.* 2009, Yu *et al.* 2015).

Accordingly, this chapter aims to establish a method for identifying and quantifying very low concentrations of SPAC. By using the method, fine carbon particles remaining after CSF process are evaluated their size and concentration. In addition, characteristics of the particles are analyzed in terms of a charge-state and a size of particles, which are related to treatment performance.

This chapter has been already published by Elsevier, and the information is described as follows:

Title: Identifying, counting, and characterizing superfine activated-carbon particles remaining after coagulation, sedimentation, and sand filtration

Author: Nakazawa, Yoshifumi; Matsui, Yoshihiko; Hanamura, Yusuke; Shinno, Koki; Shirasaki, Nobutaka; Matsushita, Taku.

Name of journal: Water Research

Year: 2018

Volume: 138

Pages: 160-168

DOI: https://doi.org/10.1016/j.watres.2018.03.046

2.2 Materials and methods

2.2.1 Carbon particles and coagulant

A commercially available wood-based PAC (Taiko W; Futamura Chemical Co., Ltd., Nagoya, Japan) was prepared as a slurry in pure water (Milli-Q water; Milli-Q Advantage A10 System; Merck KGaA, Darmstadt, Germany) and then pulverized to produce SPAC slurries of different particle sizes (Table 2-1). $SPAC_L$

was produced with a closed-chamber ball mill (Nikkato, Osaka, Japan) with 5- and 10-mm-diameter balls. $SPAC_{S1}$ and $SPAC_{S2}$ were produced using a bead mill with a re-circulation system (LMZ015; Ashizawa Finetech, Chiba, Japan) and 0.3-mm-diameter ZrO_2 beads (Pan *et al.* 2017). Standard carbon particle suspensions with predetermined mass concentrations were prepared by diluting a SPAC/PAC slurry with Sapporo City tap water filtered through a PTFE (polytetrafluoroethylene) membrane (nominal pore diameter, 0.1 μm; Φ90 mm; Toyo Roshi Kaisha, Ltd., Tokyo, Japan). Membrane-filtered tap water without the addition of carbon particles was used as blank water. The particle size distributions of the carbons were determined by using a laser light diffraction and scattering method (Microtrac MT3300EXII; MicrotracBEL Corp., Osaka, Japan). To measure the true particle size distribution of the carbon particles, a sample of the slurry was pretreated by the addition of a dispersant (Triton X-100; Kanto Chemical Co., Tokyo, Japan; final concentration, 0.08% w/v) and subjected to ultrasonic dispersion before determination of the particle size distribution via the laser light diffraction and scattering method. The apparent particle size distributions of the carbon particles were measured via the same method but without an added dispersant or ultrasonic dispersion.

Poly-aluminum chloride with a basicity of 50% and sulfate content of 3% (Taki Chemical Co., Ltd, Hyogo, Japan), a coagulant widely used in water treatment plants, was used as the coagulant in this study.

Table 2-1. Carbon particle size. The median diameters are based on the particle size distribution as determined by the laser light diffraction and scattering method.

Activated carbon		Median diameter (μm)
PAC		13.7
SPAC	$SPAC_L$	2.54
	$SPAC_{S1}$	0.91
	$SPAC_{S2}$	0.96

Note: $SPAC_L$, SPAC with a large particle size; $SPAC_{S1}$ and $SPAC_{S2}$, the first and the second, respectively, batch of SPAC with a small particle size.

2.2.2 Coagulation–flocculation, sedimentation, and rapid sand filtration

Tap water in Sapporo city was filtered through a membrane filter (nominal pore diameter, 0.1 μm; Toyo Roshi Kaisha, Ltd.) and then added with one of the carbon slurries to 30-mg/L SPAC, 7.5-mg/L SPAC, or 30-mg/L PAC to prepare raw waters. Most CSF experiments were conducted with these waters, but two CSF experiments were conducted with water from the Toyohira River (Hokkaido) after supplementing the water with SPAC at 7.5 mg/L. The river water was sampled at the location where it becomes the raw water source for the Moiwa Water Purification Plant (Sapporo, Japan).

A schematic of the experimental setup and procedure is shown in Fig. 2-1. The coagulation–flocculation and sedimentation steps were conducted in a 4-L rectangular beaker. After a predetermined volume of HCl or NaOH (0.1 N) was added to adjust the coagulation pH to 7.0, the coagulant (poly-aluminum chloride) was injected into the beaker to a final concentration of 4 mg-Al/L. The water was stirred rapidly for 20 s (coagulation; G = 600 s^{-1}, 197 rpm) and then slowly for 20 min (flocculation; 5 min at 50 s^{-1}, 38 rpm; 5 min at 20 s^{-1}, 20 rpm; 10 min at 10 s^{-1}, 13 rpm). The water was then left at rest for 1 h until the floc particles settled. Next, the top three liters of the water (supernatant) were transferred to another beaker for the determination of turbidity (2100Q portable turbidimeter; Hach

Company, Loveland, CO, USA) and for rapid sand filtration. Sand filtration was conducted for 40 min at a rate of 90 m d^{-1} in the down-flow direction using a column (Φ4 cm) filled to a depth of 50 cm with sand (effective diameter, 0.6 mm; uniformity, 1.3; Nihon Genryo Co., Ltd., Japan). The sand filtrate was collected from 13 to 40 min after the start of filtration, and the turbidity and particle count of the filtrate were determined.

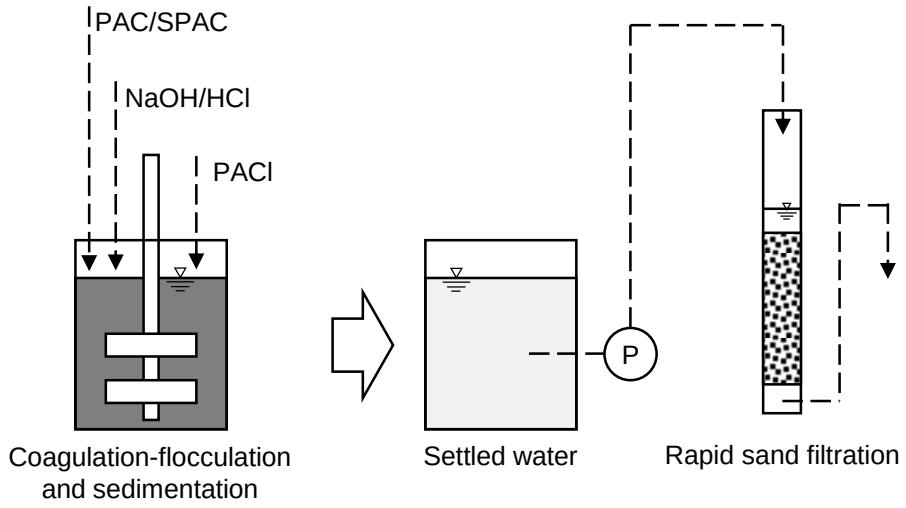

Fig. 2-1. Schematic diagram of the experimental setup for the coagulation-flocculation, sedimentation, and sand filtration experiment.

After each filtration run, the sand filter was backwashed with tap water for 1 h. Next, pure water (Milli-Q water) was passed through the sand filter for 1 h in the down-flow direction, followed by 3 L of membrane-filtered tap water, also in the down-flow direction. After the 3 L of membrane-filtered tap water was passed through the sand filter, the sand filtrate was collected. The particle count of the sand filtrate was always low (< 6 particles/mL), but this count was subtracted from the particle count of the filtrate collected in the filtration experiments to yield the net count of particles that had passed through the filter. The filter was then used for the next filtration experiment.

2.2.3 Membrane filtration and microscopic image analysis

To sample the carbon particles in the water, the water was filtered through a PTFE membrane filter (nominal pore diameter, 0.1 μm; Φ25 mm; Merck KGaA) supported by a glass filter holder (KG-25; Toyo Roshi Kaisha, Ltd.) (Fig. 2-2). After drying the filter, color digital photomicrographs were captured for nine predetermined observation zones (microscope view area, 247 × 330 μm) per filter (Fig. 2-3) with a digital microscope (VHX-2000; Keyence Corporation, Osaka, Japan) at 1000× magnification. The photomicrographs were analyzed by using the image analysis software supplied with the microscope.

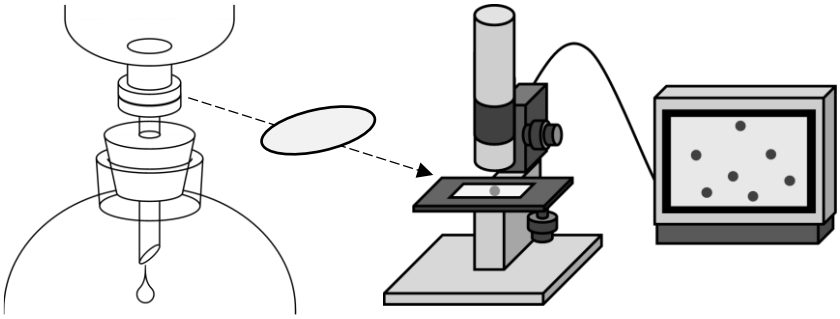

Fig. 2-2. Schematic diagram of the experimental setup for membrane filtration and microscopic image analysis.

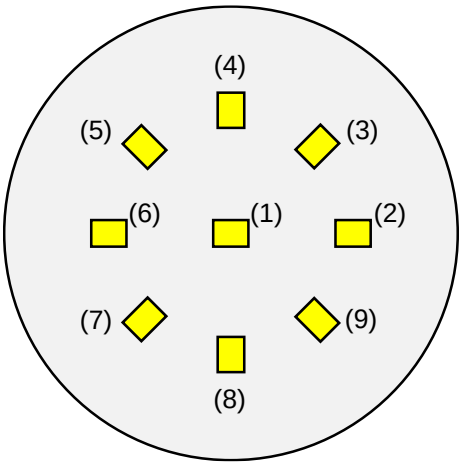

Fig. 2-3. Observation zones on a single membrane filter (Φ25 mm).

Fig. 2-4 shows two representative image analysis series. Series A shows the image analysis of a membrane through which 100 mL of standard suspension

containing 1-μg/L $SPAC_{S1}$ was filtered. Series B shows an image analysis of a membrane through which a sample of sand filtrate was filtered at a pilot-scale plant where surface water was treated by means of a CSF process after the addition of PAC (Yamaguchi *et al.* 2016). Panels A1 and B1 are the original photomicrographs of the surface of the membranes. In the photomicrographs, the black and dark gray spots in the background of the membrane texture are presumably carbon particles; very few of these colored spots were observed in the present study. After removal of the membrane texture, the images were converted to grayscale (Panels A2 and B2). The black and dark gray spots in the images were identified as carbon particles based on their lightness, with the cut-off value being 195 ± 15 in the range 0–255, because the maximum lightness of carbon particles in these photographs was ~195. Touching or overlapping spots were separated from each other by using a shrink-and-blow process in the software. Spots with a diameter > 0.2 μm were individually identified. Panels A3 and B3 show detected spots, which appear black in these panels. The original photomicrograph was then checked to confirm that the spots were present in both the photomicrograph and the processed image: false spots were removed through this process. Panels A4 and B4, which show the verified spots, were then obtained. Note that if many spots with colors but not black-and-white had been observed in the photomicrographs, more advanced image processing would have been required to identify the carbon particles (see Fig. 2-5 and Fig. 2-6). However, because the raw waters used in the present study were made by adding carbon particles to membrane-filtered water or low-turbidity river water, colored spots were not observed (Fig. 2-4). This was true even in the photomicrographs of the samples collected at the pilot-scale water treatment plant, which treated surface water in a conventional way after the addition of PAC (Fig. 2-4). In principle it is hard to distinguish between carbon particles and black mineral particles, but the interference due to black mineral particles would be small because of it low concentration compared with carbon particle concentration (Fig. 2-7).

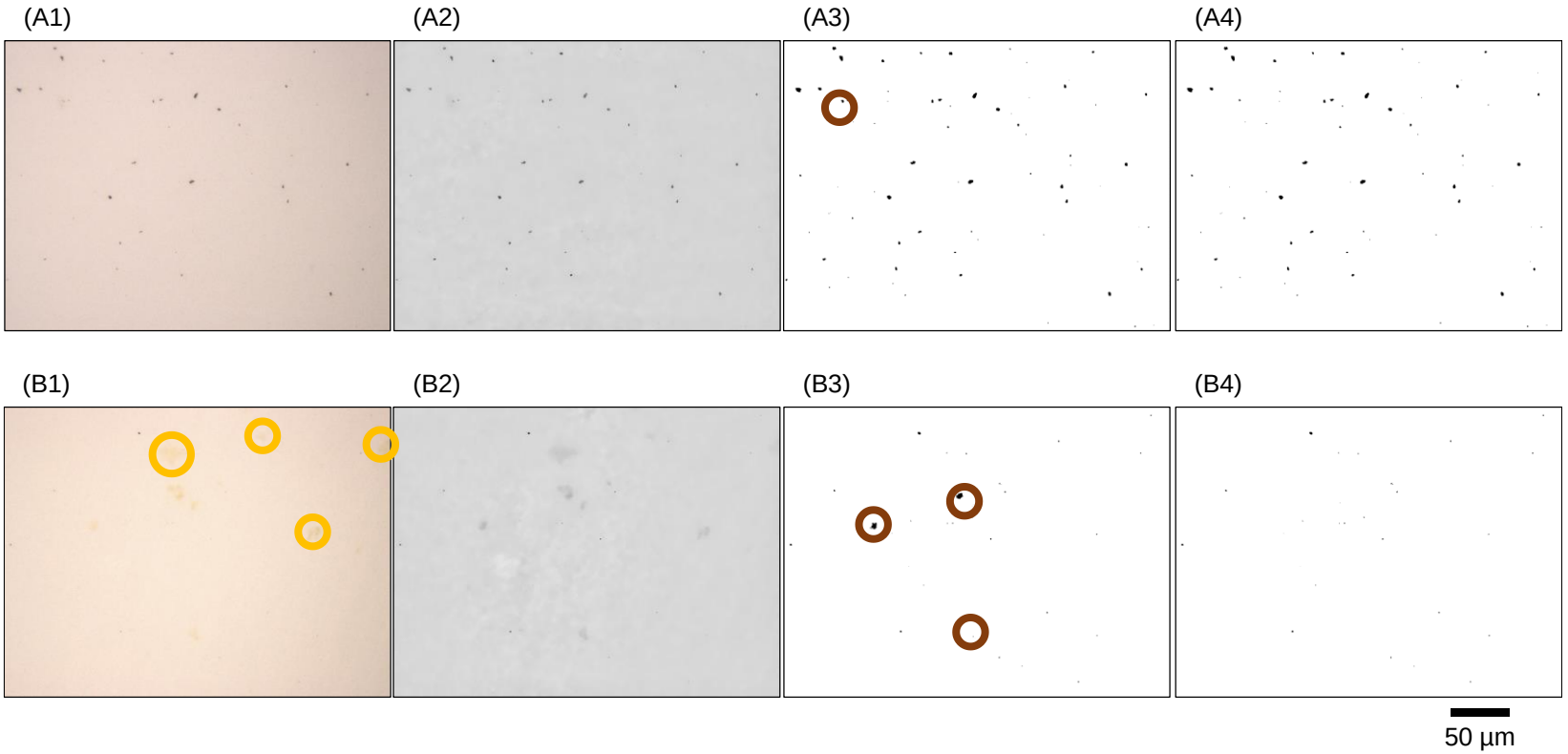

Fig. 2-4. Representative image analysis series. Series A begins with a photomicrograph captured of a filter through which 100 mL of standard suspension containing 1-µg/L $SPAC_{S1}$ was passed. Series B begins with a photomicrograph of a filter through which a sand filtrate of unknown carbon particle concentration was passed (the water was treated by a CFS after the addition of 20-mg/L PAC). Panels A2 and B2 are grayscale conversions of the original photomicrographs. The grayscale images were converted to a binary image (Panels A3 and B3) in which the spots were detected according to lightness. Panels A4 and B4 are images after visual verification that all of the black sports in Panels A3 and B3 were included in the original photomicrograph (panels A1 and B1); spots not found in the original photomicrograph were eliminated. The yellow circles indicate dots that were verified as not being carbon particles, which were removed during image processing. The brown circles indicate dots eliminated by checking the original photograph (Panels A1 and B1).

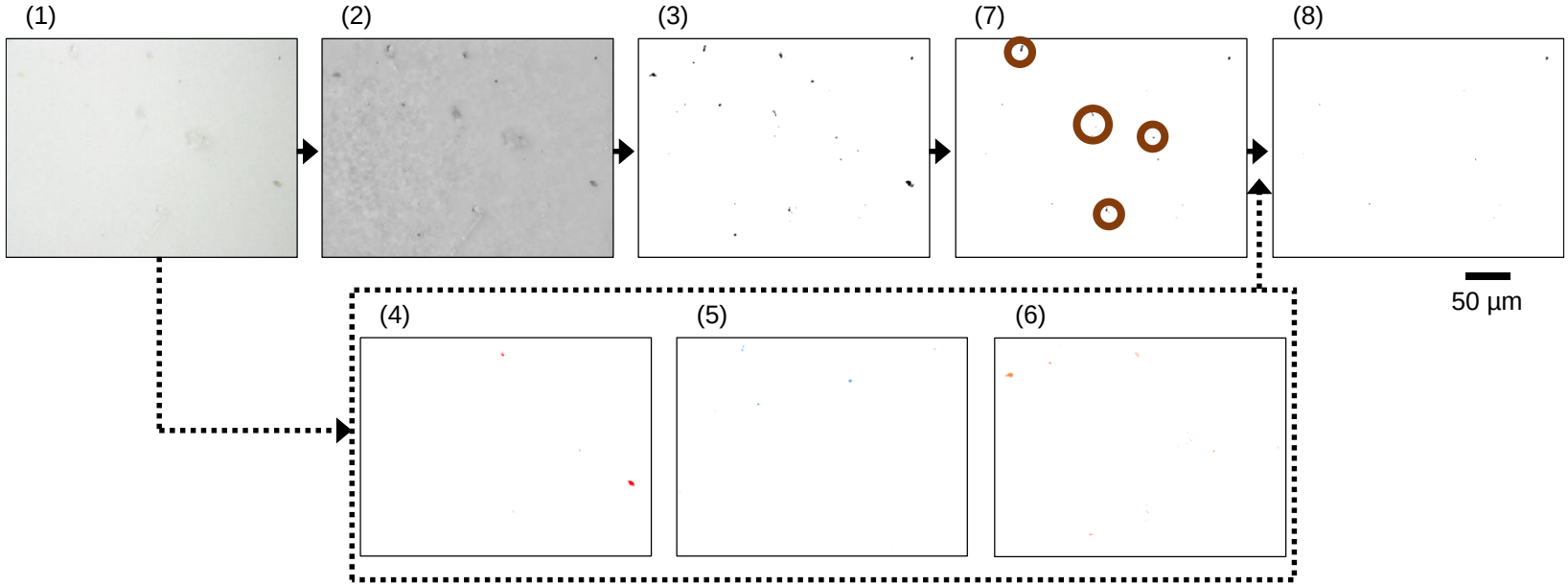

Fig. 2-5. Representative image analysis series showing the process when many colored spots were observed in the photomicrograph. Panel 1 is a photomicrograph of a filter through which 100 mL of water containing 0.1-µg/L $SPAC_{S2}$ and 30 µg/L of powdered mineral pigments (10 µg/L each of Iwaaka241 [red], Gunjo342 [blue], Yamabuki121 [yellow]; Nakagawa Gofun Enogu Co., Ltd., Kyoto, Japan) was passed. Panel 2 is a grayscale conversion of the original photomicrograph. The grayscale image was converted to a binary image (Panel 3) in which the spots were detected according to lightness. Panels 4, 5, and 6 are binary images in which red, blue, and yellow spots, respectively, were extracted according to their HSL (hue, saturation, and lightness). Panel 7 is the image after comparison with Panels 3 to 6 during which spots that were verified as not being black particles were eliminated. Panel 8 is the image after visual verification that all of the black spots in Panel 7 were included in the original photomicrograph (Panel 1); spots not found in the original photomicrograph were eliminated. The brown circles indicate spots that were eliminated by the visual examination.

When black and colored spots were both observed on the membrane, it was difficult to distinguish the black particles from the color particles using only lightness, particularly to distinguish black particles from blue particles, which resulted in an increase in the number of false positives. Therefore, black and colored particles were identified with the image in the HSL color model (Panels 3–7), and black particles could be distinguished from colored particles (Panel 4–7) by comparing the images Fig. 2-6.

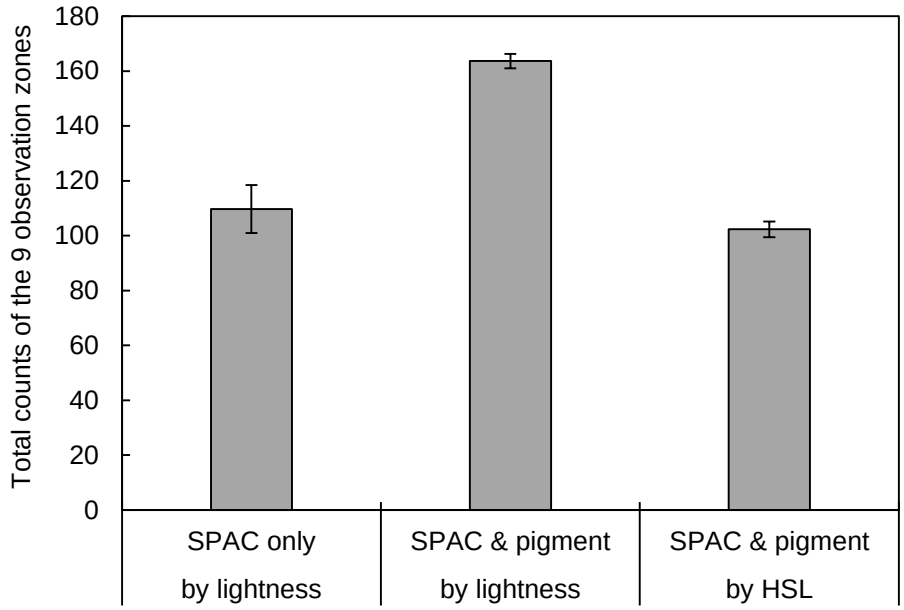

Fig. 2-6. Comparison of particle counts obtained for treated water originally containing 0.1-μg/L $SPAC_{S2}$ and 30-μg/L powdered mineral pigment particles (10 μg/L each of Iwaaka241 [red], Gunjo342 [blue], Yamabuki121 [yellow]; Nakagawa Gofun Enogu Co., Ltd., Kyoto, Japan).

When lightness only was used to identify carbon particles, the particle count for the suspension containing SPAC and pigments was larger than that for the suspension containing SPAC only because some of the pigment particles were erroneously counted as carbon particles. When the HSL (hue, saturation, lightness) color model was used (see Fig. 2-5), the counts of the suspension containing SPAC and pigment were similar to those containing SPAC, indicating that the majority of false positives were eliminated. Note that this analysis using the HSL color model still required visual examination. In the present study, however, this more advanced analysis using the HSL color model was not required because the particles in the photomicrographs were mostly black particles interspersed with a few gray particles so colored particles were hardly observed. Therefore, the detection of carbon particles according to lightness alone could be enough for analysis.

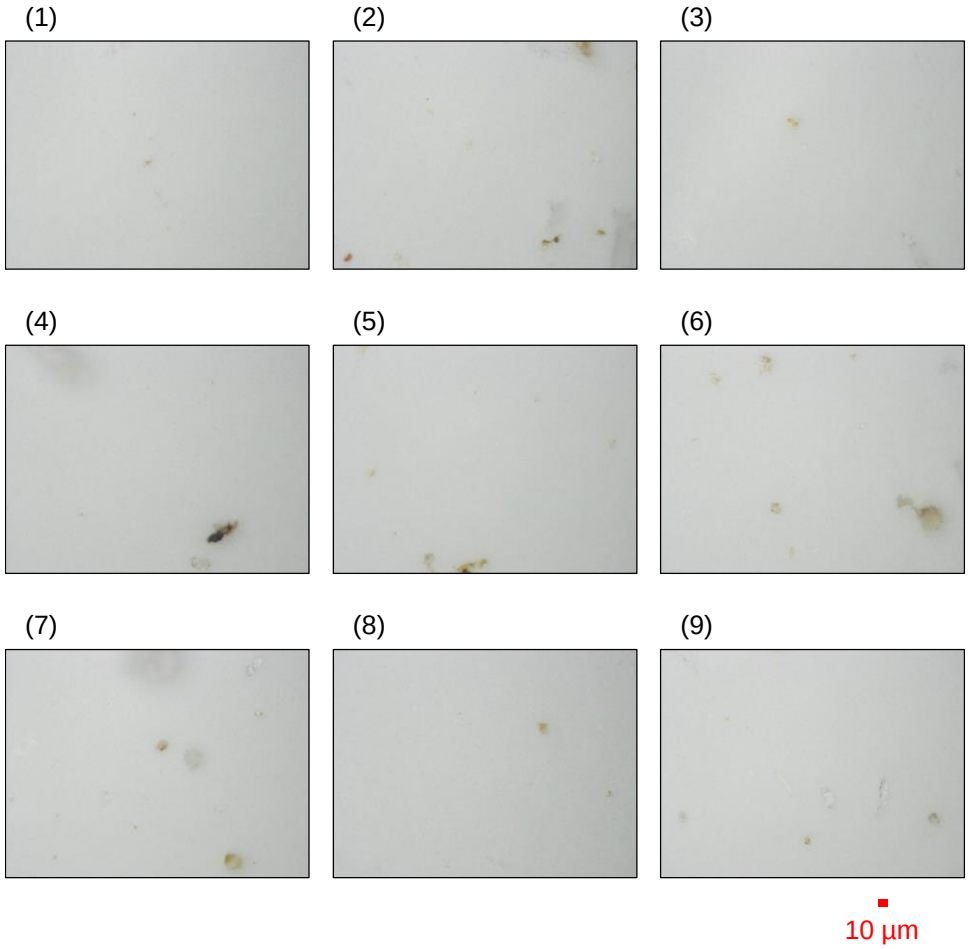

Fig. 2-7. Photomicrographs of nine observation zones on a filter that was passed river water (turbidity 5.7 NTU and DOC 0.9 mg/L) diluted 100 times by milliQ water. The concentration of black minerals looked like carbon particles from the river water was calculated as 5.1×10^3 particles/mL, that was far small compared to the concentration of carbon particles infused in the filtered tap water used in CSF experiments (3.9×10^7 particles/mL for 7.5-mg/L of $SPAC_{S2}$).

For each filter, the spot counts for the nine observation zones (Fig. 2-8 and Fig. 2-9) were summed to give the total spot count for the nine observation zones. The spot count for each whole filter was obtained by multiplying the total count by the ratio of the filtration area divided by the total area of the nine observation zones.

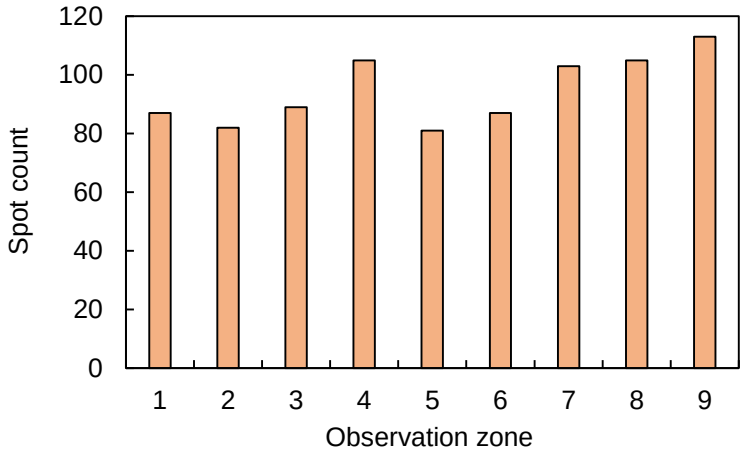

Fig. 2-8. Particle counts for the nine observation zones in a filter. An aliquot (100 mL) of standard suspension containing 1-μg/L $SPAC_{S1}$ was filtered through a membrane filter. The observation zone numbers correspond with those presented in Fig. 2-3.

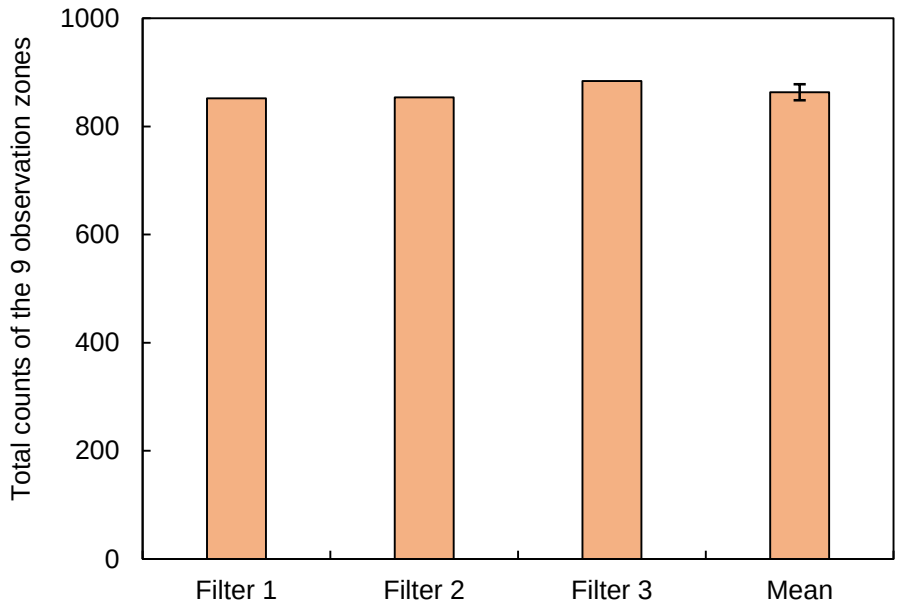

Fig. 2-9. Total particle counts for the nine observation zones in three filters and their mean value. An aliquot (100 mL) of standard suspension containing 1-μg/L $SPAC_{S1}$ was filtered through each filter. The error bar represents the standard deviation.

The filtration and counting processes were conducted three times for each water sample. The spot counts for the three filters were then averaged and corrected by subtracting the spot count of the blank water. Dividing the average-minus-blank count by the volume of the water sample gave the carbon particle number concentration.

The volume of each particle was calculated by assuming the particle to be spherical with a diameter equal to the projected area diameter of its spot on the photomicrograph. The number concentration was converted to a volume concentration by using Eq. (1):

$$\emptyset = C_N \int_0^\infty \frac{\pi}{6} d^3 f_N(d) dd \qquad (1)$$

where $\emptyset$ is the volume concentration (dimensionless), C_N is the number concentration (cm^{-3}), d is the particle diameter (cm), and f_N (d) is the particle size distribution by number (cm^{-1}).

When determining the volume concentration and the particle size distribution by volume, a blank correction was not performed. Not performing a blank correction did not substantially increase the analytical error, because the black spots observed for the blank water were very small in size and number compared to the black spots determined to be carbon particles in the sample water.

2.2.4 Measurement of zeta potential

The zeta potential of the carbon particles in the water samples after each stage of the water treatment process (i.e., coagulation, sedimentation, and rapid sand filtration) was determined by using a zeta electrometer (Zetasizer Nano ZS; Malvern, United Kingdom). Before the zeta potentials of the sand filtrate samples were determined, the samples were concentrated by a factor of 15.6. The zeta potentials of the other samples were measured without concentration.

To concentrate the sand filtrate samples, a tube containing 38.5 mL of sample water was centrifuged at 32,000 rpm (170,000 g) for 35 min at 25 °C (Ultracentrifuge L-80 XP; Beckman Coulter, Brea, CA, USA). After

centrifugation, the upper 26 mL of water in the tube was carefully removed, the tube was replenished with another 26 mL of sample water, and the tube was centrifuged again. This series of operations was repeated six times.

2.2.5 Fractionation of SPAC and PAC according to particle size

The SPAC in suspension (8.3 g/L) was fractionated by means of centrifugation. A tube containing 30 mL of SPAC suspension was centrifuged for 60 min at 0, 500, 1500, or 4000 rpm (himac CT6E; Eppendorf Himac Technologies Co., Ltd., Ibaraki, Japan). The upper 20 mL of the sample in the tube was then withdrawn, and the particle size distribution (Microtrac MT3300EXII) and zeta potential (Zetasizer Nano ZS) of the carbon particles remaining in the upper 20 mL of the sample were determined. Before measurement of the zeta potential, the turbidity of the sample was adjusted to 30 nephelometric turbidity units (NTUs) by diluting the sample with filtered tap water. Particle size distributions were determined without the addition of a dispersant or the use of ultra-sonication.

PAC in suspension (33 g/L) was fractionated by means of gravity settling. An aliquot (40 mL) of PAC suspension was left at rest in a beaker for 0, 6, 120, or 720 min. The upper 4 mL of the sample was then withdrawn, and the zeta potential and particle size distribution were determined as described above.

2.3 Results and Discussion

2.3.1 Identification and enumeration of carbon particles on the filter

The particle concentrations in the blank water and standard suspensions (0.1, 1.0, and 10 μg/L) were determined by using the membrane-filtration and microscopic-image-analysis method (Fig. 2-10). The particle counts for the three blank water samples were very low, and the counts likely included false positives arising from the texture of the membrane filter and contamination. The counts in the 100-mL blank water samples were <6 particles/mL. The counts for the same standard suspensions were comparable between filters. Particle concentrations >>6 particles/mL in a 100-mL filtered water sample could therefore be easily measured.

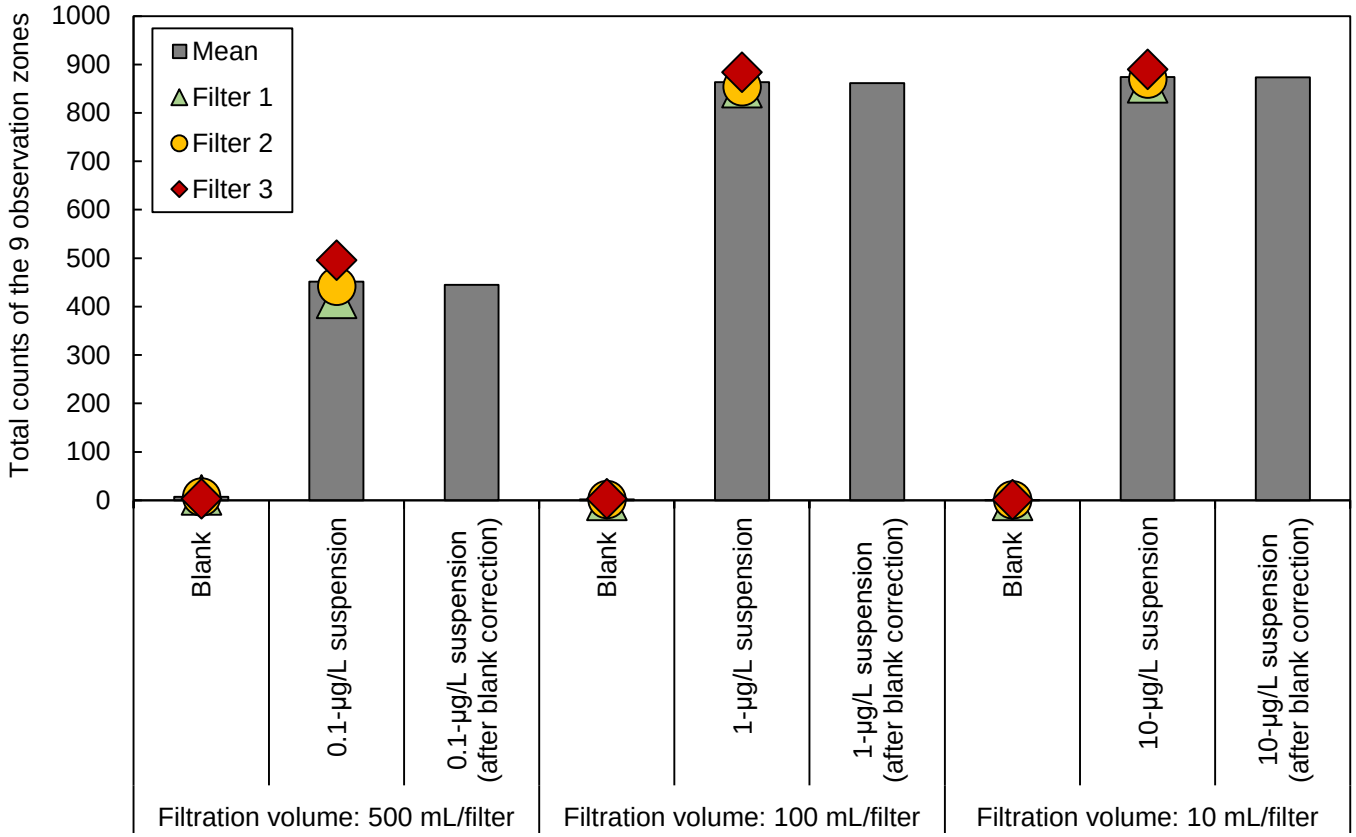

Fig. 2-10. Total particle counts for filters through which $SPAC_{S1}$ standard suspensions and blank water were passed.

Normalized standard deviations (coefficients of variation, C_V) of particle number concentrations were calculated for the counts of the three filters for a single water sample. The C_V values for all of the measurements were collected and plotted against the mean particle number concentrations. Fig. 2-11 shows the results for a filtration volume of 100 mL (results for filtration volumes of 500 and 10 mL are shown in Fig. 2-12). The C_V decreased with increasing particle number concentration, roughly in agreement with the theoretical relationship calculated by Eq. (4), which was derived by assuming the particle count to be a Poisson-distributed random variable. The expected value and variance of a Poisson-distributed random variable are equal. Therefore, the coefficient of variation is

$$C_V = 1/\sqrt{\lambda}, \qquad (2)$$

where C_V is the coefficient of variation and λ is the mean particle count.

The particle number concentration was calculated from the mean particle count by using

$$C_N = \frac{\lambda \times a_f / a_o}{V}, \qquad (3)$$

where C_N is the number concentration (cm^{-3}), a_f is the filtration area (cm^2), a_o is the total area of the nine observation zones (cm^2), and V is the filtration volume (cm^3).

Substituting Eq. (3) into Eq. (2) gives

$$C_V = \sqrt{\frac{a_f / a_o}{C_N V}}. \qquad (4)$$

The observed C_V values were all less than 0.4, with the exception of one sample for which the particle number concentration was 3 particles/mL. The C_V values were <0.2 for all the samples with particle number concentrations >200 particles/mL, which is equivalent to a SPAC concentration of >0.07 μg/L, but the C_V values varied between samples. The C_V values of some particle number concentrations were higher than predicted by the Poisson distribution, perhaps because sintered glass filter holder (nominal pore diameter, 30–50 μm, according to the manufacturer; Fig. 2-13). As a result, the filtration velocity across the membrane was uneven at the microscopic level, and the volumes of water passing through the filter at the observation zones were not exactly equal. Nevertheless, the fact that the number concentrations of the standard suspensions obtained by the membrane-filtration and microscopic-image-analysis method were linearly correlated with the mass concentrations (R^2 = 1.00; Fig. 2-14) supports the validity of the method.

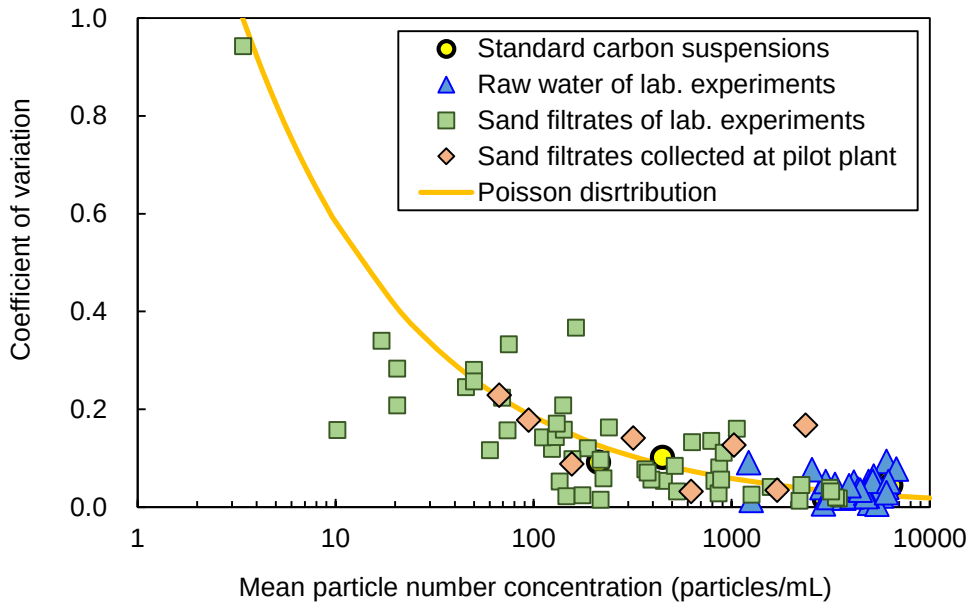

Fig. 2-11. Mean particle number concentration versus cofficient of variation for a filtration volume of 100 mL/filter. The line was calculated by using equation (4), which was derived from the Poisson distribution.

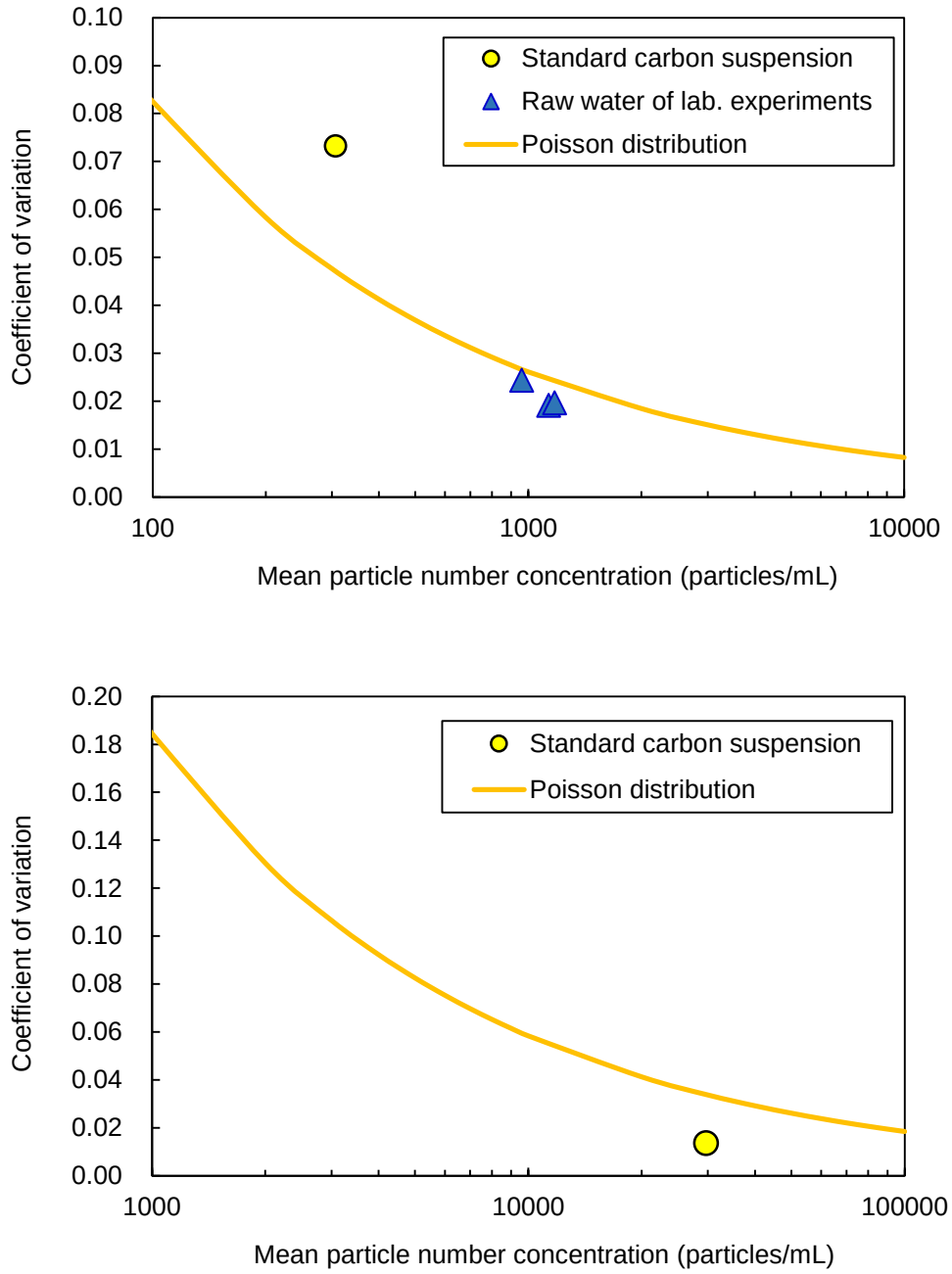

Fig. 2-12. Particle number concentration mean versus coefficient of variation. Filtration volume, 500 mL and 10 mL/filter for the upper and lower panel, respectively. The lines were calculated by using equation (4), which was derived from the Poisson distribution.

Fig. 2-13. Photograph of the sintered glass in the filter holder.

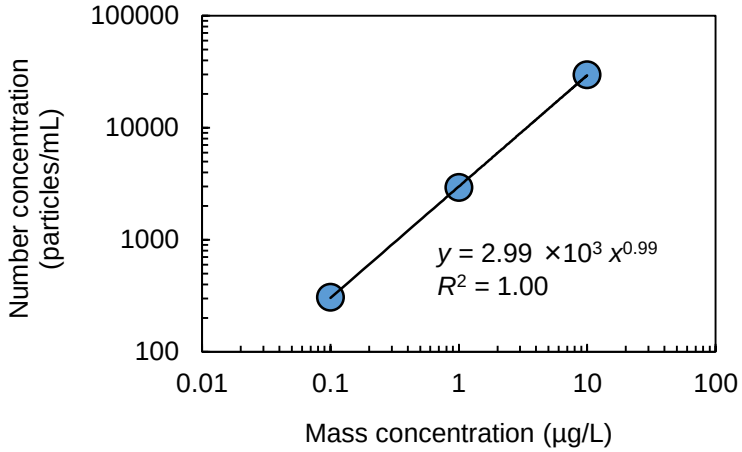

Fig. 2-14. Number concentration, as obtained by membrane-filtration and microscopic image analysis, versus mass concentration for the three $SPAC_{S1}$ standard suspensions. Error bars are hidden in the plot.

Fig. 2-15 compares the volume-based particle size distributions of the standard carbon suspensions obtained by using the membrane-filtration and microscopic-image-analysis method with those obtained by using the laser light diffraction and scattering method. The median diameter obtained by the method was in agreement with that by the laser light diffraction and scattering method. However, the ranges of the particle size distributions were not in good agreement. The poor agreement in particle size distribution could be due to the error generated

when a number distribution of a wide distribution was converted into a volume distribution (Terence 2013). The established method measures number distribution so that it could not be accurate for large particles, which influence the volume-based size distributions to a much greater extent than small particles, because they are small in number. On the other hand, the laser light diffraction and scattering method could not be accurate in measuring small particles because smaller particles scatter light with weaker intensity.

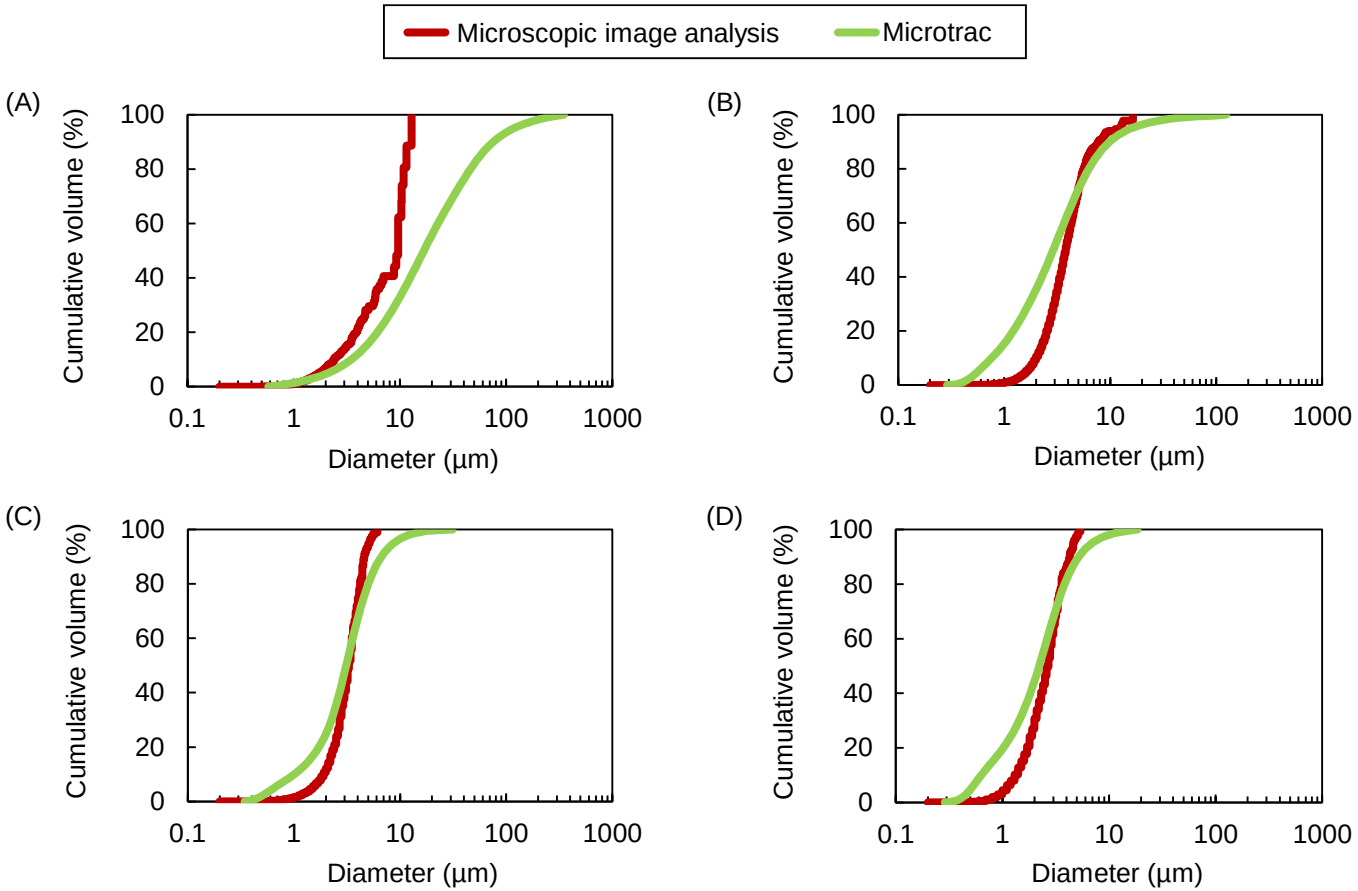

Fig. 2-15. Comparison of volume-based particle size distributions determined by means of the membrane-filtration and microscopic image analysis process and by using a Microtrac MT3300EXII instrument (laser light diffraction and scattering method; MicrotracBEL Corp., Osaka, Japan) without the addition of a dispersant or the use of ultrasonication. Panel A, PAC; panel B, $SPAC_L$; panel C, $SPAC_{S1}$; panel D, $SPAC_{S2}$.

2.3.2 Comparison of SPAC and PAC remaining after treatment

The turbidities, carbon particle number concentrations, and carbon particle volume concentrations for raw waters and sand filtrates are shown in Fig. 2-16 (the turbidities of the supernatants are shown in Fig. 2-17). The raw waters contained 30-mg/L PAC, 30-mg/L $SPAC_{S2}$, or 7.5-mg/L $SPAC_{S2}$. The turbidities of the sand filtrates were all very low (~0.05 NTU); the turbidities were almost the same as the turbidity of Milli-Q water (0.05 NTU). The false turbidity due to stray light in the turbidity measurement is <0.02 NTU, according to the specifications of the turbidity meter. Turbidity measurements could therefore not differentiate carbon particle concentrations in the filtrates of water possibly containing SPAC and PAC. However, clear differences were observed in the particle number and volume concentrations determined via microscopic image analysis of the same filtrates. A comparison of the results for raw waters containing 30 mg/L of carbon particles revealed that the SPAC number concentrations in the sand filtrate were 600–1000 particles/mL, about five times higher than the PAC number concentrations of 100–200 particles/mL. For the raw water, the SPAC number concentrations were one order of magnitude higher than the PAC number concentrations. Therefore, the removal rates in terms of number concentrations were comparable for SPAC and PAC, and that removal rates were roughly 5-log. The volume concentration in sand filtrate was higher for SPAC than for PAC. The removal rate in terms of volume concentrations was around 6-log for SPAC, but it was somewhat lower for PAC.

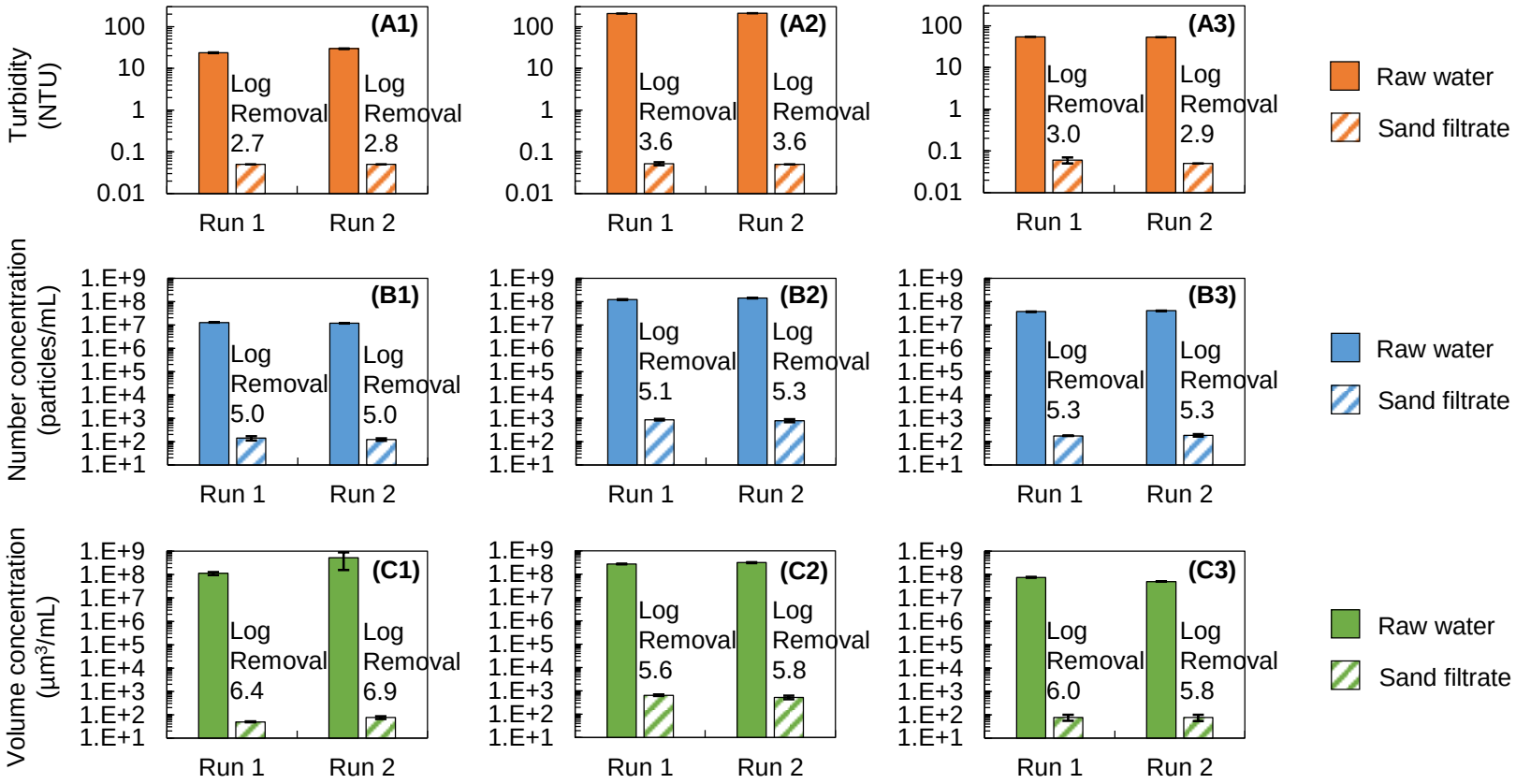

Fig. 2-16. Reduction of carbon particles by the CSF treatment. Panels A1–C1, 30-mg/L PAC; panels A2–C2, 30-mg/L $SPAC_{S2}$; panels A3–C3, 7.5-mg/L $SPAC_{S2}$. Experiments were conducted twice for each experimental condition (Run 1 and Run 2). Error bars indicate standard deviations of measurement for each experiment.

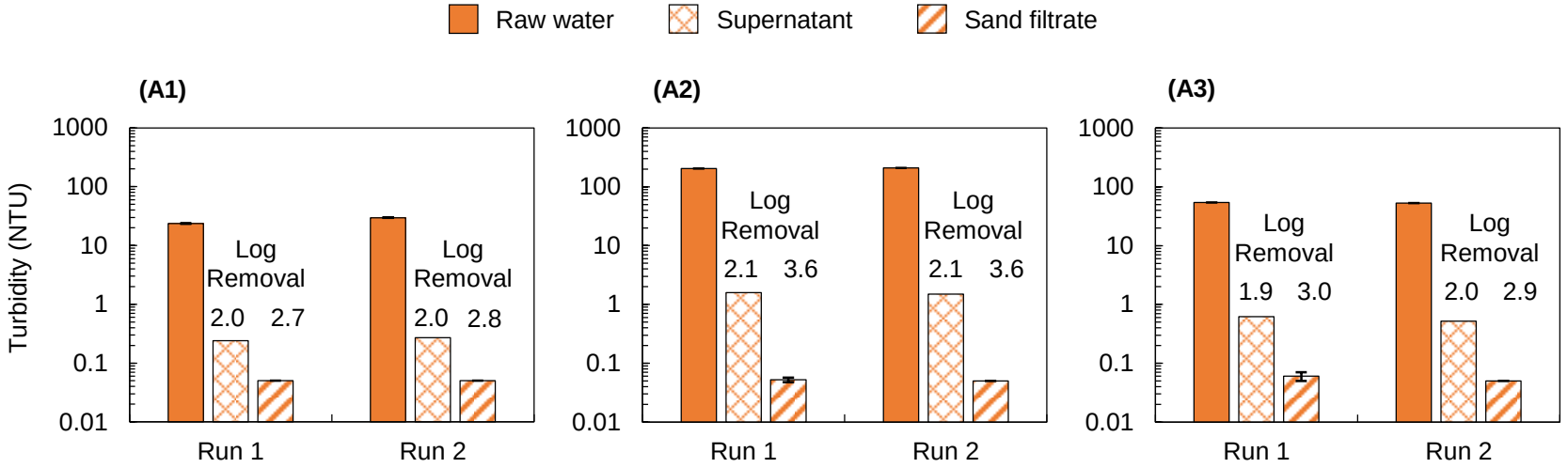

Fig. 2-17. Change of turbidity by coagulation-flocculation, sedimentation, and rapid sand filtration. Panels A1, 30-mg/L PAC; panels A2, 30-mg/L $SPAC_{S2}$; panels A3, 7.5-mg/L $SPAC_{S2}$. Experiments were conducted twice for each experimental condition (Run 1 and Run 2). Error bars indicate standard deviations.

It has been reported that the dose of SPAC is 25% of the PAC dose needed to provide a given adsorptive removal rate of a target compound, such as 2-methylisoborneol (Kanaya *et al.* 2015, Matsui *et al.* 2007, Matsui *et al.* 2005, Matsui *et al.* 2013b). I therefore compared the experimental results obtained for raw waters containing 7.5-mg/L SPAC with those obtained for raw waters containing 30-mg/L PAC. The comparison revealed that the particle number concentrations in the sand filtrates were comparable (100–200 particles/mL). The particle volume concentrations were also comparable (~100 μm^3/mL), although the removal rate in terms of particle volume concentration was lower for SPAC than for PAC. Moreover, the removal rate in terms of particle number concentration was somewhat higher for SPAC than for PAC, but the difference was small (5.3-log for 7.5-mg/L SPAC and 5.0-log for 30-mg/L PAC). In practice, the concentration of carbon particles that pass through a sand filter would therefore be no higher if SPAC were used instead of PAC.

The above-described high removals of SPAC particles were obtained in the experiments that involved use of raw water made from filtered tap water. When the raw water was made from river water, the removal rate of carbon particles was similarly high, 5.3-log (Fig. 2-18). The natural suspended solids and the organic matter contained in the river water before adding SPAC did not substantially affect the removal rate of SPAC particles, but this result could reflect the fact that the concentrations of natural suspended solids and organic matter were low (turbidity 5.7 NTU, dissolved organic carbon 0.9 mg-C/L). For example, 7.5-mg/L SPAC resulted in a turbidity of 54 NTU.

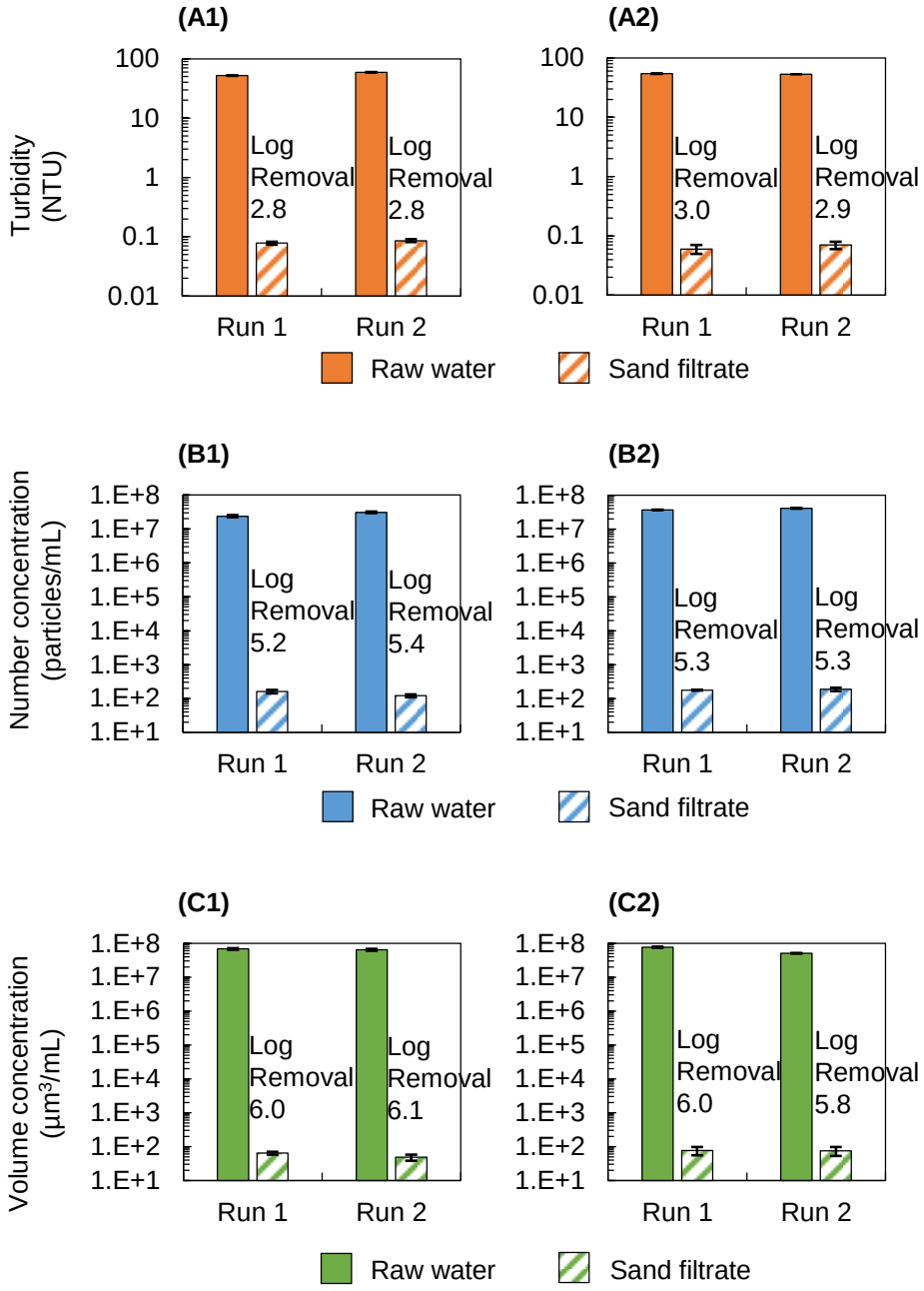

Fig. 2-18. Reduction of carbon particles by the CSF treatment. Panels A1–C1, river water (turbidity 5.7 NTU and DOC 0.9 mg/L) supplemented with $SPAC_{S2}$ at 7.5 mg/L; panels A2–C2, filtered tap water (turbidity < 0.07 NTU and DOC 0.5 mg/L) supplemented with $SPAC_{S2}$ at 7.5 mg/L. Experiments were conducted twice for each experimental condition (Run 1 and Run 2). Error bars indicate standard deviations of measurement for each experiment.

If the principal mechanism responsible for carbon particle removal via coagulation is charge neutralization (Edzwald 2011), the coagulant dosage required to remove all of the carbon particles is determined by the total external surface area of the carbon particles (Dentel 1988, Stumm and O'Melia 1968). The

total external surface area of 7.5-mg/L SPAC was similar to that of 30-mg/L PAC (Table 2-2). The similarity of the particle number concentrations in raw waters treated with 7.5-mg/L SPAC and 30-mg/L PAC may be due to the similarity of the total external surface areas. However, further studies are needed to better understand the effect of carbon particle size on the carbon particle concentrations in the treated water.

Table 2-2. External surface area concentration.

Activated carbon	Mass concentration (mg/L)	External surface area concentration (cm^2/L)	
		Microscopic image analysis	Microtrac
PAC	30	1.4×10^3	2.5×10^2
$SPAC_{S2}$	7.5	2.0×10^3	3.3×10^2
$SPAC_{S2}$	30	7.9×10^3	1.3×10^3

2.3.3 Characteristics of carbon particles remaining in the sand filtrate

Fig. 2-19 shows the particle size distributions of carbon particles in raw water and sand filtrate. Compared to the raw water, the particle size distribution of SPAC in the sand filtrate was shifted toward smaller particles, an indication that smaller particles were less efficiently removed by CSF and therefore tended to pass through the filter. This tendency was more apparent for PAC. This tendency is also consistent with the observation that more SPAC than PAC remained in the sand filtrate when the raw waters with the same mass concentration of SPAC and PAC were treated, as described in Section 2.3.2 (Fig. 2-16). Because particles of smaller size tended to be less efficiently removed, the particle size distributions of PAC and SPAC in the sand filtrate would eventually become similar.

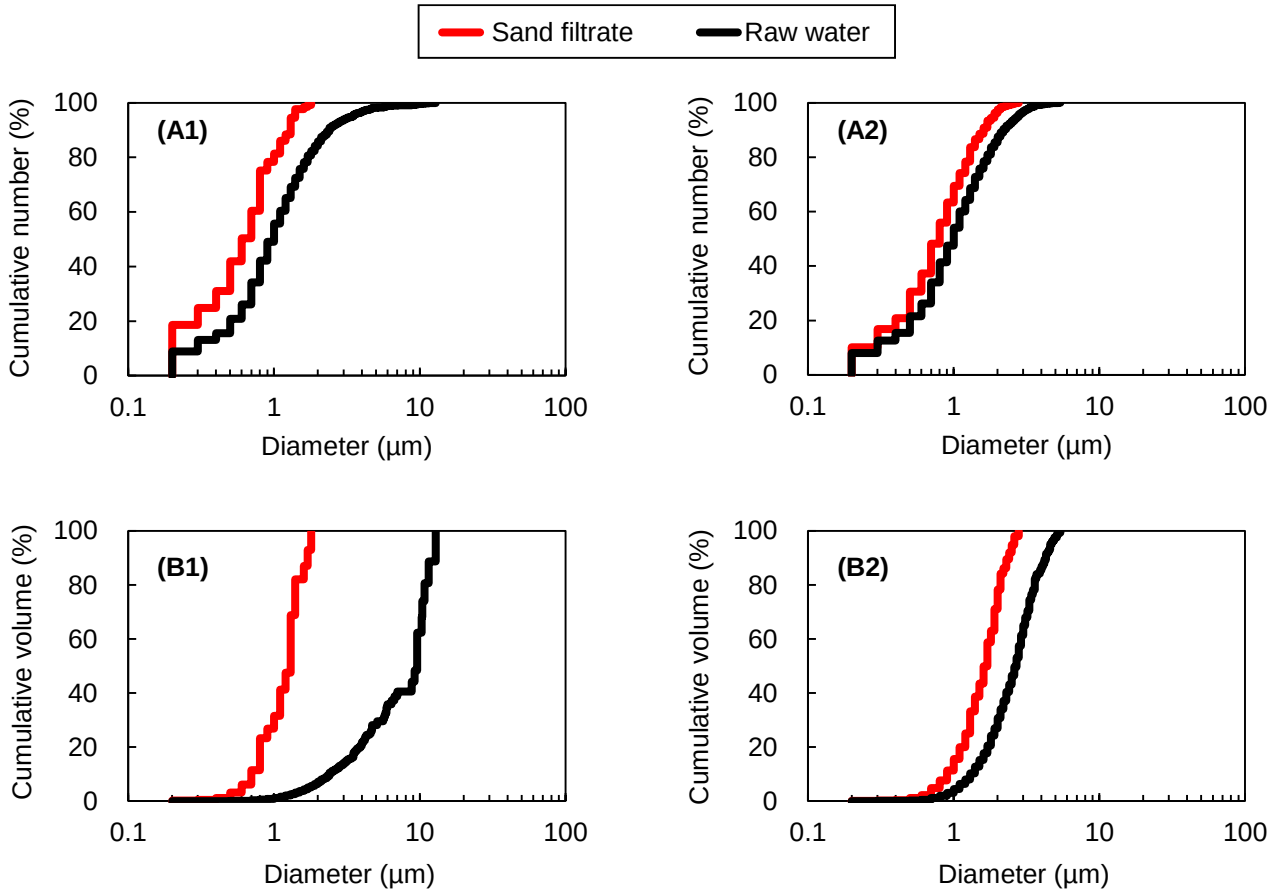

Fig. 2-19. Particle size distributions before and after treatment. Panels A1 and B1, 30-mg/L PAC (Run 1); panels A2 and B2, 30-mg/L $SPAC_{S2}$ (Run 1). Particle size distributions were obtained by means of membrane-filtration and microscopic image analysis.

Turbidity is quantified based on the amount of light scattered by particles. Specific turbidity (turbidity normalized to volume concentration) is inversely proportional to the average particle diameter calculated from the ratio of the volume to the surface area of particles with diameters larger than the wavelength of light (Kissa 1999). The implication is that turbidity is proportional to particle concentration quantified by external surface area (external surface area concentration), which is the total external surface area of the particles divided by the volume of the suspension. For standard suspensions of PAC and SPAC, turbidities were well correlated with external surface area concentrations (Fig. 2-20). The external surface area concentration of the carbon particles remaining in the sand filtrate was calculated from the data obtained for the carbon particles remaining in the sand filtrate by using the membrane-filtration and microscopic-image-analysis method. When the turbidity resulting from the carbon particles remaining in the sand filtrate was estimated from the regression equation (Fig. 2-20) and the calculated external surface area concentration, the turbidity ranged from 2×10^{-5} to 3×10^{-4} NTU (Table 2-3). These values were much smaller than the turbidities actually observed for the sand filtrates (~0.05 NTU, Fig. 2-16). It is therefore reasonable that turbidity measurement could not differentiate carbon particle concentrations in sand filtrates, as described in Section 2.3.2.

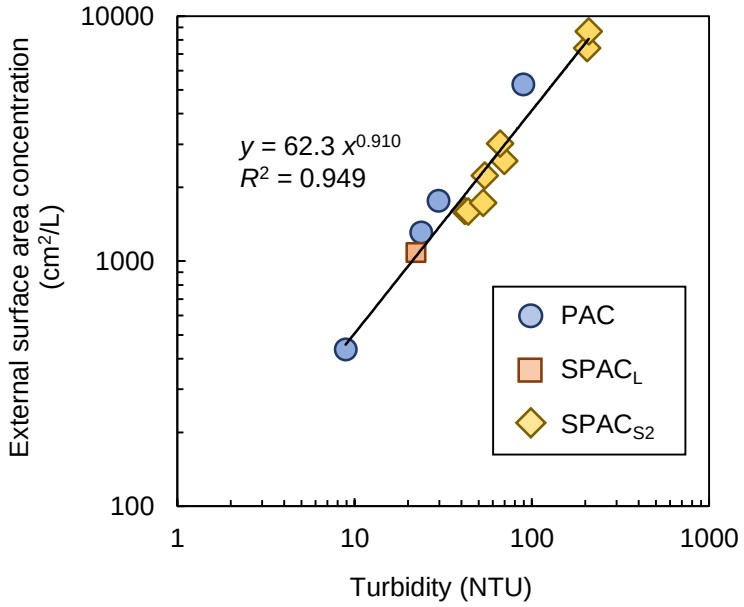

Fig. 2-20. External surface area concentration, as obtained by membrane-filtration and microscopic image analysis, versus turbidity. Standard suspensions of PAC (10, 30, and 80 mg/L), $SPAC_L$ (10 mg/L), and $SPAC_{S2}$ (6.0, 7.5, 10, and 30 mg/L).

Table 2-3. Estimation of turbidity arising from carbon particles remaining in the sand filtrate.

Raw water			**Sand filtrate**			
Activated carbon	**Mass concentration**	**Turbidity**	**Turbidity**	**Number concentration of carbon particles**	**External surface area concentration of carbon particles**	**Turbidity attributable to carbon particles**
		Turbidity meter	**Turbidity meter**	**Microscopic image analysis**	**Microscopic image analysis**	**Estimation from external surface area concentration**
	mg/L	**NTU**	**NTU**	**mL^{-1}**	**cm^2/L**	**NTU**
PAC	30	27	0.05	1.3×10^{2}	3.1×10^{-3}	1.9×10^{-5}
$SPAC_{S2}$	7.5	54	0.06	1.8×10^{2}	3.9×10^{-3}	2.4×10^{-5}
$SPAC_{S2}$	30	207	0.05	8.3×10^{2}	2.5×10^{-2}	1.9×10^{-4}

2.3.4 Mechanisms for lower removal rate of smaller carbon particles

The main mechanism underlying rapid sand filtration is interception. When particles follow streamlines which lie very close to the surface of sand grains, the particles contact the surface of a sand grain and are captured. The probability of particles coming into contact with sand grains decreases as particle size decreases (Ives 1973). According to orthokinetic aggregation theory, particle–particle collisions during flocculation occur less frequently as particles become smaller (Ives 1978). Therefore, the lower removal efficiency of small carbon particles during CSF can be explained by the interception and orthokinetic aggregation mechanisms.

To determine whether the lower removal efficiency of small carbon particles was due solely to interception and orthokinetic aggregation or was related to other characteristics of the carbon, a further investigation was conducted. Even if carbon particles are transported to the surface of the sand grain, they are not captured if there are strong electrokinetic repulsive forces between the sand grains and the carbon particles. Particle–particle collisions do not result in aggregation if significant repulsion exists. I therefore examined the zeta potential of the carbon particles, a commonly used index of the electrokinetic potential in colloidal dispersions or aggregations that is correlated with coagulation and filtration performance. Fig. 2-21 shows the zeta potential of carbon particles in raw water, water sampled after coagulation, supernatant after sedimentation, and sand filtrate. The zeta potential of the carbon particles in the raw water was approximately −23 mV, but it increased to −4 − 8 mV after coagulation, an indication that the charge on the carbon particles had been almost fully neutralized during the coagulation process. However, the particles remaining in the supernatant had a more negative charge (−9 − 5mV) than the particles after

coagulation. The particles in the sand filtrate, which were smaller in size than the particles before CSF, had a more negative charge (−15 − 5mV) than those in the supernatant.

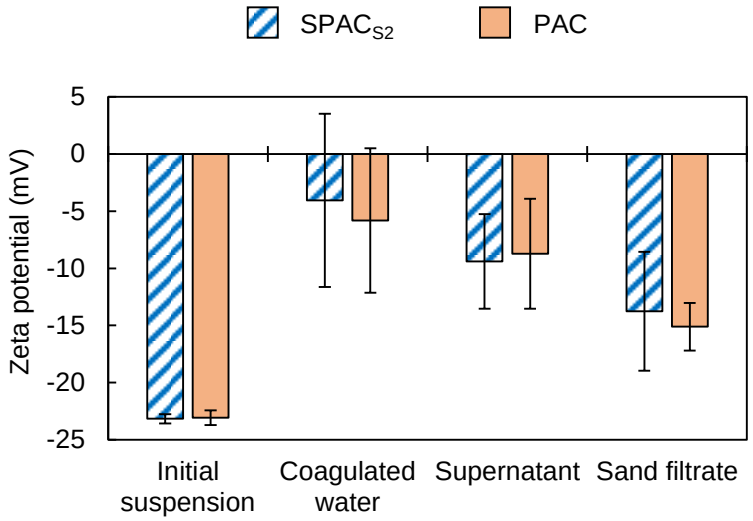

Fig. 2-21. Changes in the zeta potential of PAC and SPAC$_{S2}$ during coagulation-flocculation, sedimentation, and rapid sand filtration. The carbon particle concentration of the initial suspension was 30 mg/L. Error bars indicate standard deviations.

The zeta potentials of the untreated SPAC and PAC particles did not vary as a function of particle size. Fig. 2-22 shows the zeta potential of the carbon particles as a function of carbon particle size. SPAC and PAC were separated by particle size based on the differences in the settling velocities of the particles. The original SPAC and PAC particles had a similar zeta potential of −20 to −25 mV. The negative charge was slightly higher for particles with a diameter of 3 μm, and it then decreased with decreasing particle size, although the decrease was small. The reason for this small change in charge is unclear; however, the data indicate that the smaller carbon particles were not intrinsically more negatively charged than the larger carbon particles, and the surface charges were not very different between the large and small carbon particles. However, the small carbon particles that remained in the sand filtrate had a more negative charge than the carbon particles after coagulation. Therefore, small carbon particles were charge-neutralized and destabilized at a lower rate than large carbon particles during the

coagulation process. A possible explanation for the weak neutralization of the small particles during the coagulation process is that the adsorption of aluminum hydroxide species onto particles is a transport-limited process that depends on the particle size, and the rate of adsorption onto small particles is low (Elimelech *et al.* 1995, Gregory 1988). Finally, I conclude that the low destabilization rate during the coagulation process, the low frequency of particle–particle collisions during flocculation, and the low probability of the particles coming into contact with sand grains during the sand filtration process could collectively make it difficult for small carbon particles to be captured during filtration, the result being that small carbon particles tended to remain in the sand filtrate.

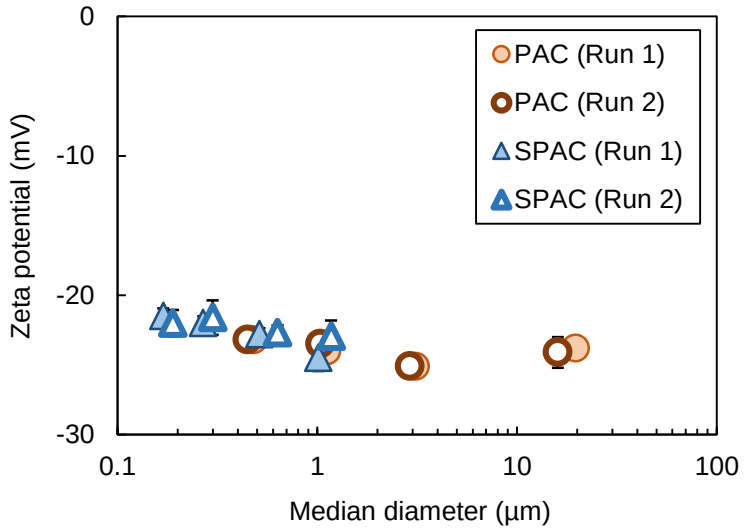

Fig. 2-22. Zeta potential and median diameter of carbon particles remaining after sedimentation (PAC) or centrifugation ($SPAC_{S2}$). Error bars indicate standard deviations.

2.4 Summary

I developed a method to detect and measure the number of carbon particles remaining in sand filtrate. The method used membrane filtration, digital microscopy, and image analysis. I used this method to identify carbon particles

with diameters > 0.2 μm at a concentration as low as 0.1 μg/L. By using this method, I was able to determine the trace concentration of residual carbon particles in sand filtrates, concentrations below the limit of detection by turbidity measurements.

The residual concentration of SPAC was similar to that of PAC when the SPAC was used at 25% of the PAC mass concentration, a percentage that resulted in comparable adsorption of dissolved organic contaminants by SPAC and PAC (SPAC mass dose is 25% of the PAC mass dose, but the SPAC enables comparable adsorptive removal to PAC). This result suggests that when SPAC is used instead of PAC, the risk that some activated carbon particles may pass through the CSF process and remain in the treated water would not substantially increase. The number concentrations in the sand filtrate were 100–200 particles/mL when 7.5 mg/L SPAC and 30 mg/L PAC were treated. Reductions of approximately 5-log in terms of particle number concentrations and 6-log in terms of particle volume concentrations were attained via CSF.

Carbon particles remaining after CSF treatment were smaller in size than were the carbon particles before treatment. The small carbon particles remaining after CSF treatment had a more negative charge than the carbon particles after coagulation treatment. The tendency of smaller particles to appear in the sand filtrate was therefore related to their lower destabilization rate during the coagulation process as well as their lower collision rates in the flocculation and filtration processes.

2.5 References

Amaral, P., Partlan, E., Li, M., Lapolli, F., Mefford, O.T., Karanfil, T. and Ladner, D.A. (2016) Superfine powdered activated carbon (S-PAC) coatings on microfiltration membranes: Effects of milling time on contaminant removal and flux. Water Research 100, 429-438.

Ando, N., Matsui, Y., Kurotobi, R., Nakano, Y., Matsushita, T. and Ohno, K. (2010) Comparison of natural organic matter adsorption capacities of super-powdered activated carbon and powdered activated Carbon. Water Res 44(14), 4127-4136.

Ando, N., Matsui, Y., Matsushita, T. and Ohno, K. (2011) Direct observation of solid-phase adsorbate concentration profile in powdered activated carbon particle to elucidate mechanism of high adsorption capacity on super-powdered activated carbon. Water Research 45(2), 761-767.

Apul, O.G., Hoogesteijn von Reitzenstein, N., Schoepf, J., Ladner, D., Hristovski, K.D. and Westerhoff, P. (2017) Superfine powdered activated carbon incorporated into electrospun polystyrene fibers preserve adsorption capacity. Science of The Total Environment 592, 458-464.

Ateia, M., Erdem, C.U., Ersan, M.S., Ceccato, M. and Karanfil, T. (2019) Selective removal of bromide and iodide from natural waters using a novel AgCl-SPAC composite at environmentally relevant conditions. Water Research 156, 168-178.

Bonvin, F., Jost, L., Randin, L., Bonvin, E. and Kohn, T. (2016) Super-fine powdered activated carbon (SPAC) for efficient removal of micropollutants from wastewater treatment plant effluent. Water Research 90, 90-99.

Carns, K.E. and Stinson, K.B. (1978) Controlling Organics: The East Bay Municipal Utility District Experience. Journal (American Water Works Association) 70(11), 637-644.

Decrey, L., Bonvin, F., Bonvin, C., Bonvin, E. and Kohn, T. (2020) Removal of trace organic contaminants from wastewater by superfine powdered activated carbon (SPAC) is neither affected by SPAC dispersal nor coagulation. Water Research 185, 116302.

Dentel, S.K. (1988) Application of the precipitation-charge neutralization model of coagulation. Environmental Science & Technology 22(7), 825-832.

Dunn, S.E. and Knappe, D.R.U. (2019) DBP Precursor and Micropollutant Removal by Powdered Activated Carbon.

Edzwald, J.K. (2011) WATER QUALITY & TREATMENT A Handbook on Drinking Water, American Water Works Association, American Society of Civil Engineers, McGraw-Hill.

Elimelech, M., Gregory, J., Jia, X. and Williams, R.A. (1995) Particle Deposition & Aggregation. Elimelech, M., Gregory, J., Jia, X. and Williams, R.A. (eds), pp. xiii-xv, Butterworth-Heinemann, Woburn.

Gifford, J.S., George, D.B. and Adams, V.D. (1989) Synergistic effects of potassium permanganate and PAC in direct filtration systems for THM precursor removal. Water Research 23(10), 1305-1312.

Gregory, J. (1988) Polymer adsorption and flocculation in sheared suspensions. Colloids and Surfaces 31, 231-253.

Ives, K.J. (1973) The scientific basis of filtration : proceedings of the NATO Advanced Study Institute, Leyden, Noordhoff, Cambridge, U.K.

Ives, K.J. (1978) The Scientific Basis of Flocculation, Springer Netherlands.

Jiang, W., Xiao, F., Wang, D.S., Wang, Z.C. and Cai, Y.H. (2015) Removal of emerging contaminants by pre-mixed PACl and carbonaceous materials. RSC Advances 5(45), 35461-35468.

Kanaya, S., Kawase, Y., Mima, S., Sugiura, K., Murase, K. and Yonekawa, H. (2015) Drinking Water Treatment Using Superfine PAC (SPAC): Design and Successful Operation History in Full-scale Plant, pp. 624-631, Salt Lake City, Utah, USA.

Kissa, E. (1999) Dispersions

Characterization, Testing, and Measurement, Taylor & Francis, New York.

Lee, B.-B., Choo, K.-H., Chang, D. and Choi, S.-J. (2009) Optimizing the coagulant dose to control membrane fouling in combined coagulation/ultrafiltration systems for textile wastewater reclamation. Chemical Engineering Journal 155(1), 101-107.

Matsui, Y., Aizawa, T., Kanda, F., Nigorikawa, N., Mima, S. and Kawase, Y. (2007) Adsorptive removal of geosmin by ceramic membrane filtration with super-powdered activated carbon. Journal of Water Supply: Research and Technology-Aqua 56(6-7), 411-418.

Matsui, Y., Murase, R., Sanogawa, T., Aoki, N., Mima, S., Inoue, T. and Matsushita, T. (2005) Rapid adsorption pretreatment with submicrometre powdered activated carbon particles before microfiltration. Water Science and Technology 51(6-7), 249-256.

Matsui, Y., Nakao, S., Sakamoto, A., Taniguchi, T., Pan, L., Matsushita, T. and Shirasaki, N. (2015) Adsorption capacities of activated carbons for geosmin and 2-methylisoborneol vary with activated carbon particle size: Effects of adsorbent and adsorbate characteristics. Water Res 85, 95-102.

Matsui, Y., Nakao, S., Taniguchi, T. and Matsushita, T. (2013a) Geosmin and 2-methylisoborneol removal using superfine powdered activated carbon: shell adsorption and branched-pore kinetic model analysis and optimal particle size. Water Research 47(8), 2873-2880.

Matsui, Y., Nakao, S., Taniguchi, T. and Matsushita, T. (2013b) Geosmin and 2-methylisoborneol removal using superfine powdered activated carbon: Shell adsorption and

branched-pore kinetic model analysis and optimal particle size. Water Research 47(8), 2873-2880.

Matsui, Y., Yoshida, T., Nakao, S., Knappe, D.R. and Matsushita, T. (2012) Characteristics of competitive adsorption between 2-methylisoborneol and natural organic matter on superfine and conventionally sized powdered activated carbons. Water Res 46(15), 4741-4749.

Murray, C.C., Vatankhah, H., McDonough, C.A., Nickerson, A., Hedtke, T.T., Cath, T.Y., Higgins, C.P. and Bellona, C.L. (2019) Removal of per- and polyfluoroalkyl substances using super-fine powder activated carbon and ceramic membrane filtration. Journal of Hazardous Materials 366, 160-168.

Pan, L., Nishimura, Y., Takaesu, H., Matsui, Y., Matsushita, T. and Shirasaki, N. (2017) Effects of decreasing activated carbon particle diameter from 30 μm to 140 nm on equilibrium adsorption capacity. Water Res 124, 425-434.

Partlan, E., Ren, Y., Apul, O.G., Ladner, D.A. and Karanfil, T. (2020) Adsorption kinetics of synthetic organic contaminants onto superfine powdered activated carbon. Chemosphere 253, 126628.

Stumm, W. and O'Melia, C.R. (1968) Stoichiometry of Coagulation. Journal AWWA 60(5), 514-539.

Terence, A. (2013) Particle size measurement, Springer US.

Yamaguchi, J., Yamaguchi, D. and Kawase, Y. (2016) Application study of superfine powdered activated carbon in coagulation, sedimentation and filtration (II), pp. 284-285, Kyoto, Japan.

Yu, W.-z., Qu, J.-h. and Gregory, J. (2015) Pre-coagulation on the submerged membrane fouling in nano-scale: Effect of sedimentation process. Chemical Engineering Journal 262, 676-682.

3 REDUCTION OF SUPERFINE ACTIVATED-CARBON PARTICLES IN SAND FILTRATE

3.1 Introduction

If coagulation and flocculation are performed well, there should be few residual particles in the treated water. Plenty of studies have been conducted for the effect of coagulants and coagulation conditions on floc formation and turbidly removal (Edzwald 2011). Several studies have focused on particle charge neutralization, the size and growth of floc particles, settling velocity, permeability, carbon particles as a ballasting agent for settling, nuclei for coagulation, or a pretreatment agent of coagulation-hindering compounds, and the reduction of turbidity after sedimentation and filtration with respect to the use of PAC (Aguilar *et al.* 2003, Matsui *et al.* 2009, Younker and Walsh 2016). However, few studies have focused on the particles remaining in treated water after sedimentation and filtration (Carns and Stinson 1978, Gifford *et al.* 1989).

Accordingly, this chapter aims to find better coagulation conditions and find a better coagulant for the removal of SPAC. In this context, mixing operation conditions including mixing intensity, mixing time, and reactor configuration are examined. The effects of coagulant type and coagulant dose on the removal of SPAC are also examined.

This chapter has been already published by Elsevier, and the information is described as follows:

Title: Minimizing residual black particles in sand filtrate when applying super-fine powdered activated carbon: Coagulants and coagulation conditions

Author: Nakazawa, Y.; Matsui, Y.; Hanamura, Y.; Shinno, K.; Shirasaki, N.; Matsushita, T.

Name of journal: Water Research

Year: 2018

Volume: 147

Pages: 311-320

DOI: https://doi.org/10.1016/j.watres.2018.10.008

3.2 Materials and Methods

3.2.1 Activated carbon particles

A commercially available wood-based PAC (Taiko W; Futamura Chemical Co., Ltd., Nagoya, Japan) was prepared as a slurry in pure water (Milli-Q water; Merck KGaA, Darmstadt, Germany) at a concentration of ~15% (w/w). The PAC in the slurry were milled in a closed-chamber ball mill (Nikkato, Osaka, Japan) with 5- and 10-mm-diameter Al_2O_3 balls at 45−50 rpm for 4–5 h to afford the particles with D_{95} (the diameter larger than 95% of the entire distribution) < 30 μm (Pan *et al.* 2017). The slurry was taken out from the chamber of the ball mill and then milled with a bead mill (LMZ015; Ashizawa Finetech, Ltd., Chiba,

Japan) with 0.3-mm-diameter ZrO_2 beads at a rotational speed of 8 m/s (2590 rpm) in recirculation mode for 20 min to produce a SPAC slurry (Table 3-1).

Table 3-1. Activated carbon particle size. The median diameters were determined by laser light diffraction and scattering.

Activated carbon		Median diameter (μm)
PAC		13.7
SPAC	$SPAC_1$	0.96
	$SPAC_2$	0.90
	$SPAC_3$	1.02

The true particle size distributions of the carbons were determined using a laser light diffraction and scattering method (Microtrac MT3300EXII; MicrotracBEL Corp., Osaka, Japan), which followed addition of a dispersant (Triton X-100; Kanto Chemical Co., Inc., Tokyo, Japan; final concentration, 0.08% w/v) and ultrasonic dispersion with 150 W for 1 min (Fig. 3-1).

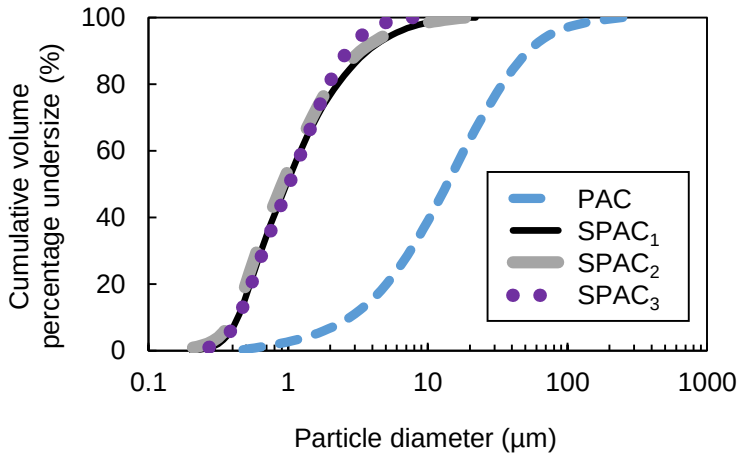

Fig. 3-1. Particle size distributions of PAC, $SPAC_1$, $SPAC_2$, and $SPAC_3$.

3.2.2 Coagulants

Twenty-three kinds of PACls were used as coagulants in the present study. Among them, PACl-70 (basicity 2.1; the number, 70, in the name indicates the % basicity; sulfate ion 2% w/w) and PACl-50 (basicity 1.5, sulfate ion 3% w/w) are

commercial products provided by Taki Chemical Co., Ltd. (Hyogo, Japan), which are produced by dissolving $Al(OH)_3$ into HCl and H_2SO_4 [as described by, e.g., (Sato and Matsuda 2009)]. On the other hand, B70ns, B70s0.11, B70s0.12, B70s0.13, B70s0.14, B70s0.15, and B70s0.17 (the numbers after "B" and "s" represent the "% basicity" and "mole ratio of sulfate ion to aluminum: SO_4/Al" respectively, and "ns" stands for "non-sulfated") were produced in the authors' laboratory by the following method named $Al(OH)_3$-dissolution.

Predetermined amounts of $AlCl_3 \cdot 6H_2O$ (FUJIFILM Wako Pure Chemical Corporation, Osaka, Japan) and $Al_2(SO_4)_3 \cdot 14\sim18H_2O$ (FUJIFILM Wako Pure Chemical Corporation) were dissolved into pure water (Milli-Q water) to get aluminum aqueous solution. This solution was mixed with $Al(OH)_3$ powder (FUJIFILM Wako Pure Chemical Corporation) to form a milk-like slurry and then heated with microwaves (ETHOS TC; Milestone S.r.l., Sorisole (BG), Italy) at 150 °C for 3 h. After that, the slurry was centrifuged by a centrifugal separator (H-9R; Kokusan Co., Ltd., Tokyo, Japan) at a rotation speed of 3,000 rpm (6,000 g) for 10 min at 20 °C, and then the clear top of the liquid was filtered by a membrane filter (pore size 0.45 μm, PTFE; Toyo Roshi Kaisha, Ltd., Tokyo, Japan) to obtain a solution of PACl with basicity of 40~50%. The solution was poured into a beaker, stirred with a rotation speed of >600 rpm, and heated at 50 °C using a hot plate/magnetic stirrer, and then a predetermined amount of aqueous solution of sodium carbonate (FUJIFILM Wako Pure Chemical Corporation) was dripped into the solution to adjust the basicity up to 70%. The basicity was calculated by the following formula.

$$Basicity\ (\%) = \frac{[OH^-]}{3[Al_t]} \times 100$$

where $[Al_t]$ is the total aluminum concentration determined by an inductively coupled plasma mass spectrometer (ICPMS, 7700x, Agilent

Technologies, Inc., Santa Clara, CA, USA), [OH^-] is the concentration of hydroxyl groups from the ingredients $Al(OH)_3$ and sodium carbonate. The total mass of OH^- introduced to the final product was calculated by taking a mass balance.

PACls produced by the method named base-titration were used in the CSF experiments described in supplementary experiments. The method is described in Section 7.2.

The distributions of aluminum species in the coagulants were analyzed by the ferron method. On the basis of their reaction rates with ferron reagent (8-hydroxy-7-iodo-5-quinoline sulfonic acid; FUJIFILM Wako Pure Chemical Corporation), the aluminum species were divided into three categories: Ala, Alb, and Alc. Ala denotes aluminum species that reacted with ferron instantaneously (within 30 s). Alb denotes species that reacted with ferron within 120 min. Alc denotes species that did not react with ferron. These species were assumed to be monomeric, polymeric, and colloidal aluminum species, respectively (Wang *et al.* 2004). Ferron analyses of the PACls were conducted immediately after dilution with Milli-Q water to 2.7 g-Al/L (0.1 mol-Al/L) (Jia *et al.* 2004, Wang et al. 2004). Dilution reportedly has little effect on the ferron speciation distribution of PACl (Kimura *et al.* 2013, Wang *et al.* 2002).

3.2.3 Batch-reactor tests of coagulation–flocculation, sedimentation, and rapid sand filtration

Tap water in Sapporo city was filtered through a membrane filter (nominal pore diameter, 0.1 μm; Toyo Roshi Kaisha, Ltd.) to remove suspended matter, and then the water was adjusted for M alkalinity to 30 mg/L as $CaCO_3$ by adding $NaHCO_3$ (FUJIFILM Wako Pure Chemical Corporation). The water was supplemented with an activated carbon slurry to make a raw water for CSF

experiments: activated carbon concentrations were 30 mg/L for PAC; 6 mg/L, 7.5 mg/L, 10 mg/L, or 30 mg/L for SPAC. Most CSF experiments were conducted with these waters, but some CSF experiments were additionally conducted with water from the Toyohira River (Sapporo, Japan) after supplementing it with SPAC at 10 mg/L. The river water was sampled at the location where it becomes the raw water source for the Moiwa Water Purification Plant (Sapporo).

The experimental setup and procedure were basically the same as those of Nakazawa *et al.* (2018) but are shown in Fig. 3-2. The coagulation–flocculation and sedimentation steps were conducted in a 4-L rectangular beaker. After a predetermined volume of HCl or NaOH (0.1 N) was added to adjust the coagulation pH to 7.0, the coagulant (PACl) was injected into the beaker to a final concentration of 4 mg-Al/L, unless otherwise noted. Then the water was mixed rapidly followed by slow mixing with a three-stage mixing intensity. The mixing intensities (G value: velocity gradient, see Section 7.1 for the G value calculation) and times (T value: mixing time) of the flash (indicated by subscript F) and slow mixing (indicated by subscript S, with the order: 1, 2, and 3) were varied depending on each experiment, and these values are described in each case in the Results and Discussion section (see also Table 3-2). The water was then left at rest for 1 h. Next, the top three liters of the water (supernatant) were transferred to another beaker for determination of the turbidity (2100Q portable turbidimeter; Hach Company, Loveland, CO, USA) and for rapid sand filtration. Sand filtration was conducted for 40 min at a rate of 90 m d^{-1} in the down-flow direction using a column (Φ4 cm) filled to a depth of 50 cm with sand (effective diameter, 0.6 mm; uniformity, 1.3; Nihon Genryo Co., Ltd., Japan). The sand filtrate was collected from 13 to 40 min after the start of filtration, and the turbidity and carbon particle count of the filtrate were determined. After each filtration run, the sand filter was backwashed with tap water, then washed forward with pure water (Milli-Q water) and membrane-filtered tap water.

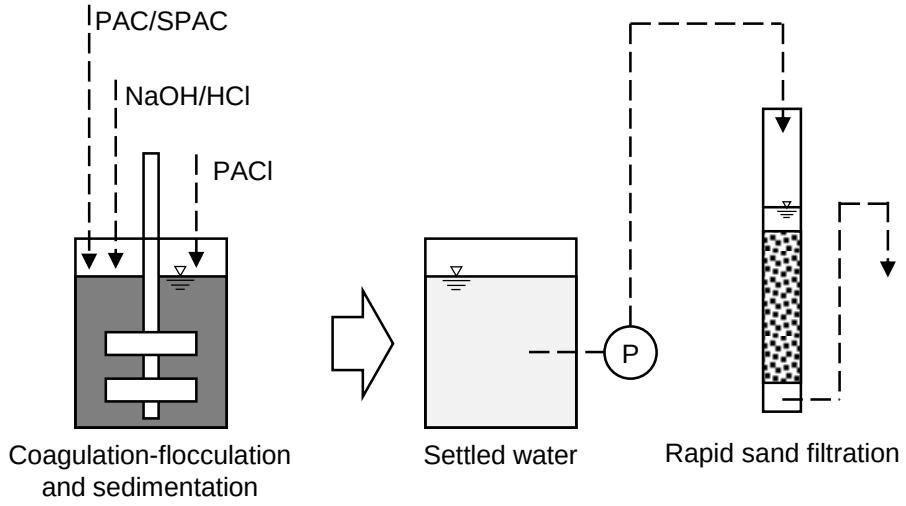

Fig. 3-2. Schematic diagram of the experimental setup for the coagulation-flocculation, sedimentation, and sand filtration experiment.

Table 3-2. The experimental conditions of coagulation in CSF experiments.

	Coagulant		Flash mixing						Slow mixing								Flash + slow mixing
	Name	Dosage (mg-Al L^{-1})	G_{F1} (s^{-1})	T_{F1} (s)	G_{F2} (s^{-2})	T_{F2} (s)	G_{F3} (s^{-3})	T_{F3} (s)	G_{S1} (s^{-1})	T_{S1} (s)	G_{S2} (s^{-1})	T_{S2} (s)	G_{S3} (s^{-1})	T_{S3} (s)	G_{S4} (s^{-2})	T_{S4} (s)	$G_T T_T$ (dimensionless)
Fig. 3-6	PACl-50 and PACl-70	4	600	20					50	300	20	300	10	600			39,000
Fig. 3-12	PACl-50 and PACl-70	4	600	10					50	150	20	150	10	300			19,500
			600	20					50	300	20	300	10	600			39,000
			600	40					50	600	20	600	10	1,200			78,000
Fig. 3-15	PACl-50 and PACl-70	4	600	10					50	375	20	375	10	675			39,000
			600	20					50	300	20	300	10	600			39,000
			600	40					50	170	20	170	10	320			39,100
Fig. 3-16	PACl-70	4	600	20					50	170	20	170	10	320			27,100
			600	40					50	170	20	170	10	320			39,100
			600	60					50	170	20	170	10	320			51,100
			600	100					50	170	20	170	10	320			75,100
Fig. 3-17	PACl-70	4	150	160					50	170	20	170	10	320			39,100
			300	80					50	170	20	170	10	320			39,100
			600	40					50	170	20	170	10	320			39,100
Fig. 3-18	PACl-70	1.5, 2.25	600	100					12.5	600	12.5	600	12.5	600	12.5	600	90,000
Fig. 3-20	PACl-50 and PACl-70	1.5	600	100					12.5	600	12.5	600	12.5	600	12.5	600	90,000
Fig. 3-23,	PACl-50 and	1.5	600	100					12.5	600	12.5	600	12.5	600	12.5	600	90,000
Fig. 3-24	PACl-70		600	33	600	33	600	33	12.5	600	12.5	600	12.5	600	12.5	600	90,000
Fig. 3-25,	PACl-50 and	1.5	600	100					12.5	2,400							
Fig. 3-26	PACl-70		600	100					12.5	600	12.5	600	12.5	600	12.5	600	90,000
Fig. 3-27	PACl-50 and	1.5	600	100					12.5	600	12.5	600	12.5	600	12.5	600	90,000
	PACl-70		600	33	600	33	600	33	12.5	600	12.5	600	12.5	600	12.5	600	90,000
			600	100					12.5	2,400							
Fig. 3-28	PACl-50 and PACl-70	1.5~8	600	40					50	600	20	600	10	1,200			78,000

	Coagulant		Flash mixing						Slow mixing								Flash + slow mixing
	Name	Dosage (mg-Al L^{-1})	G_{F1} (s^{-1})	T_{F1} (s)	G_{F2} (s^{-2})	T_{F2} (s)	G_{F3} (s^{-3})	T_{F3} (s)	G_{S1} (s^{-1})	T_{S1} (s)	G_{S2} (s^{-1})	T_{S2} (s)	G_{S3} (s^{-1})	T_{S3} (s)	G_{S4} (s^{-2})	T_{S4} (s)	$G_T T_T$ (dimensionless)
Fig. 3-35	PACl-70 and PACls by $Al(OH)_3$ -dissolution	4	600	20					50	300	20	300	10	600			39,000
Fig. 3-36	PACl-70 and B70s0.14	4	600	20					50	170	20	170	10	320			27,100
			600	40					50	170	20	170	10	320			39,100
			600	60					50	170	20	170	10	320			51,100
			600	100					50	170	20	170	10	320			75,100

G and T stand for velocity gradient and mixing time, respectively. Subscripts F, S, and the numbers after S mean flash mixing, slow mixing, and the order of the slow mixing part, respectively.

3.2.4 Flow-through reactor tests of coagulation–flocculation, sedimentation, and rapid sand filtration

A series of flow-through mode CSF tests were performed using a bench-

scale CSF plant comprising five components: preparation unit, rapid mixing unit for coagulation, slow mixing unit for flocculation, sedimentation unit, and sand filter (Fig. 3-3 and Table 3-3). The rapid mixing unit constituted a single-chambered reactor or a 3-chambered-reactor with three equally-sized chambers; the two reactors had the same total hydraulic retention time (HRT) of 100 s. The slow mixing unit constituted a single-chambered reactor or a 4-chambered reactor, both with four mixing impellers and the same total HRT of 2400 s. Regardless of reactor configuration, rapid mixing for coagulation was conducted at a fixed mixing intensity (G value: velocity gradient) of 600 s^{-1} for 100 s, and slow mixing for flocculation was conducted at a fixed G value of 12.5 s^{-1} for 2400 s. Residence time distributions of the reactors were measured via a step tracer test using NaCl as the tracer and conductivity detection (Crittenden *et al.* 2012). To prevent the effects of wind and temperature-induced density current, the bench-scale CSF plant was installed in a constant-temperature room with no wind, and the water temperature was kept at the same as the room temperature.

Toyohira River water, collected at the Moiwa Water Purification Plant, Sapporo, Japan (hereafter ‘River water’), was used as the raw water. Dechlorinated Sapporo municipal water (Municipal waters 1–4; Table 3-4) was also used because only a limited volume of River water was available. Raw water was pumped into the first mixing chamber of the preparation unit, and SPAC was added in the second mixing chamber at a concentration of 2 mg/L (3–5 × 10^6 particles/mL), which is a typical dose when SPAC is used as an adsorbent (Matsui *et al.* 2007). After the addition of NaOH or HCl to adjust the pH to 7.0, a coagulant (PACl) was injected into the coagulation reactor at a dose of 1.5 mg-Al/L, unless otherwise noted; the dose was predetermined to bring the settling turbidity down

to less than 2 NTU. After coagulation–flocculation, the water flowed through a sedimentation reactor, which had a HRT of 65 min. After sedimentation, the supernatant flowed to a sand filter. Sand filtration was conducted at a rate of 90 or 150 m d^{-1} using a 4-cm diameter column filled with sand (effective diameter, 0.94 mm; uniformity, 1.24; Nihon Genryo Co., Ltd., Japan) to a depth of 50 cm.

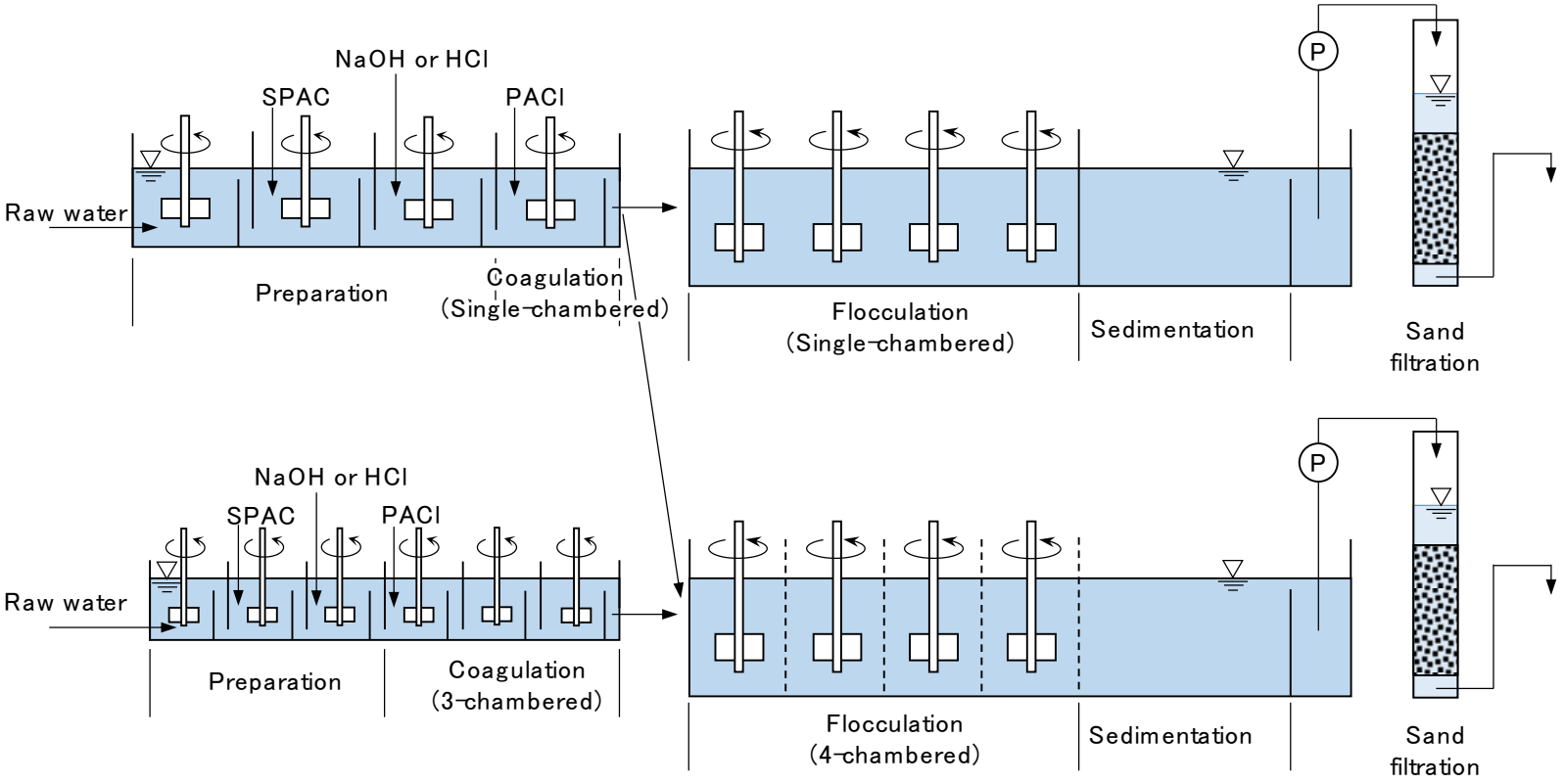

Fig. 3-3. Schematic diagram of the bench-scale CSF plant.

Table 3-3. Specifications of the bench-scale coagulation–flocculation, sedimentation, and rapid sand filtration plant.

Component	Type	Number of chambers	Length × width × height per chamber	Water depth	Volume per chamber	Hydraulic retention time per chamber	G value
			cm	cm	L	s	s^{-1}
Preparation unit	Connected to the single-chambered coagulation reactor	3	9.5 × 9.5 × 15	9.2	0.83	100	600
	Connected to the 3-chambered coagulation reactor	3	6.6 × 6.6 × 12	6.4	0.28	33	600
Coagulation reactor	Single-chambered reactor	1	9.5 × 9.5 × 15	9.2	0.83	100	600
	3-chambered reactor	3	6.6 × 6.6 × 12	6.4	0.28	33	600
Flocculation reactor	Single-chambered reactor	1	56 × 19 × 25	19	20	2400	12.5
	4-chambered reactor	4	14 × 19 × 25	19	5	600	12.5

Component	Length × width × height	Water depth	Volume	Hydraulic retention time	Overflow rate
	cm	cm	L	s	mm min^{-1}
Sedimentation reactor	88 × 19 × 25	19	32	3900	3.0

Component	Outer diameter of column	Inner diameter of column	Length of column	Effective diameter of sand	Uniformity coefficient of sand	Sand depth	Filtration rate
	cm	cm	cm	mm		cm	m d^{-1}
Sand filter	4	3.6	140 or 90	0.94	1.24	50	90 or 150

Table 3-4. Raw waters used in the Flow-through reactor tests.

Raw water	**DOC**	**Alkalinity**	**Na^+**	**K^+**	**Mg^{2+}**	**Ca^{2+}**	**Cl^-**	**NO_3^-**	**SO_4^{2-}**	
	mg/L	**mg/L as $CaCO_3$**	**mg/L**	**mg/L**	**mg/L**	**mg/L**	**mg/L**	**mg/L**	**mg/L**	
River water	0.8	16	12	2.1	1.8	10	21	1.5	20	Fig. 3-18 (a), Fig. 3-19 (a, b)
Municipal water 1	0.6	18	15	2.3	2.4	11	23	0.8	21	Fig. 3-18 (b), Fig. 3-19 (c)
Municipal water 2	no data	16	13	1.7	1.8	9	23	0.9	18	Fig. 3-20, Fig. 3-23, Fig. 3-25, Fig. 3-27
Municipal water 3	0.4	20	11	0.8	3.1	8	14	1.3	19	Fig. 3-24
Municipal water 4	0.5	20	12	1.6	2.4	11	18	1.0	19	Fig. 3-26

3.2.5 Membrane filtration and microscopic image analysis

To sample the carbon particles in the water, the water was filtered through a PTFE membrane filter (nominal pore diameter, 0.1 μm; Φ25 mm; Merck KGaA) supported by a glass filter holder (KG-25; Toyo Roshi Kaisha, Ltd.) (Fig. 3-4). After drying the filter, color digital photomicrographs were captured for nine or eighteen predetermined observation zones (microscope view area, 247×330 μm) per filter (Fig. 3-5) with a digital microscope (VHX-2000; Keyence Corporation, Osaka, Japan) at 1000× magnification. The photomicrographs were analyzed using the image analysis software supplied with the microscope. Details of the analytical procedures are described in Section 2.2.3.

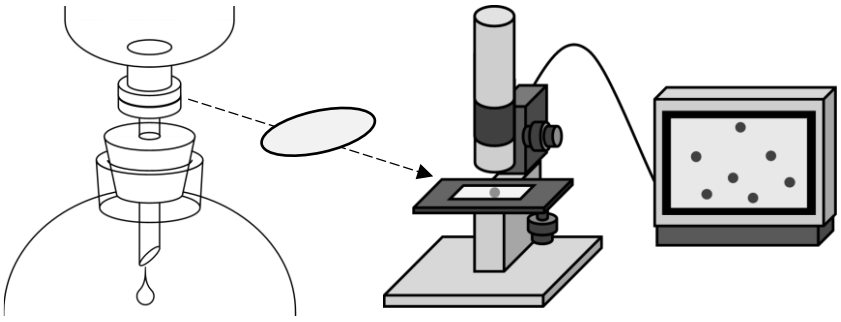

Fig. 3-4. Schematic diagram of the experimental setup for membrane filtration and microscopic image analysis.

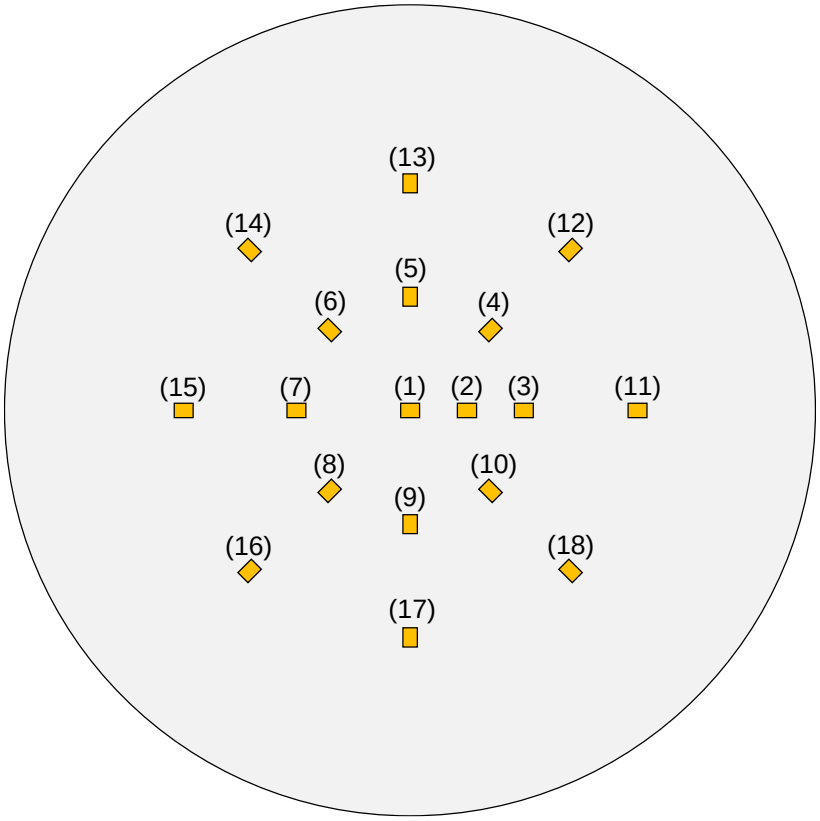

Fig. 3-5. The position of observation zones on a membrane filter. The observation was conducted with 18 zones in the case that the particle number concentration was expected to be lower than 200 particles/mL. In the other case, the observation was conducted with 9 zones (zone numbers 1 and from 3 to 10).

3.3 Results and Discussion

3.3.1 Comparison of commercially-available PACl-50 and PACl-70

Fig. 3-6 shows the number concentrations of residual carbon particles in sand filtrate after CSF when water containing SPAC or PAC of various mass concentrations was coagulated using PACl-70 (a high-basicity PACl) or PACl-50 (a conventional PACl having normal basicity). When PAC at the initial concentration 30 mg/L was treated with PACl-70, the residual concentrations were around 200 particles/mL, and PACl-70 resulted in a slightly higher residual concentration than PACl-50, but the difference was small.

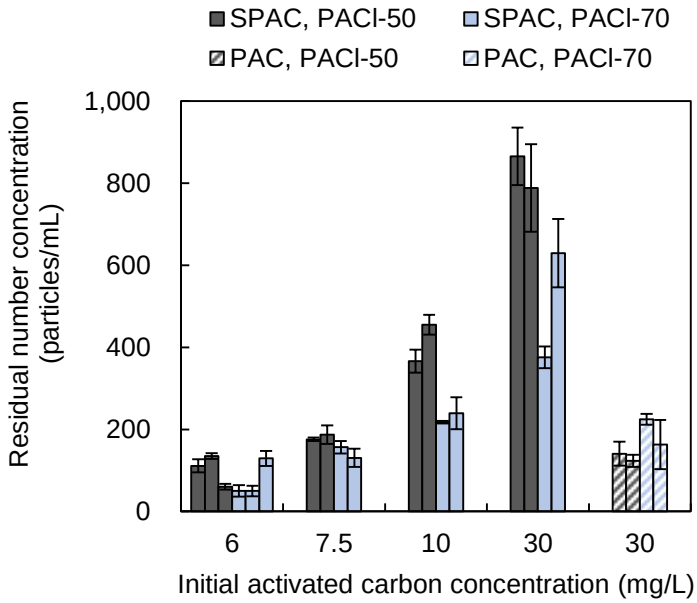

Fig. 3-6. Particle number concentration of residual activated carbon vs. initial activated carbon concentration at a fixed mixing intensity (G_TT_T: 39,000, G_F: 600 s^{-1}, T_F: 20 s; G_{S1}: 50 s^{-1}, T_{S1}: 300 s, G_{S2}: 20 s^{-1}, T_{S2}: 300 s, G_{S3}: 10 s^{-1}, T_{S3}: 600 s). PAC and $SPAC_1$ were used. Error bars indicate standard deviations of measurements.

When SPAC of the same initial concentration (30 mg/L) was treated using conventional PACl-50, the residual concentration was much higher (800 particles/mL). When PACl-70 was used to treat the SPAC, the residual concentration was reduced to 400 particles/mL. The lower the initial concentration of SPAC was, the lower the residual concentration, both for PACl-50 and PACl-70; and at the initial concentration of 7.5 mg/L or less, the difference of residual concentrations between the two cases of using PACl-50 or PACl-70 became smaller. Overall, high-basicity PACl-70 was superior to PACl-50 to remove SPAC. With PACl-70, the removal rates in terms of particle number concentrations depended on the concentration of SPAC: 5.3 log removal was lowest at an SPAC concentration of 10 mg/L. Nevertheless, the removal rates with PACl-70 were slightly higher than with PACl-50 (Fig. 3-7). In contrast, the turbidity of the supernatant after sedimentation following coagulation by PACl-50 was slightly lower than that by PACl-70, and the result was opposite to the residual number concentration mentioned above (Fig. 3-8).

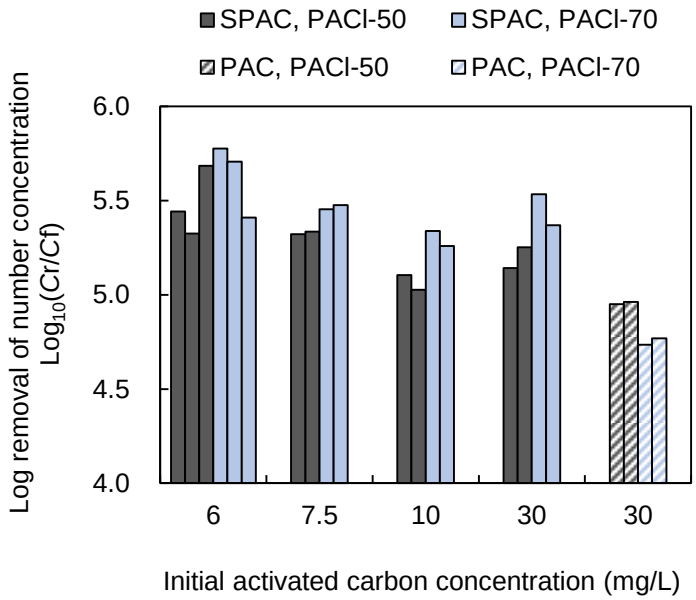

Fig. 3-7. Removal rate in terms of particle number concentration after CSF in the experiments of Fig. 3-6. *C*r and *C*f indicate the particle number concentration of carbon in raw water and sand filtrate, respectively.

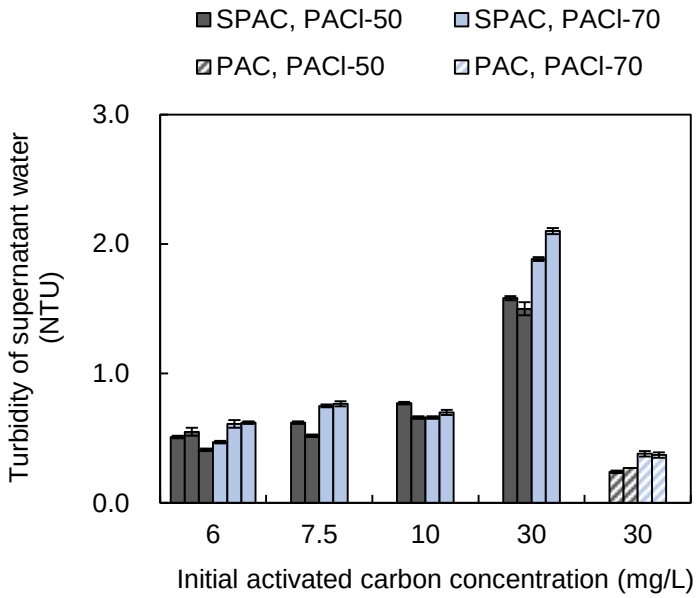

Fig. 3-8. Turbidity of supernatant after coagulation, flocculation, and sedimentation in the experiments of Fig. 3-6. Error bars indicate standard deviations of measurements.

Higher-basicity PACls (e.g. PACl-70) are known to neutralize negative charges more according to the results of colloid titration (Fig. 3-9) (Matsui *et al.* 2017). Accordingly, although PACl-70 is not superior compared with PACl-50 in terms of forming large flocs bringing a lower turbidity of supernatant water, PACl-70 is inferred to neutralize the negative charges of carbon particles

efficiently due to its high capacity in charge neutralization. The high capacity in charge neutralization seemed to contribute to the removal of carbon particles.

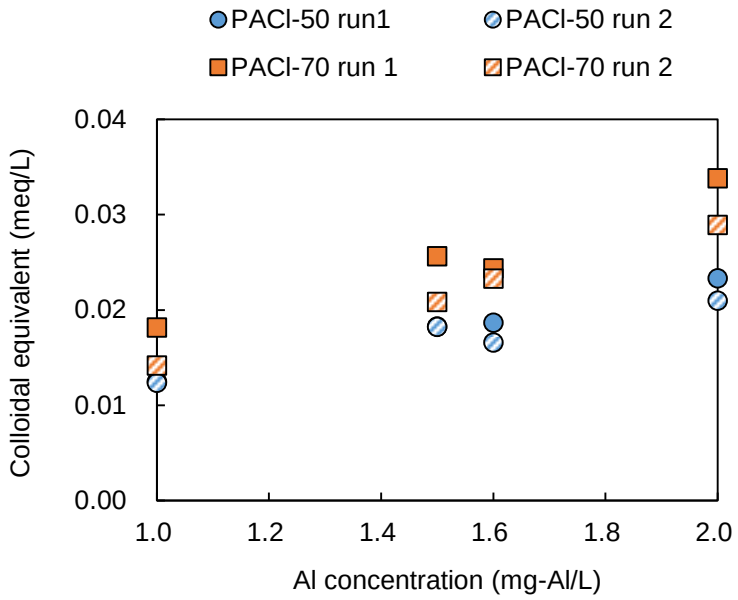

Fig. 3-9. Colloid charge capacity of PACl-50 and PACl-70 (Matsui et al. 2017).

The particles remaining after CSF were smaller in size than the particles before CSF (see Fig. 2-19). Although the tendency of small carbon particles to remain after CSF is overall attributable to their size, the size effect is comprised of the following three reasons: 1) low destabilization rate during the coagulation process, 2) low frequency of particle–particle collisions during flocculation, and 3) low probability of the particles coming into contact with sand grains during the sand filtration process. Therefore, particle destabilization is a key to reduce remaining carbon particles after CSF. When comparing the zeta potentials of residual carbon particles after CSF treatments with PACl-70 and PACl-50, they were not different (Fig. 3-10). Therefore, particles with a certain zeta potential value or lower regardless of PACl-70 or 50 passed through the filter. Accordingly, the merit of PACl-70 in reducing carbon particle concentration after CSF was due to its high capacity to minimize the number of non-neutralized carbon particles (with a certain zeta potential value or lower) rather than due to its high positive charge to neutralize the negative charge of particles to nearly zero level.

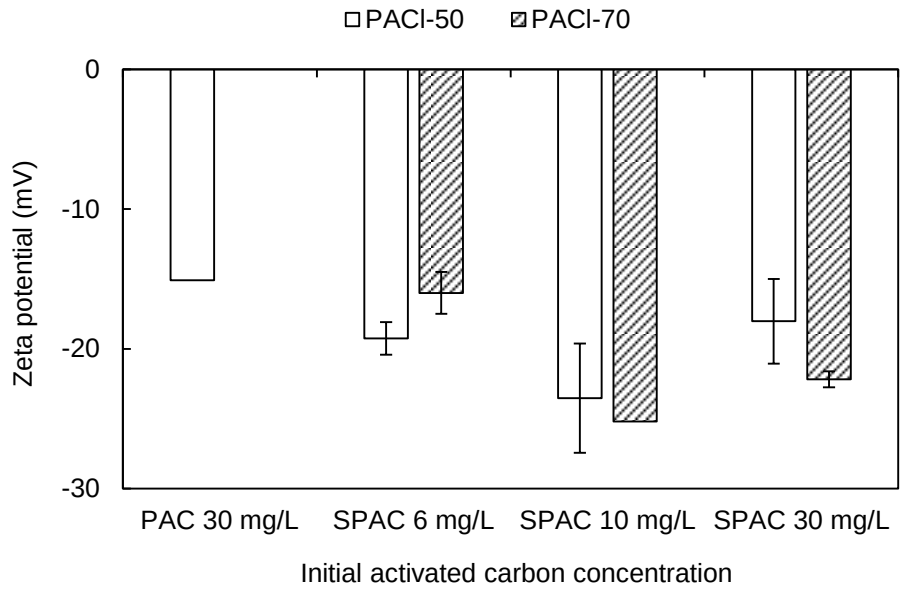

Fig. 3-10. Zeta potentials of residual carbon particles in sand-filtrate vs. initial activated carbon concentration. Experimental conditions were the same as those described for Fig. 3-6. The number of measurements was described as follows: with PACl-70, two measurements for SPAC 6 mg/L and 30 mg/L, and one measurement for SPAC 10 mg/L; with PACl-50, three measurements for SPAC 30 mg/L, two measurements for SPAC 6 mg/L and 10 mg/L, and one measurement for PAC 30 mg/L. Error bars indicate standard deviations of measurements.

When the SPAC suspension was coagulated using PACl-70, the formation of micro floc particles was not confirmed in the photograph taken soon after flash mixing (Fig. 3-11). When the PAC suspension was coagulated with PACl-70, the formation of micro floc particles was confirmed marginally. In contrast, when PACl-50 was used in the coagulation process, the formation of micro floc particles was clearly observed in the experiments of all experimental conditions. However, floc size at the end of slow mixing was not different between each pair of experiments using PACl-50 and PACl-70.

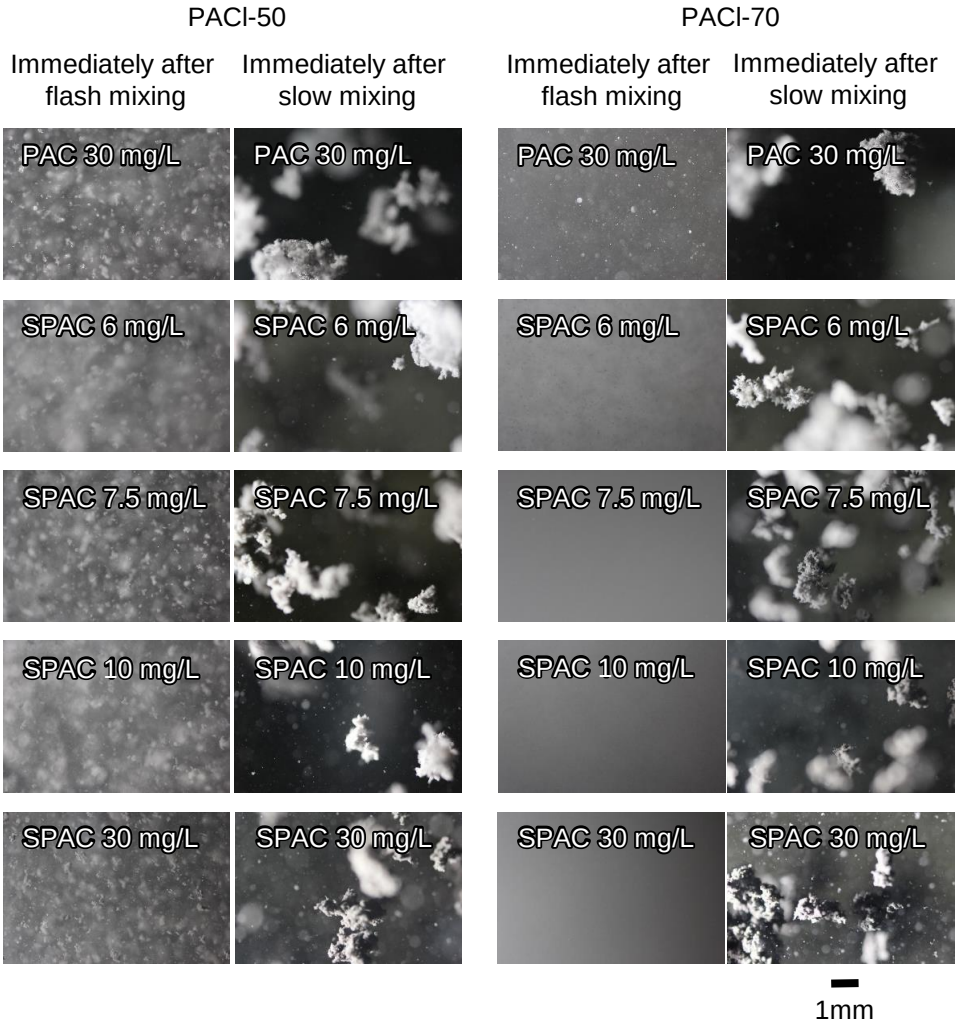

Fig. 3-11. Photos of floc particles during the experiments of Fig. 3-6. The two columns of the left side are experiments using PACl-50. The two columns of the right side are experiments using PACl-70. The photos in the first column in each set of two rows were taken immediately after flash mixing was finished. The photos in the second column in each set of two rows were taken immediately after slow mixing was finished.

Therefore, it can be said that the rapid formation of large-size floc particles and the lowered turbidity of supernatant water, although such information can be obtained by a conventional jar test, are not indicators for a lower residual carbon particle concentration after CSF. PACls are rich in diversity in terms of two different aspects: charge-neutralization capacity to destabilize particles and the bridge-formation ability to form large floc particles, but the charge-neutralization capacity is not related to the bridge-formation ability (Zhao *et al.* 2010). Consequently the present study revealed that PACls having a feature of the

charge-neutralization capacity to destabilize particles rather than the bridge-formation ability to form large-size floc particles are beneficial for lowering residual carbon particle concentration after CSF.

3.3.2 Effect of mixing intensity in coagulation and flocculation

As mentioned in the preceding paragraph, the high-basicity PACl (PACl-70) formed flocs slowly, but it had a high charge neutralizing capacity. Hence, it was hypothesized that optimizing the mixing intensity and time would lead to further reduction of residual carbon particle concentration in sand filtrate, and experiments were conducted. Fig. 3-12 illustrates the residual SPAC concentrations in sand filtrates when coagulation-flocculation were conducted with three different G_TT_T values ranging from 19,500 to 78,000 by adjusting T_T. (The G_TT_T value means total GT, which is the sum of flash-mixing GT (G_FT_F) and slow-mixing GT) In the case with the small G_TT_T value of 19,500, the residual carbon particle concentration was 800-particles/mL after CSF using PACl-50, whereas a much higher residual concentration of 2,200 particles/mL was observed using PACl-70. In such a low mixing intensity, large floc particles were seen in the photographs at the end of slow mixing, but many small floc particles were also observed in the same photographs, in both cases of PACl-50 and PACl-70 (Fig. 3-13); the mixing intensity was obviously insufficient. In contrast, as the G_TT_T value increased from 39,000 to 78,000, small floc particles diminished, seen in the photographs taken at the end of slow mixing (Fig. 3-13). At the same time, the turbidity of supernatant water (Fig. 3-14) and the residual carbon particle concentration of sand filtrate also decreased substantially. As shown in Fig. 3-12 and Fig. 3-14, furthermore, the effect of G_TT_T on the turbidity of supernatant water and the residual carbon particle concentration of sand filtrate was more pronounced for PACl-70, which had a higher capacity for charge neutralization, than PACl-50.

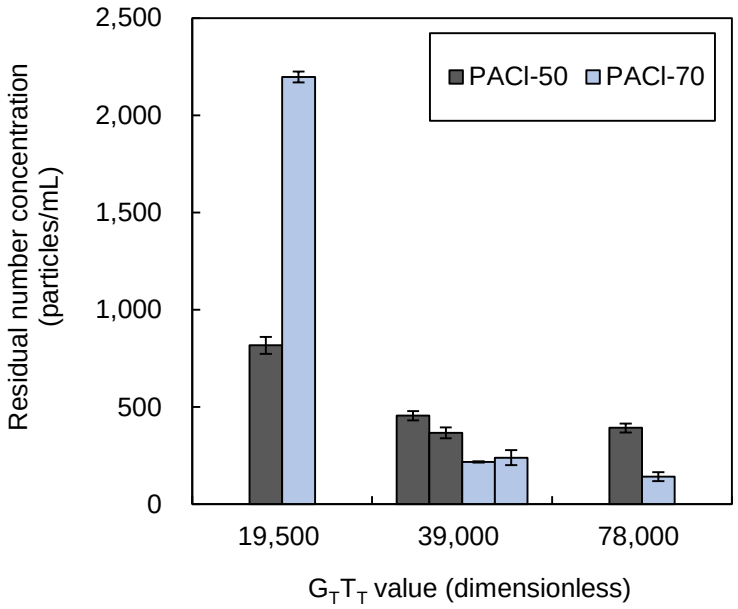

Fig. 3-12. Effect of total mixing intensity (G_TT_T value=G_FT_F value of flash mixing+G_ST_S value of slow mixing) on the particle number concentration of residual carbon. $SPAC_1$ was used. Initial $SPAC_1$ concentration was 10 mg/L. Details of the mixing conditions are shown in Table 3-2. The number of experiments for each mixing condition was described as follows: with total GT 39,000, two experiments; with total GT 19,500 and 78,000, one experiment each. Error bars indicate standard deviations of measurements.

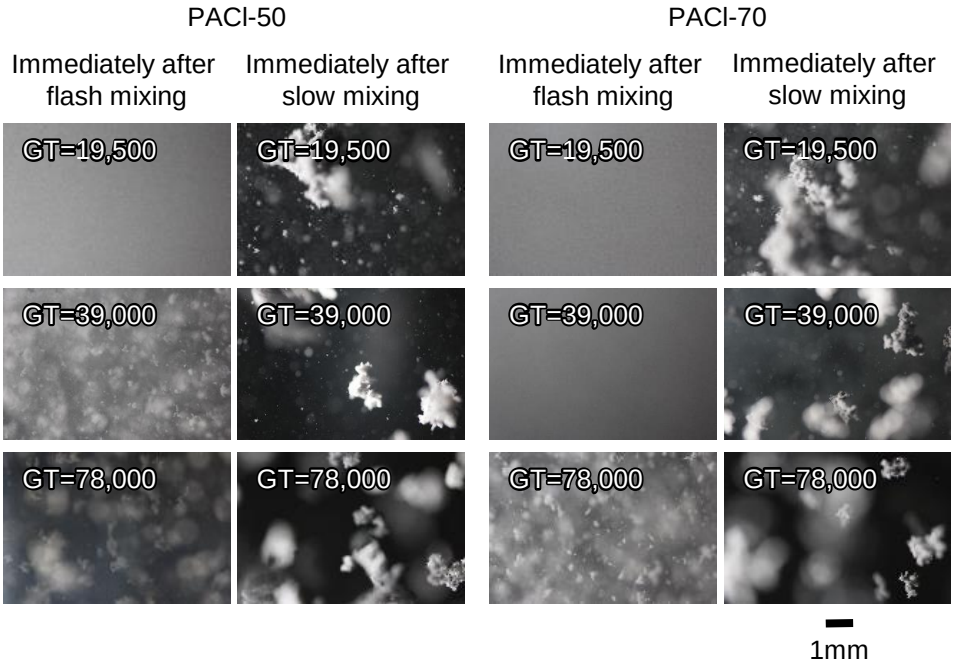

Fig. 3-13. Photos of floc particles during the experiments of Fig. 3-12. The two columns of the left side are experiments using PACl-50. The two columns of the right side are experiments using PACl-70. The photos in the first column in each set of two rows were taken immediately after flash mixing was finished. The photos in the second columns in each set of two rows were taken immediately after slow mixing was finished.

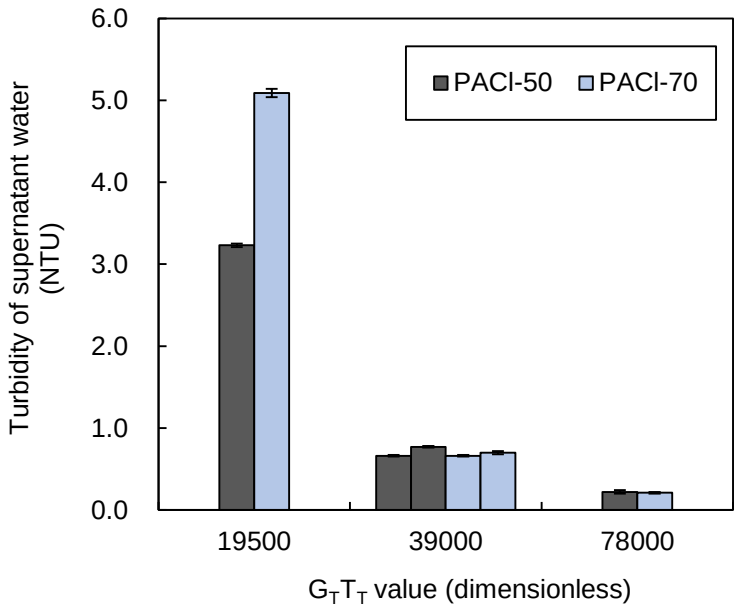

Fig. 3-14. Turbidity of supernatant after coagulation, flocculation, and sedimentation in the experiments of Fig. 3-12. Error bars indicate standard deviations of measurements.

3.3.3 Effect of flash mixing intensity in coagulation

Because charge neutralization occurs mostly during the flash mixing stage, I hypothesized that the residual carbon particle concentration of sand filtrate is influenced more by the flash mixing conditions than by the slow mixing conditions, so I conducted other series of CSF experiments. In the first series of experiments, the G_TT_T was fixed at 39,000, but its allocation to flash mixing was changed; i.e. the larger the G_FT_F value of flash-mixing was, the smaller the G_ST_S value of slow-mixing. The results are shown in Fig. 3-15. When the flash-mixing G_FT_F was small (6,000), the residual carbon particle concentration was high at 900 particles/mL. The residual concentration, however, decreased as the flash-mixing G_FT_F increased. The effect of the flash-mixing G_FT_F was more prominent with PACl-70 than with PACl-50. At the largest flash-mixing G_FT_F (24,000), the residual carbon particle concentration was reduced to <200 particles/mL.

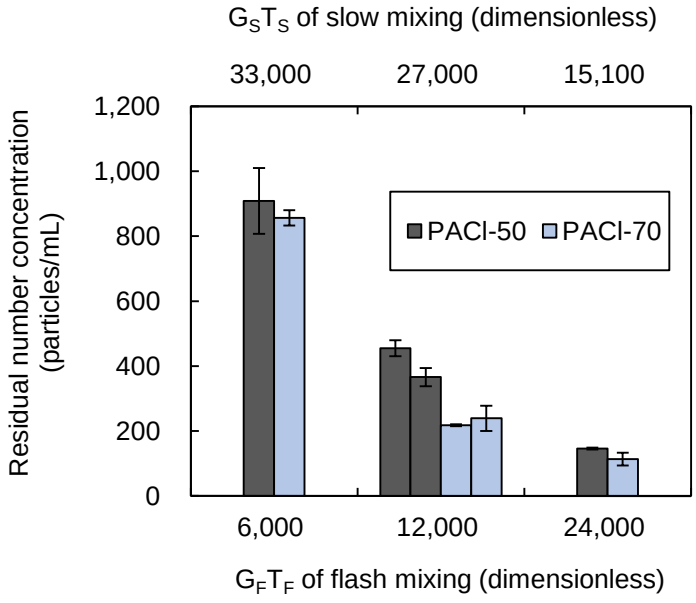

Fig. 3-15. Effect of mixing intensity in flash and slow mixing on the particle number concentration of residual carbon at a fixed total mixing intensity. $SPAC_1$ was used. Initial $SPAC_1$ concentration was 10 mg/L. G_TT_T value (=G_FT_F of flash mixing+G_ST_S of slow mixing) was fixed at about 39,000. Details of the mixing conditions are shown in Table 3-2. The number of experiments for each mixing condition was described as follows: with G_TT_T 39,000 (G_FT_F=12,000), two experiments; with G_TT_T 39,000 (G_FT_F=6,000) and 39,100 (G_FT_F=24,000), one experiment. Error bars indicate standard deviations of measurements.

In a series of experiments for which flash-mixing G_FT_F was changed by adjusting T_F but slow mixing intensity was fixed at a constant value (G_ST_S=15,100), a G_FT_F >24,000 resulted in a low residual carbon particle concentration (Fig. 3-16), indicating that there is a certain minimal value for G_FT_F required for lowering the carbon particle concentration in sand filtrate. Next, the effect of G_F value on residual carbon particles was examined in the condition where GT values of both flash and slow mixing intensities were fixed (G_FT_F =24,000 and G_ST_S =15,100). Residual carbon particle concentration became smaller with a larger GF value (smaller T_F value) (Fig. 3-17). It was minimal at G_F=600 s^{-1} (experiments at G value>600 s^{-1} could not be conducted because the mixing caused the water to splash out of the container.

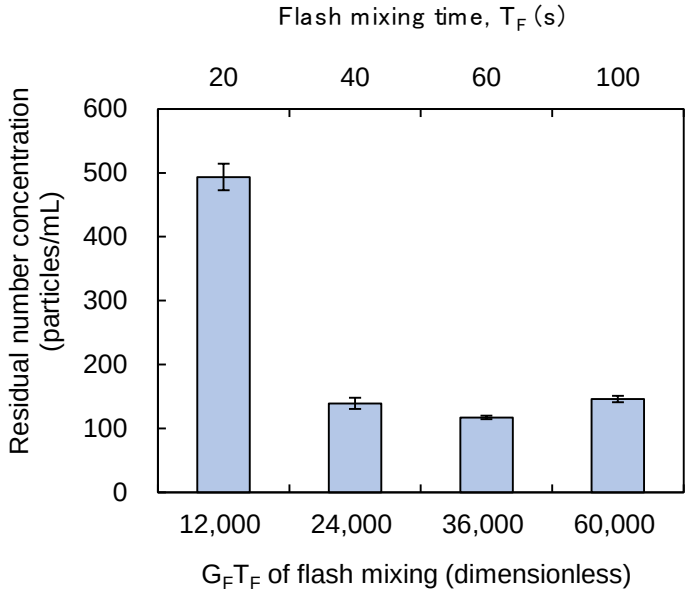

Fig. 3-16. Effect of flash mixing time (T_F) on the particle number concentration of residual carbon. $SPAC_2$ was used. Initial $SPAC_2$ concentration was 10 mg/L. PACl-70 was used. G_F value was fixed at 600 s^{-1}. G_ST_S of slow mixing=15,100. Details of the mixing conditions are shown in Table 3-2. Error bars indicate standard deviations of measurements.

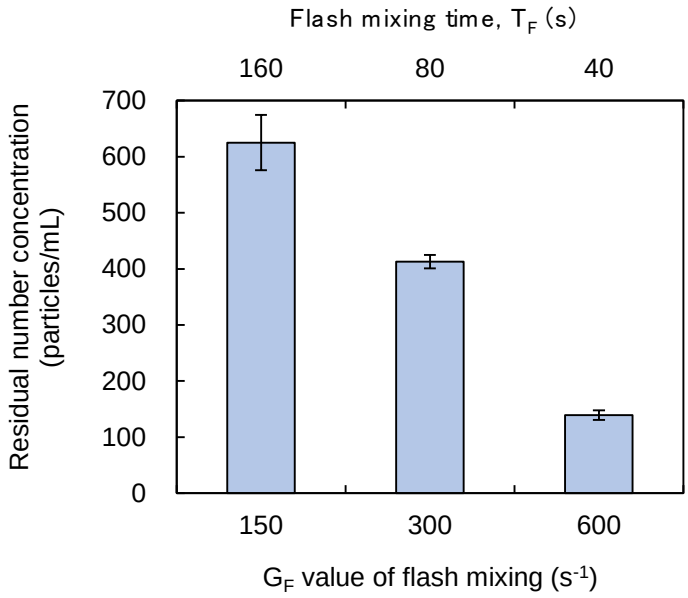

Fig. 3-17. Effect of mixing speed (G_F) and time in flash mixing on the particle number concentration of residual carbon at a fixed flash mixing intensity (G_FT_F=24,000) and a fixed slow mixing intensity (G_ST_S=15,100). $SPAC_2$ was used. Initial $SPAC_2$ concentration was 10 mg/L. PACl-70 was used. Error bars indicate standard deviations of measurements.

Kan *et al.* (2002) conducted jar tests by using alum and commercially-available PACl to investigate the effect of flash-mixing time on the removal of clay particle. They report that the residual turbidity decreased sharply with increasing duration of flash-mixing. Lin *et al.* (2013) also conducted jar tests by using turbid surface-water and commercially-available PACl to investigate the effect of flash-mixing intensity on the turbidity and DOC removal. They reported that the removal performances of turbidity and DOC were improved as flash-mixing intensity increased. In the present study, fine carbon particles were used as the target matter, but the tendency that the turbidity after settling and residual carbon particles remaining in sand filtrate reduced as flash-mixing intensity or time increased was much the same as those previous studies.

It is of great interest that the trace residual-carbon-particle concentration as an outcome after the fourth step of sand-filtration in the CSF was largely affected by the mixing intensity of the first step of coagulation in the CSF, although the flocculation and sedimentation processes occurred in between the coagulation and

the sand-filtration. The flocculation and sedimentation processes had long detention time, and most of the carbon particles were removed by the sedimentation process. During the flash mixing process for coagulation, the PACls hydrolyzed in water and formed a hydrolyzing aluminum polymer, which efficiently neutralized the negative charge of carbon particles. Thus, providing both rapid dispersion of dosed PACls and high-frequent contact between the hydrolyzing aluminum polymer and the carbon particles, in particular very fine carbon particles, was necessary to decrease charge-un-neutralized particles. Finally, achieving these conditions produced low residual carbon particles, which penetrated through the sand bed situated in the last stage in the CSF. A high G_F value created such conditions of the rapid dispersion and the high-frequent contact.

3.3.4 Residual carbon particles after treatment with a bench-scale CSF plant

The residual carbon particle concentration in sand filtrate with increasing filtration time was examined, using a bench-scale CSF plant, a SPAC dose of 2 mg/L, and PACl-70 as the coagulant at 1.5 or 2.25 mg-Al/L (Fig. 3-18). At each time point examined, the residual carbon particle concentration was lower when the higher concentration of coagulant was used than when the lower concentration was used. Irrespective of coagulant dose, the residual carbon particle concentration started high and then decreased with increasing filtration time until a steady state was reached at less than 200 particles/mL; this particle concentration is similar to that reported for a full-scale CSF water purification plant using PAC (Kobayashi *et al.* 2019). The high concentration of particles during the initial period of filtration was not due to residual backwash water remaining in the filter because the filter media was washed with pure water (Milli-Q Advantage A10 System; Merck KGaA) during the final washing process. Therefore, I concluded that the filter underwent a ‘ripening’ process, which is

when clean sand media captures particles that cause the filter to become more efficient at capturing additional particles over time (Crittenden et al. 2012).

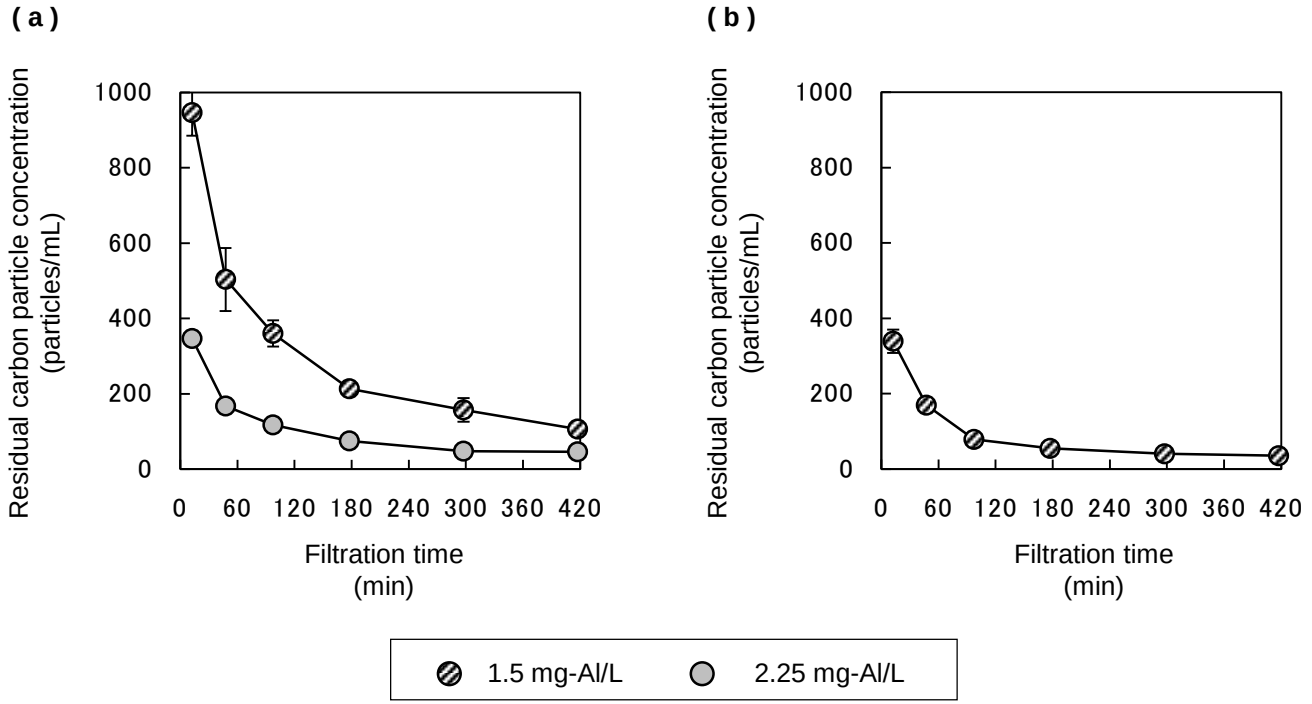

Fig. 3-18. Residual carbon particle concentration in sand filtrate after treatment of river water (a) or municipal water (b, Municipal water 1) with a bench-scale CSF plant. Coagulation: single-chambered reactor, G = 600 s^{-1}; flocculation: 4-chambered reactor, G = 12.5 s^{-1}; filtration rate, 90 m d^{-1}. $SPAC_3$ initial concentration, 2.0 mg/L; coagulant (PACl-70), 1.5 or 2.25 mg-Al/L.

Although a clear decrease in residual carbon particle concentration was observed as the filter ripened, no clear change in the particle size distribution of the residual particles was observed (range, 0.3–2 μm; Fig. 3-19). Therefore, the increased removal of carbon particles with increasing filtration time was not related to the particle size of the carbon particles. In conjunction with my previously reported finding that the carbon particles remaining in sand filtrate had a higher negative charge than the carbon particles entering the sand filter (Nakazawa et al. 2018), I interpreted this increased removal efficacy as follows. The sand filter treats the sedimentation supernatant, which contains particles with varying degrees of charge neutralization. Clean sand media has a high negative charge (Edzwald 2011), so the charge-neutralized particles attach to the surface of the sand particles and remain in the sand filter. In contrast, the less-charge-neutralized particles are unable to attach to the sand particles due to repulsive forces and therefore exit the filter. However, as the filter ripens by the accumulation of charge-neutralized particles, the ability of the less-charge-neutralized particles to attach to the immobilized charge-neutralized particles results in increased removal efficacy over time. To examine the role of particle attachment in more detail, I conducted experiments at two different filtration rates (Fig. 3-20) under the assumption that the filtration mechanism comprises two steps: transport, where suspended particles are transported to the surface of sand grains, and attachment, where the particles attach to the sand grains (Edzwald 2011). In my experiments, I observed that the higher filtration rate resulted in decreased attachment efficiency [the number of particle sand-grain adhesions divided by the number of particle sand-grain collisions (Crittenden et al. 2012)] of the carbon particles to the filter.

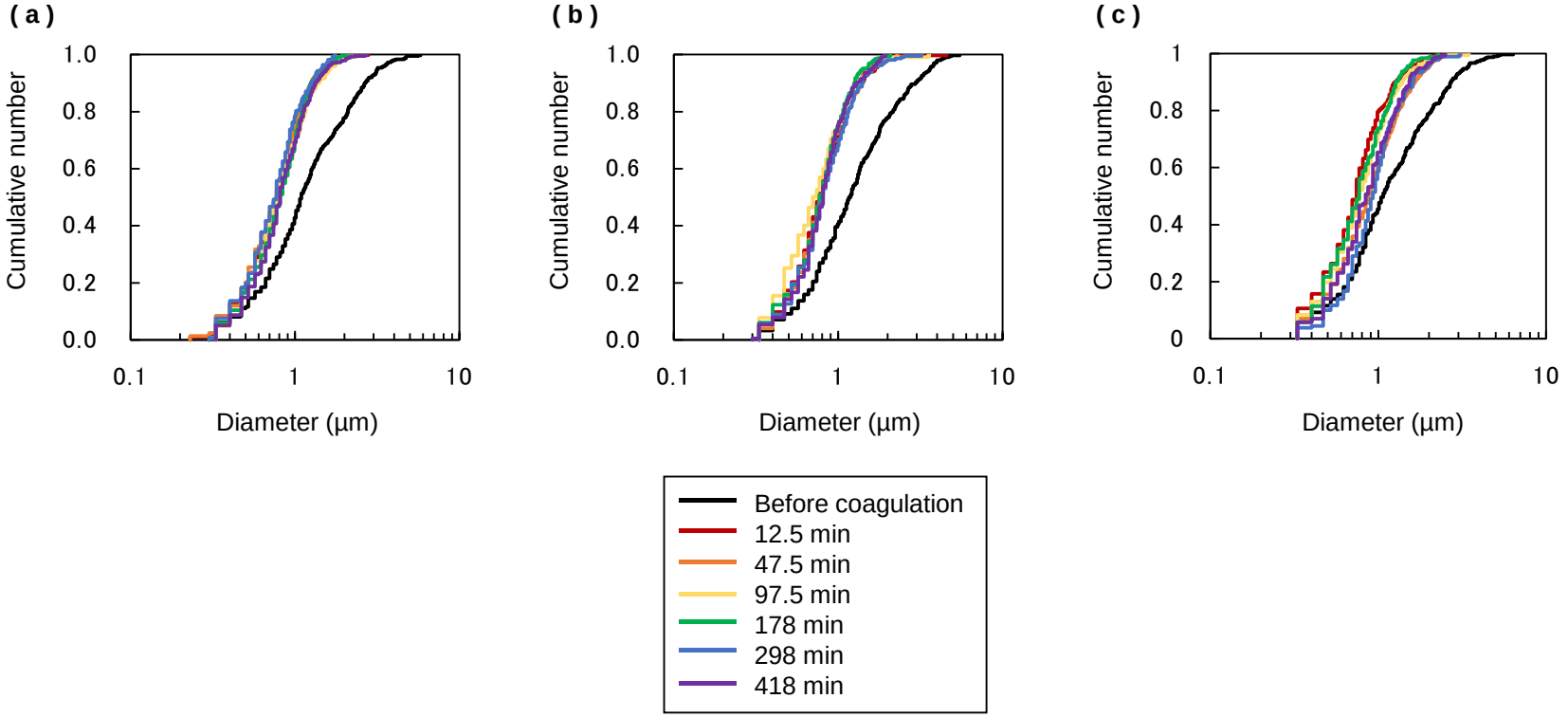

Fig. 3-19. Particle size distributions of carbon particles in water sampled from the preparation unit before coagulation or in sand filtrate. The numbers in the legend indicate the filtration time. Particle sizes were determined by using membrane filtration and microscopic image analysis. River water (a, b) or Municipal water 1 (c) was used as the raw water. Coagulant (PACl-70) dose, 1.5 mg-Al/L (a, c) or 2.25 mg-Al/L (b). The experimental conditions were the same as those described in the caption to Fig. 3-18.

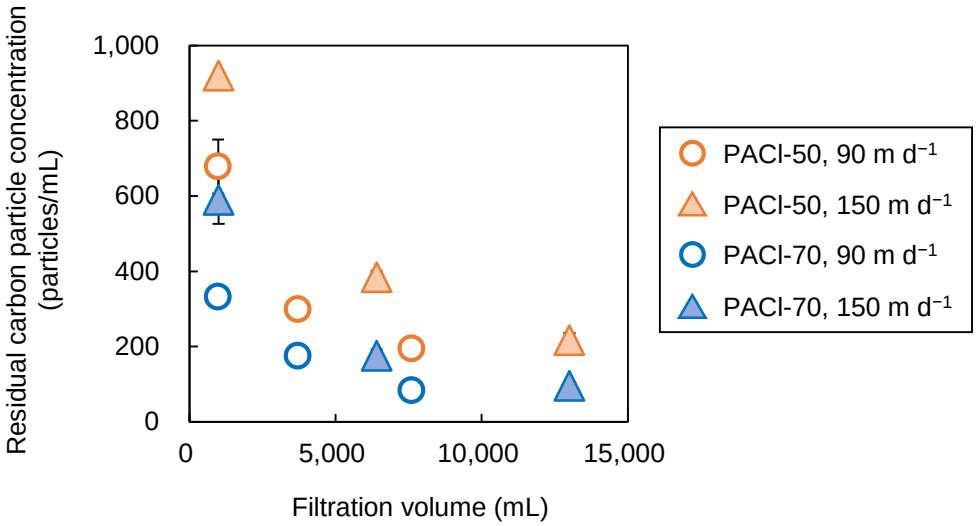

Fig. 3-20. Effect of filtration rate on residual particle concentration in sand filtrate. Filtration rate, 90 or 150 m d^{-1}. Municipal water 2 was used as the raw water. $SPAC_3$ initial concentration, 2.0 mg/L; coagulant (PACl-50 or PACl-70), 1.5 mg-Al/L. Coagulation, single-chambered reactor, G = 600 s^{-1}; flocculation, 4-chambered reactor, G = 12.5 s^{-1}.

3.3.5 Effect of mixing reactor configuration on the concentrations of residual particles

Another important mixing condition is the distribution of residence time. The experiments of Sections 3.3.1-3.3.3 were conducted as batch tests, which results in a constant and uniform residence time. However, actual water treatment systems use a continuous flow reactor, which results in a residence time that varies. In other words, even if the average residence time is long enough, if the residence time has a wide variance over time, the fact that some particles may not have sufficient opportunity to come into contact with the coagulant (Bratby 2006, Crittenden et al. 2012).

Thus, in this section, flow-through reactors with different set-ups were used to investigate the effect of mixing reactor configuration on residual particle concentration. In these experiments, a single-chambered reactor or a 3-chambered reactor, with the same total HRT and same size impellors (one per chamber), was used for coagulation treatment with rapid mixing. In addition, a single-chambered

reactor or a 4-chambered reactor, with the same total HRT and same total number of impellors with the same size and rotational speed, was used for flocculation with slow mixing. According to the residence time distributions determined for the coagulation and flocculation reactors (Fig. 3-21 and Fig. 3-22), the proportion of the distributions indicating a short residence time (less than half of the HRT) was larger for the single-chambered reactor than for the 3- or 4-chambered reactors.

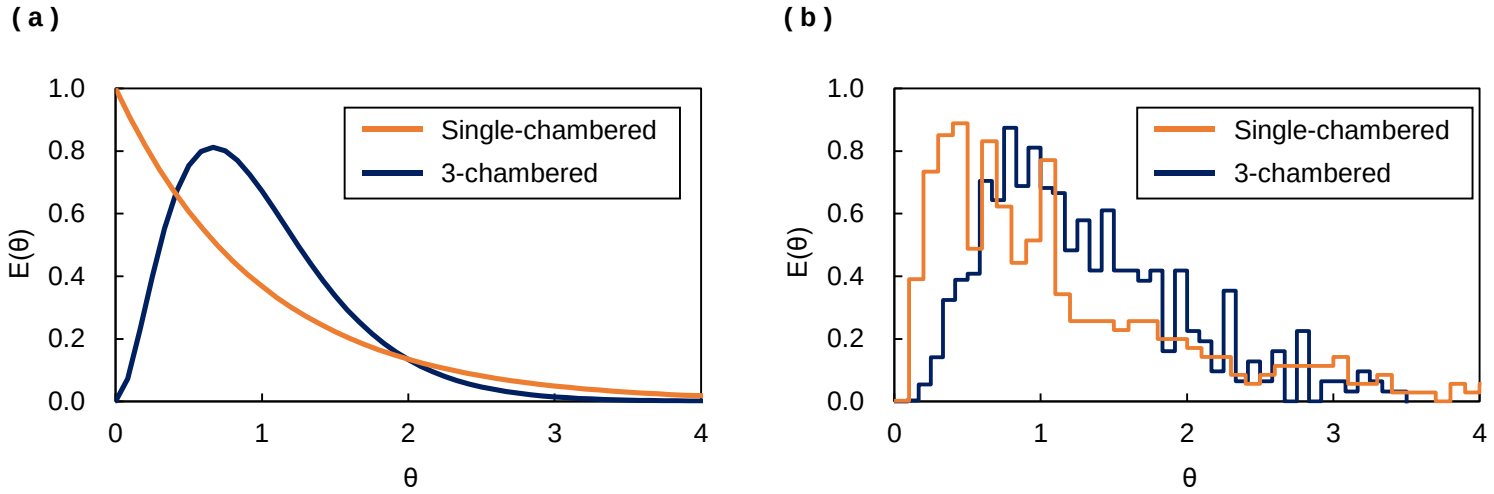

Fig. 3-21. Theoretical (a) and experimental (b) residence time distributions for the single-chambered or 3-chambered coagulation reactor with rapid mixing. θ is normalized residence time divided by HRT, and E(θ) is residence time distribution (Crittenden et al. 2012).

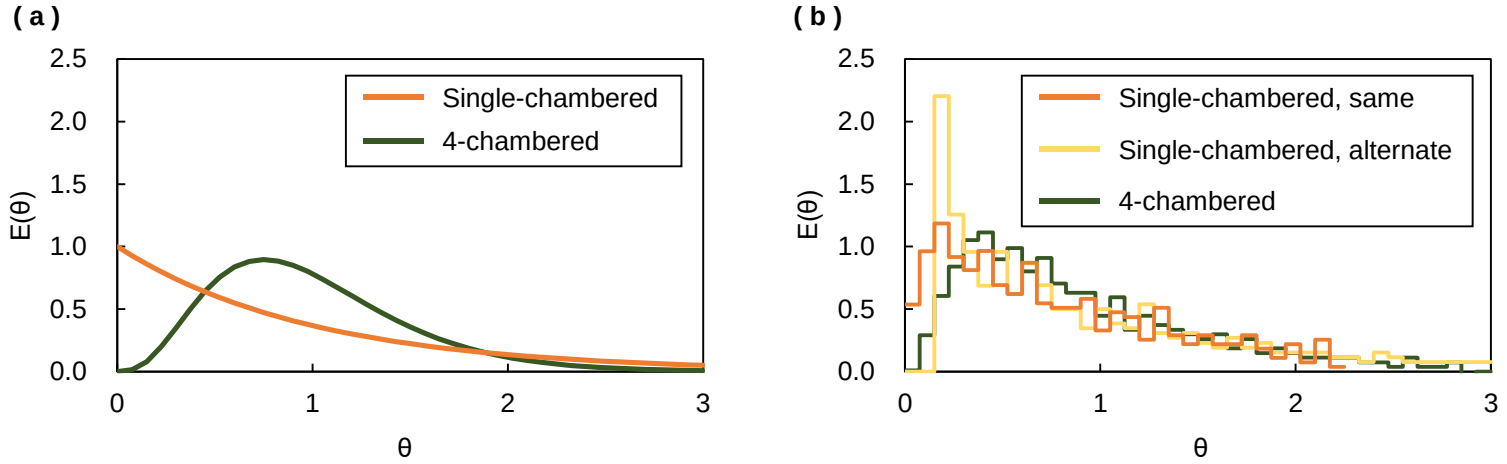

Fig. 3-22. Theoretical (a) and experimental (b) residence time distributions for the single-chambered or 4-chambered flocculation reactor with slow mixing. “alternate” means that the direction of rotation of the 4 mixers alternated; “same” means that the direction of rotation of the 4 mixers was the same. θ is normalized residence time, time divided by HRT, and E(θ) is residence time distribution (Crittenden et al. 2012).

First, the effect of coagulation reactor (rapid mixing unit) configuration on residual carbon particle concentration in sand filtrate was examined. Although the single-chambered reactor and the 3-chambered reactor had the same mixing intensity (G value) and HRT, a lower residual carbon particle concentration was obtained with the 3-chambered reactor than with the single-chamber reactor (Fig. 3-23 and Fig. 3-24). This suggests that the different residence time distributions of the two types of reactor influenced the residual carbon particle concentration in the sand filtrate. Thus, when a large proportion of the residence time distribution included short residence times, which was observed in the distribution for the single-chambered reactor (Fig. 3-21 and Fig. 3-22), which increased the residual carbon particle concentration in the sand filtrate.

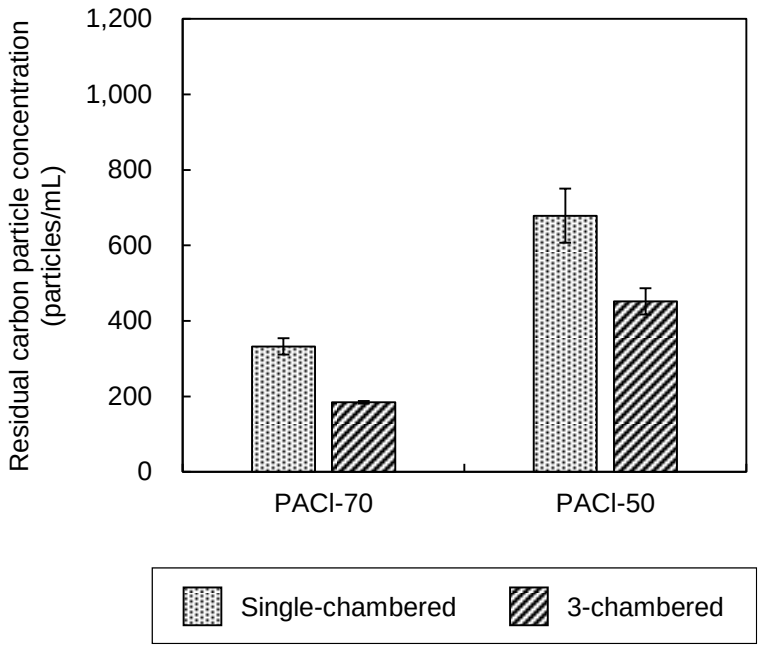

Fig. 3-23. Effect of rapid mixing reactor configuration (a single-chambered or 3-chambered coagulation reactor) on residual particle concentration in sand filtrate. Both reactors used the same mixing intensity (G = 600 s^{-1}) and same total HRT (100 s), and were followed by a 4-chambered flocculation reactor (G = 12.5 s^{-1}) and a sand filter. Municipal water 2 was used as the raw water. $SPAC_3$ initial concentration, 2.0 mg/L; coagulant (PACl-50 or PACl-70), 1.5 mg-Al/L; filtration rate, 90 m d^{-1}.

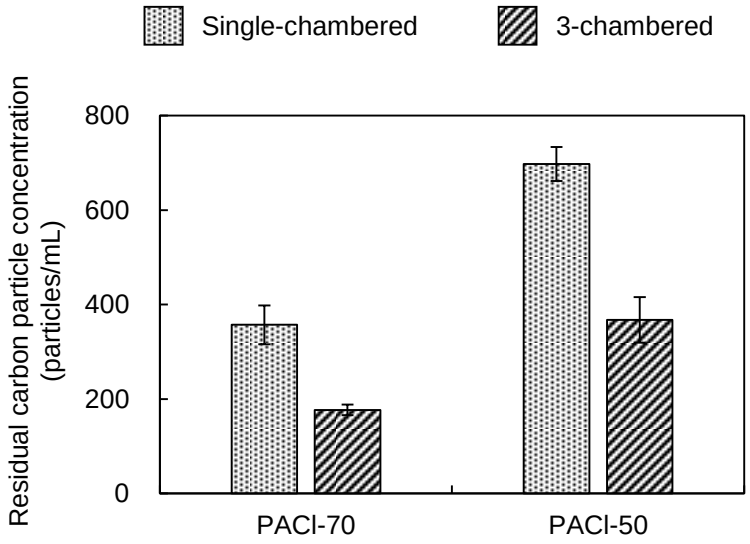

Fig. 3-24. Effect of coagulation reactor configuration on residual carbon particle concentration in sand filtrate. A single-chambered or 3-chambered coagulation reactor with the same mixing intensity (G = 600 s^{-1}) and same total HRT (100 s) was used. Both reactors were followed by a 4-chambered flocculation reactor (G = 12.5 s^{-1}) and a sand filter. Municipal water 3 was used as the raw water. SPAC initial concentration, 2.0 mg/L; coagulant (PACl-50 or PACl-70), 1.5 mg-Al/L; filtration rate, 90 m d^{-1}.

Next, the effect of flocculation reactor (slow mixing unit) configuration on residual carbon particle concentration in sand filtrate (Fig. 3-25 and Fig. 3-26) was examined. The 4-chambered reactor resulted in a lower residual particle concentration in the sand filtrate than the single-chambered reactor when PACl-50 was used as the coagulant. However, when PAC-70 was used, this trend was not observed. This phenomenon was discussed in Chapter 4.

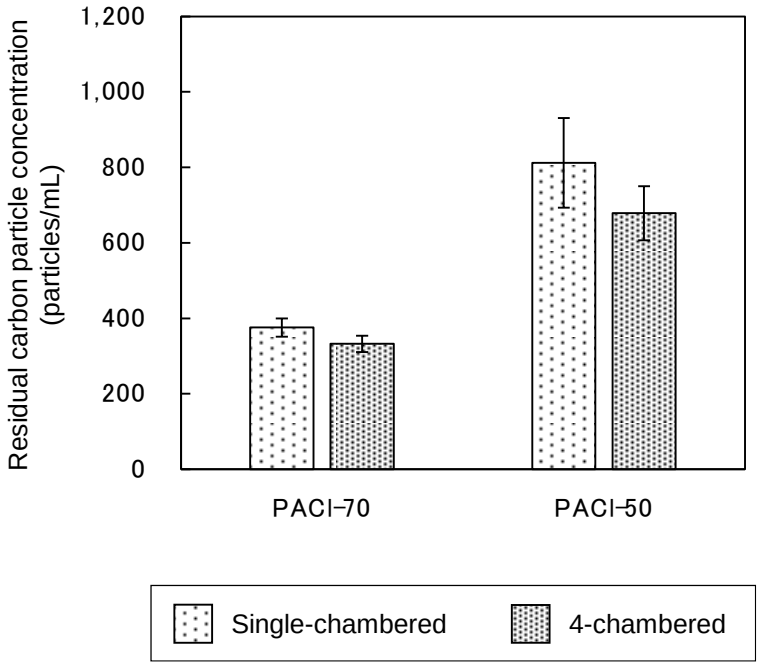

Fig. 3-25. Effect of slow mixing reactor configuration (a single-chambered or 4-chambered flocculation reactor) on residual particle concentration in sand filtrate. Both reactors used the same mixing intensity (G = 12.5 s^{-1}) and same total HRT (2400 s) and were preceded by a single-chambered coagulation reactor (G = 600 s^{-1}). The experimental conditions were the same as described in the caption to Fig. 3-23.

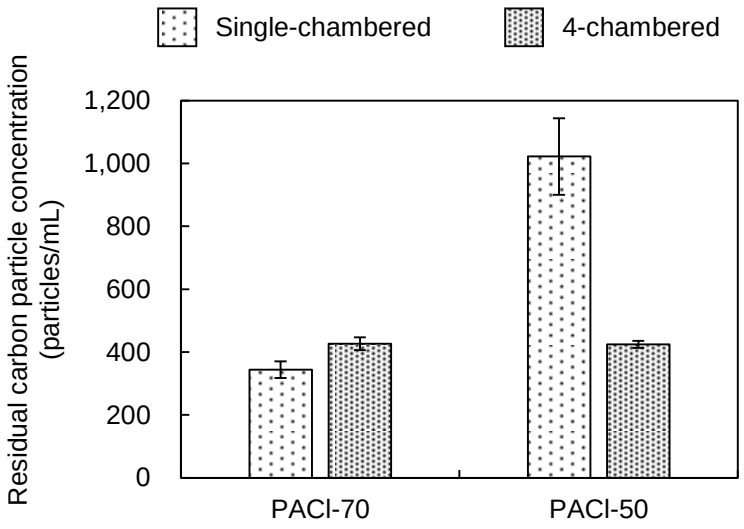

Fig. 3-26. Effect of flocculation reactor configuration on residual particle concentration in sand filtrate. A single-chambered coagulation reactor (G value of 600 s^{-1}) followed by a single-chambered or 4-chambered flocculation reactor with the same mixing intensity (G = 12.5 s^{-1}) and same total HRT (2400 s) were used. Municipal water 4 was used as the raw water. $SPAC_3$ initial concentration, 2.0 mg/L; coagulant (PACl-50 or PACl-70), 1.5 mg-Al/L; filtration rate, 90 m d^{-1}.

The turbidity of settled water was found to also be influenced by the residence time distribution of the coagulation and flocculation reactors (Fig. 3-27).

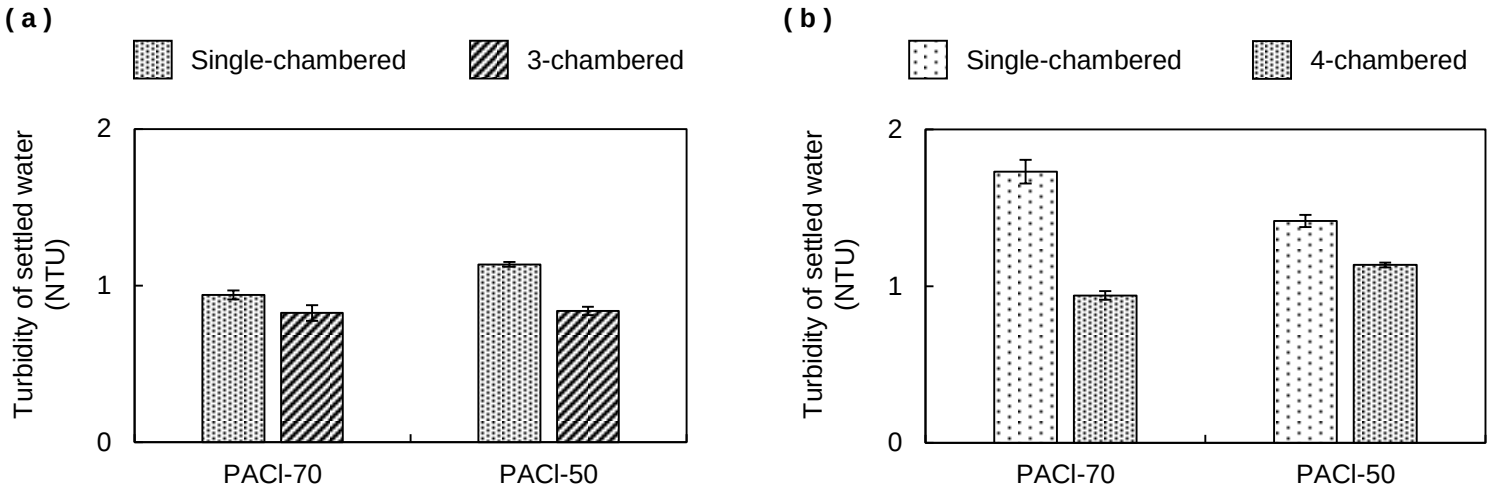

Fig. 3-27. Effect of mixing reactor configuration on the turbidity of settled water after sedimentation. (a) Effect of a single-chambered or 3-chambered coagulation reactor. Both reactors used the same mixing intensity (G = 600 s^{-1}) and the same total HRT (100 s) and were followed by a 4-chambered flocculation reactor (G = 12.5 s^{-1}). (b) Effect of a single-chambered or 4-chambered flocculation reactor. Both reactors used the same mixing intensity (G = 12.5 s^{-1}) and same total HRT (2400 s) and were preceded by a single-chambered coagulation reactor (G = 600 s^{-1}). Municipal water 2 was used as the raw water. $SPAC_3$ initial concentration, 2.0 mg/L; coagulant (PACl-50 or PACl-70), 1.5 mg-Al/L; settling time, 65 min. The experimental conditions were the same as described in the caption to Fig. 3-23 and Fig. 3-25.

3.3.6 Effect of coagulant dosage

It is generally known that turbidity removal by coagulation-sedimentation improves as the dosage of coagulant increases when the coagulation processes are mainly due to sweep flocculation mechanism, which operates at near neutral pH, but not due to charge-neutralization mechanism, which operates at pH < 6 (Edzwald 2011, Hendricks 2010). The present study of CSF, which was conducted at pH 7, also confirmed the relationship between the dosage of coagulant and the residual concentration of SPAC or the turbidity of supernatant water in CSF (Fig. 3-28 and Fig. 3-29); increasing coagulant dosage resulted in an increase in the removal of carbon particles both after sedimentation and sand filtration. Additionally, the superiority of PACl-70 to PACl-50 was held in the entire range of coagulant dosages tested in terms of residual carbon particle concentration. The very low residual concentration of 6 particles/mL was attained with the highest coagulant dosage of PACl-70.

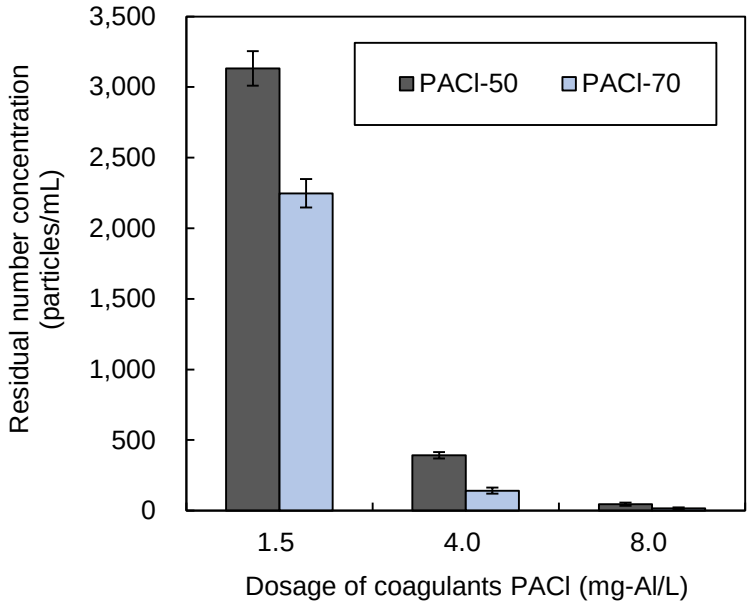

Fig. 3-28. Effect of coagulant dosage on the particle number concentration of residual carbon in sand filtrate. $SPAC_1$ was used. Initial $SPAC_1$ concentration was 10 mg/L. G_TT_T value was fixed at 78,000 (G_FT_F=24,000, G_ST_S=54,000). Error bars indicate standard deviations of measurements.

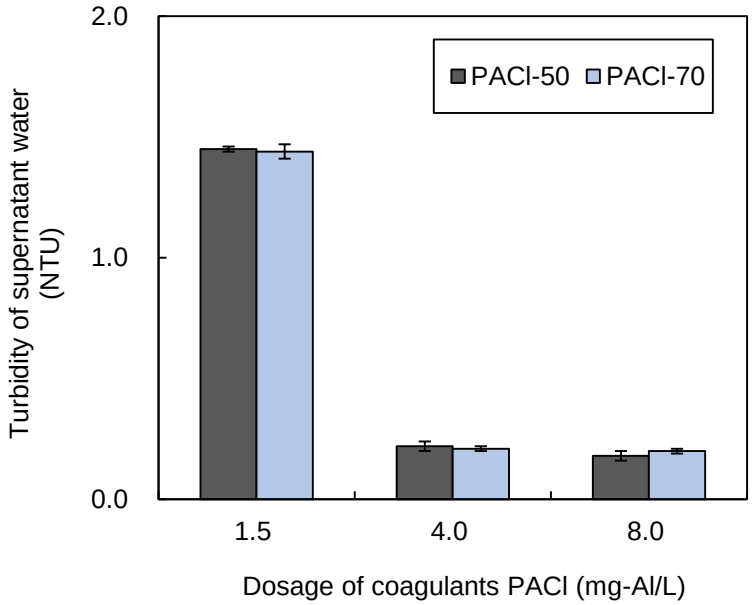

Fig. 3-29. Turbidity of supernatant after coagulation, flocculation, and sedimentation in the experiments of Fig. 3-28. Error bars indicate standard deviations of measurements.

3.3.7 Development and performance of coagulants by base-titration

The above described investigation suggests the importance of decreasing the number of charge-un-neutralized particles in order to enhance the separation of SPAC particles and lower the number of residual SPAC particles after CSF. Available techniques for decreasing the number of charge-un-neutralized particles were enumerated using a coagulant with high a charge-neutralization capacity, such as high-basicity PACl with the optimized flash mixing intensity, as well as increasing the dosage of coagulant. I further searched for a better PACl that lowered the number of residual SPAC particles. I produced a series of PACls with high basicity (Table 3-5; see also Section 7.2) and conducted jar tests (Table 3-6; see also Section 7.3).

Table 3-5. Coagulants made by base-titration.

Name	Basicity	SO4/Al	Cl/Al	Na/Al	Al content	Heating process	
						Time	Temperature
	%	molar ratio	molar ratio	molar ratio	mol/L	h	℃
B65ns	65	0	3	1.95	0.1		
B65ns-heat	65	0	3	1.95	0.1	5	121
B79s0.10-1	79	0.1	2.8	2.38	0.04		
B79s0.10-2-heat	79	0.1	2.8	2.38	0.09	5	121
B80ns-1	80	0	3	2.4	0.05		
B80ns-2	80	0	3	2.4	0.1		
B80ns-2-heat	80	0	3	2.4	0.1	0.33	120
B82s0.11	82	0.11	2.79	2.45	0.1		
B82s0.11-heat	82	0.11	2.79	2.45	0.1	72	90~95
B88s0.10	88	0.1	2.8	2.64	0.05		

Table 3-6. The mixing conditions of coagulation in the jar-test (Fig. 3-31 to Fig. 3-34).

SPAC	Coagulant	Flash		Slow						Total
Median diameter	Dosage	G_F	T_F	G_{S1}	T_{S1}	G_{S2}	T_{S2}	G_{S3}	T_{S3}	G_TT_T
μm	mg-Al/L	s^{-1}	s	s^{-1}	s	s^{-1}	s	s^{-1}	s	dimensionless
1.0	0~1.5	190	60	19	600					22,800
1.0	0~1.5	200	60	20	600	15	600	10	1,200	45,000
1.1	1.5	200	120	20	600	15	600	10	1,200	57,000

It is widely known that the Al_{13} species in PACl have a high charge-neutralizing ability (Gao *et al.* 2005, Lin *et al.* 2008, Parthasarathy and Buffle 1985, Wu *et al.* 2007, Zhao *et al.* 2009), and Alb analyzed by the ferron method corresponds to the Al_{13} species (Parker and Bertsch 1992, Parthasarathy and Buffle 1985). In the present study, some PACls with a high content of Alb (Alb-type PACl) were produced by base-titration (Fig. 3-30), and experiments of coagulation-flocculation and sedimentation were conducted. The zeta potential of carbon particles became zero at a lower dosage of Alb-type PACl (B80ns-1) than of PACl-70 (Fig. 3-31), and Alb-type PACls (B65ns, B80ns-1, B80ns-2) supplied a higher positive charge to carbon particles than PACl-70 at the same coagulant dosage (Fig. 3-32). These results indicate that Alb-type PACls actually had a higher charge-neutralizing ability than PACl-70. However, these Alb-type PACls could not flocculate carbon particles, and consequently resulted in a high turbidity after sedimentation, even given large mixing intensity (Fig. 3-32). Even at the coagulant dose, which brought the zeta potentials of carbon particles to around zero, the turbidities after sedimentation were still high, compared with those obtained by PACl-70 (Fig. 3-31).

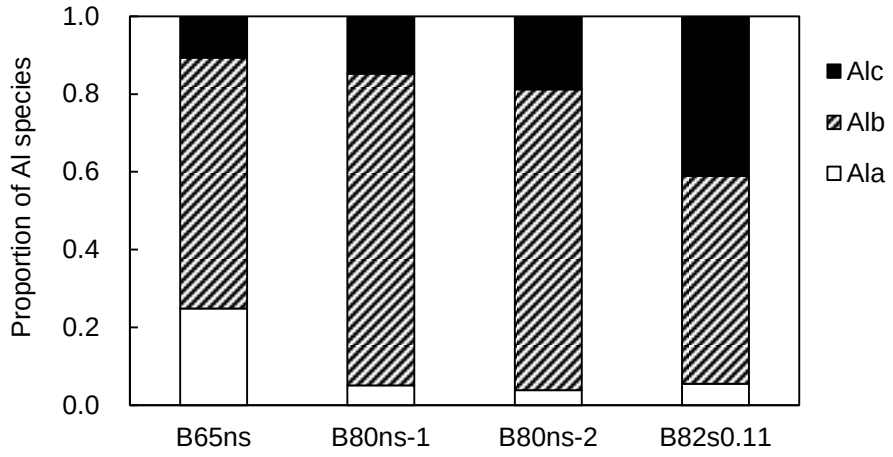

Fig. 3-30. Proportions of Al species in PACl coagulants made by base-titration.

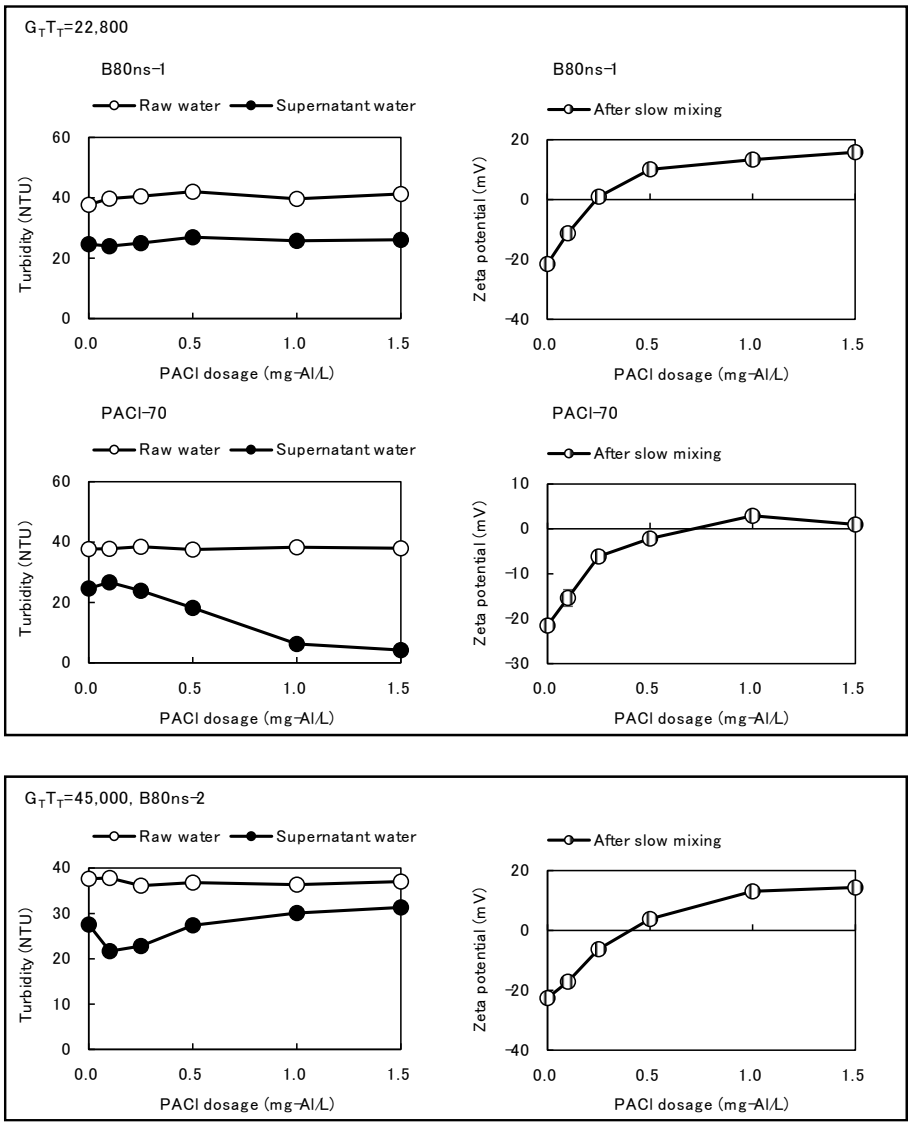

Fig. 3-31. Turbidity removal of and zeta potential of carbon particles. Initial SPAC concentration was 10 mg/L. Alb type base-titration PACls (B80ns-1, B80ns-2) and PACl-70 were used as coagulant with a dosage of 0 to 1.5 mg-Al/L. Coagulation pH was 7.0. Settling time was 60 min. Error bars of turbidity and zeta potential indicate standard deviations of three measurements and five measurements, respectively. Details of the mixing conditions are shown in Table 3-6.

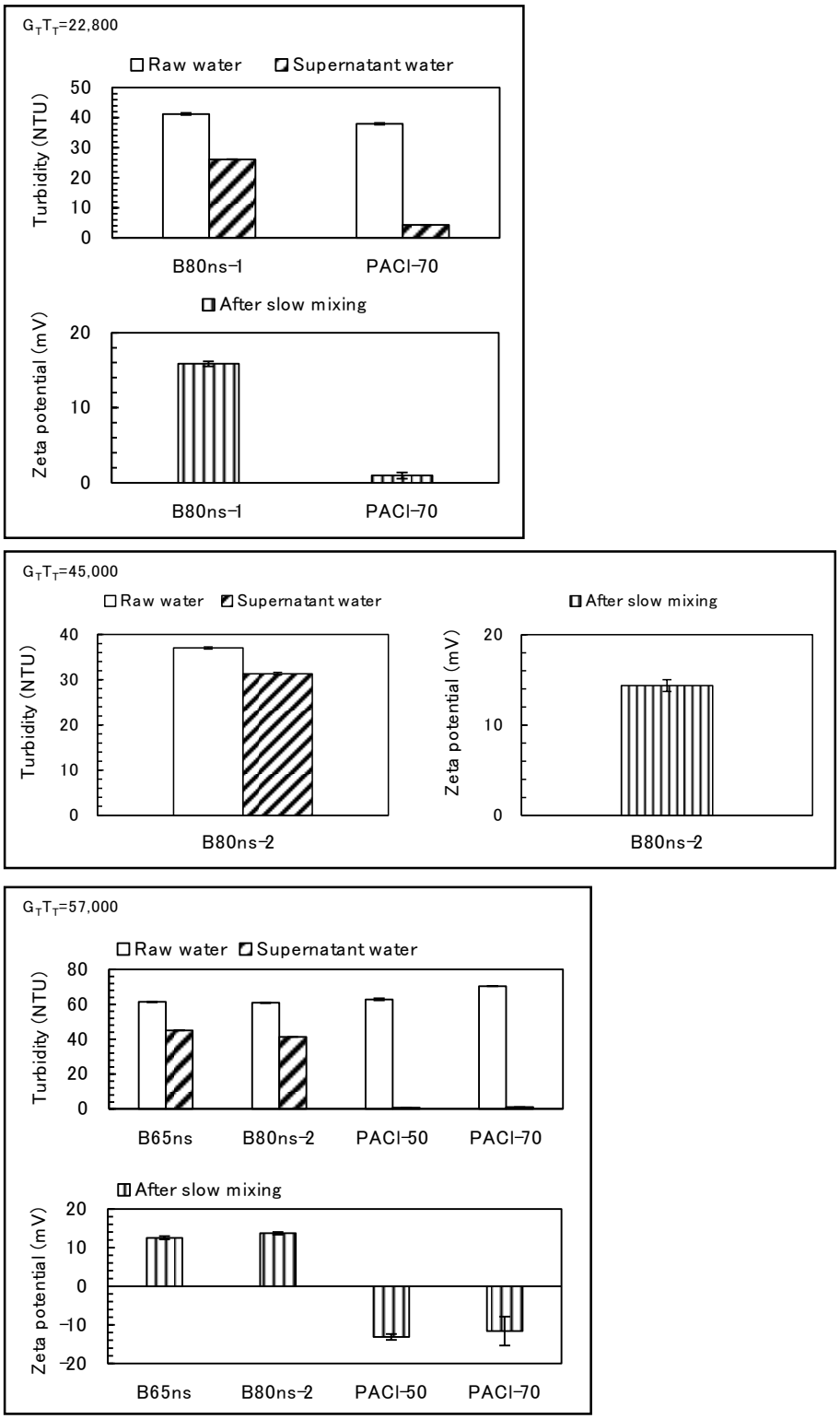

Fig. 3-32. Turbidity removal of and zeta potential of carbon particles. Initial SPAC concentration was 10 mg/L. Alb type base-titration PACls (B65ns, B80ns-1 and B80ns-2), PACl-50, and PACl-70 were used as coagulant with a dosage of 1.5 mg-Al/L. Coagulation pH was 7.0. Settling time was 60 min. Error bars of turbidity and zeta potential indicate standard deviations of three measurements and five measurements, respectively. Details of the mixing conditions are shown in Table 3-6.

It was reported that sulfate ions in PACl play a role in enhancing floc formation (Wang et al. 2002). Actually, the commercial PACl products, PACl-50 and PACl-70, both of which produce larger floc particles than the Alb-type PACl, contain sulfate ion. Accordingly, I supplemented sulfate ion and prepared three Alb-type PACls (Fig. 3-33). One PACl (B82s0.11) among the sulfated Alb-type PACls slightly flocculated carbon particles at a large mixing intensity (as a GT value of 57,000). However, turbidity-removal performance was considerably inferior to PACl-50 and PACl-70.

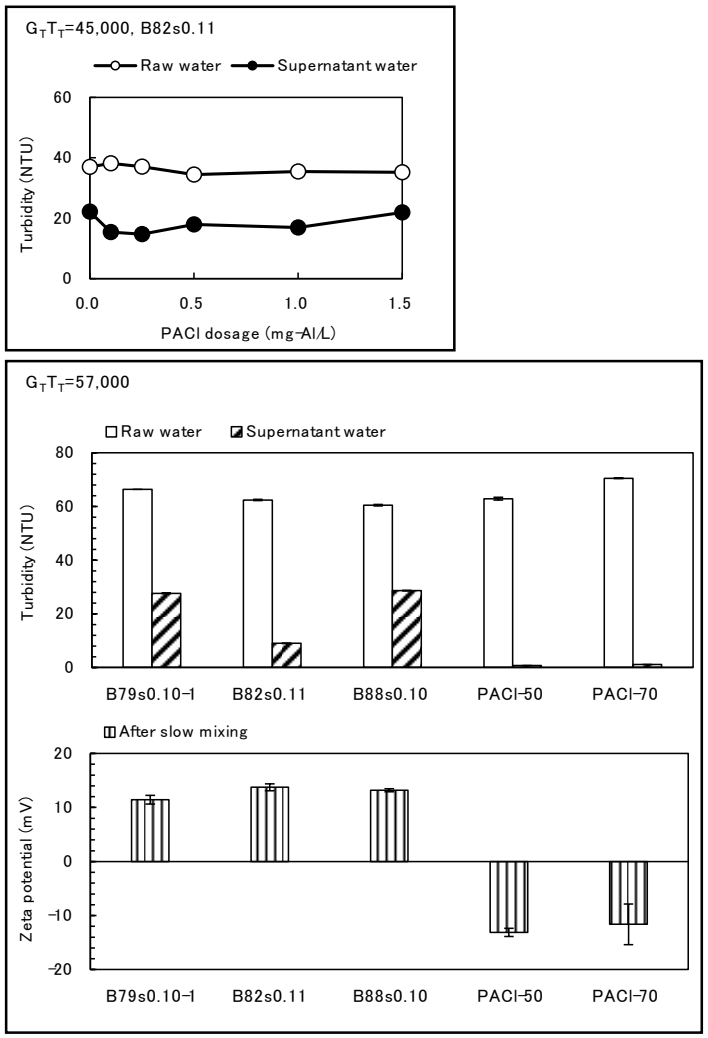

Fig. 3-33. Turbidity removal and zeta potential of carbon particles. Initial SPAC concentration was 10 mg/L. Base-titration PACls that contained sulfate ion (B79s0.10-1, B82s0.11, B88s0.10), PACl-50, and PACl-70 were used as coagulant with a dosage of 0 to 1.5 mg-Al/L. Coagulation pH was 7.0. Settling time was 60 min. Error bars of turbidity and zeta potential indicate standard deviations of three measurements and five measurements, respectively. Details of the mixing conditions are shown in Table 3-6.

Gao and Yue (2005) produced sulfated PACls of different SO_4/Al ratios by base-titration at ambient temperature and reported that a sulfated high-basicity PACl (basicity 67%) with SO_4/Al=0.066 in the range from 0 to 0.15 reduced residual turbidity the most when an experiment consisting of coagulation-flocculation and sedimentation was conducted with lake water. In my experiments, however, the production of sulfated high-basicity PACls at ambient temperature by base-titration was unsuccessful due to the occurrence of aluminum hydroxide precipitation during titration, and I was not able to apply the sulfated high-basicity PACl. Shi *et al.* (2007) also mentioned that room temperature was not suitable for preparation of PACl because a large amount of aluminum precipitate could form during titration.

Yan *et al.* (2008) investigated the relationship between Al species and their behavior in coagulation targeting NOM. They reported that Ala (monomeric species) combined with NOM but most of the flocs formed by Ala were small and difficult to settle. Alb (polymeric species) had high charge-neutralizing ability but flocs formed by Alb were not larger and did not settle faster than those formed by Alc (colloidal species), and Alc adsorbs and removes the target matter most efficiently. In the present study, in addition, given that the major aluminum fraction in PACl-50 and PACl-70 was not Alb but Alc, Alc-type PACls (rich in content of Alc fraction) were also produced (see SI for the preparation method). Those Alc-type PACls showed high charge-neutralization ability, however their flocculation performances were almost the same as the Alb-type PACls and had a low removal efficiency (Fig. 3-34). In summary, Alb or Alc in PACls prepared by base-titration had a high capacity for charge-neutralization, but the bridge-formation ability to form floc particles was poor and resulted in high turbidity after sedimentation.

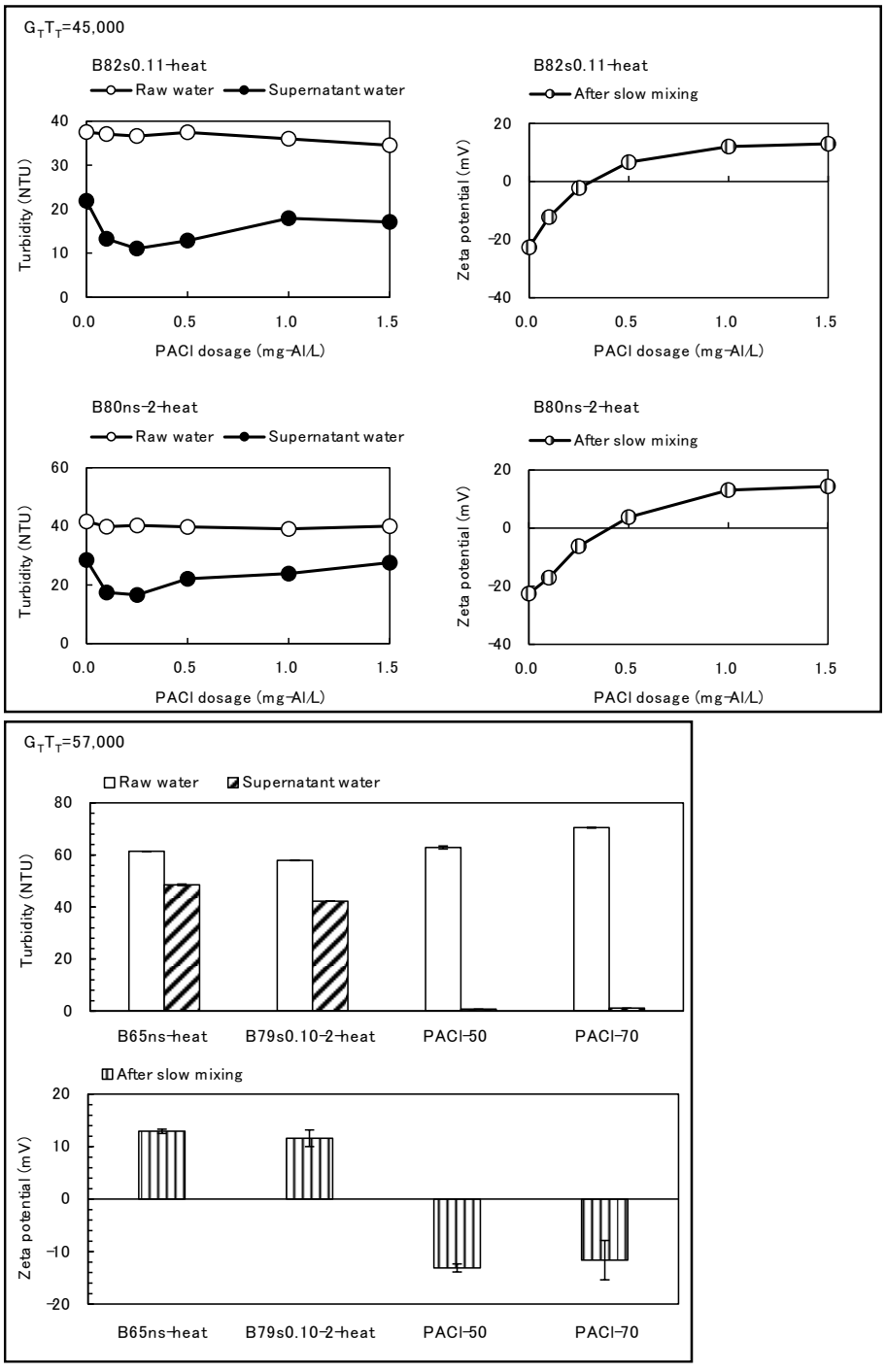

Fig. 3-34. Turbidity removal and zeta potential of carbon particles. Initial SPAC concentration was 10 mg/L. Alc-type base-titration PACls (B82s0.11-heat, B80ns-2-heat, B65ns-heat, and B79s0.10-2-heat), PACl-50, and PACl-70 were used as coagulant with a dosage of 0 to 1.5 mg-Al/L. Coagulation pH was 7.0. Settling time was 60 min. Error bars indicate standard deviations of measurements. Details of the mixing conditions are shown in Table 3-6.

3.3.8 Development and performance of coagulants by $Al(OH)_3$-dissolution

Subsequently, I applied another method to produce PACls: $Al(OH)_3$-dissolution (Table 3-7). Eleven PACls with a basicity of 70% and with a variety of sulfate ion contents were produced (Table 3-7): it was impossible to produce PACls with a basicity >70% because of the gelation of Al solution or the presence of too much undissolved residue. As shown in Fig. 3-35, the performance on reducing residual SPAC particles increased as sulfate content increased from $SO_4/Al=0$ to $SO_4/Al=0.14$ but decreased for $SO_4/Al>0.14$. The preparation of PACls with $SO_4/Al>0.14$ required rising the temperature from 50 °C to 80 °C when adjusting the basicity. In terms of high temperature, this process was similar to the process of base-titration PACls, which do not have sufficient bridge-formation ability. The loss of the bridge-formation ability might be related with a high temperature in production process.

Table 3-7. Coagulants made by $Al(OH)_3$-dissolution.

Name	**Basicity**	**SO_4/Al**	**Cl/Al**	**Na/Al**	**Al content**	**Titrating process**	
						Time	**Temperature**
	%	**mole ratio**	**mole ratio**	**mole ratio**	**mol/L**	**h**	**℃**
B70ns	70	0	1.68	0.78	2	1	50
B70s0.11	70	0.11	1.46	0.79	2	1	50
B70s0.12	70	0.12	1.36	0.69	2.2	1	50
B70s0.13	70	0.13	1.36	0.72	2	1.3	50
B70s0.14-1	70	0.14	1.43	0.79	2.1	1.3	50
B70s0.14-2	70	0.14	1.44	0.81	2.1	1.4	50
B70s0.14-3	70	0.14	1.37	0.75	1.9	1.4	50
B70s0.14-4	70	0.14	1.37	0.75	1.9	1.4	50
B70s0.15-1	70	0.15	1.31	0.71	2.2	1.4	50~77
B70s0.15-2	70	0.15	1.29	0.68	2.1	1.3	50~77
B70s0.17	70	0.17	1.34	0.78	2.1	1	50~80

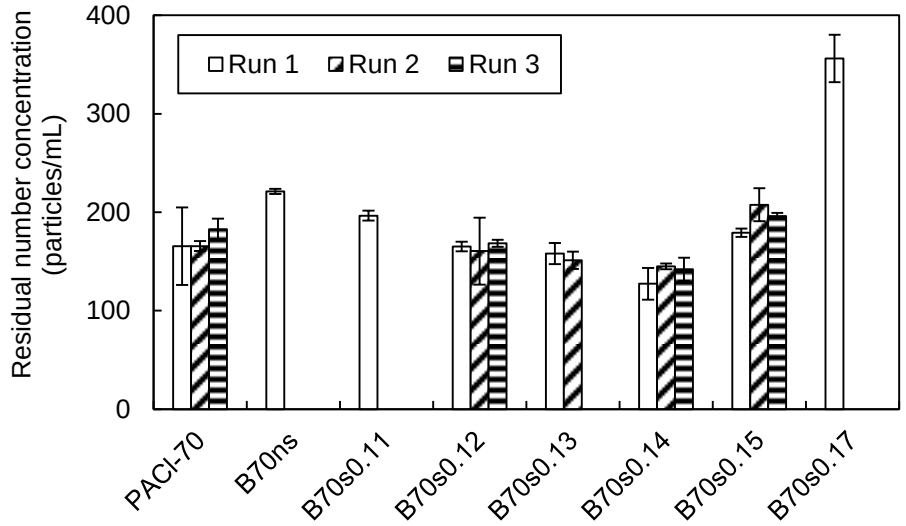

Fig. 3-35. Particle number concentration of residual carbon after CSFs with various PACls. $SPAC_1$ was used. Initial $SPAC_1$ concentration was 10 mg/L. G_TT_T value was fixed at 39,000. Three runs were conducted for PACl-70, B70s0.12, B70s0.14 (B70s0.14-1 was used for all Runs), and B70s0.15 (B70s0.15-1 was used for Run 1, and B70s0.15-2 was used for Run 2 and 3). Two runs were for B70s0.13. One run was conducted for B70ns, B70s0.11, and B70s0.17. Error bars indicate standard deviations of three measurements.

Among the PACls prepared by $Al(OH)_3$-dissolution, B70s0.14 with the SO_4/Al=0.14 showed the highest performance on reducing residual SPAC particles after CSF. B70s0.14 outperformed commercially available PACl-70, which was used in the experiments of the Section 3.3.1-3.3.6 and effectively removed SPAC. As shown in Fig. 3-36A, B70s0.14 highly reduced residual carbon particles at a higher mixing intensity, and was superior to PACl-70 for all mixing conditions tested. The superiority of B70s0.14 to PACl-70 was also confirmed in the experiments where natural water supplemented with SPAC was used (Fig. 3-36B). Moreover, the trend that high G_FT_F results in low concentration of residual carbon particles, which described in the Section 3.3.3, was also observed in the data of natural water. In case of very high G_FT_F (60,000) applied, very low concentrations of residual carbon particles were attained with both B70s0.14 and PACl-70 and their difference was small. Residual carbon particle concentrations obtained in the experiments using river water (Fig. 3-36B) were somewhat lower than those using filtered tap water (Fig. 3-36A). However the

effect of organic matter concentrations and turbidity should not be inferred by the comparison of these two data because the two waters differed in ionic composition as well as organic matter concentrations and turbidity, all of which affect coagulation performance.

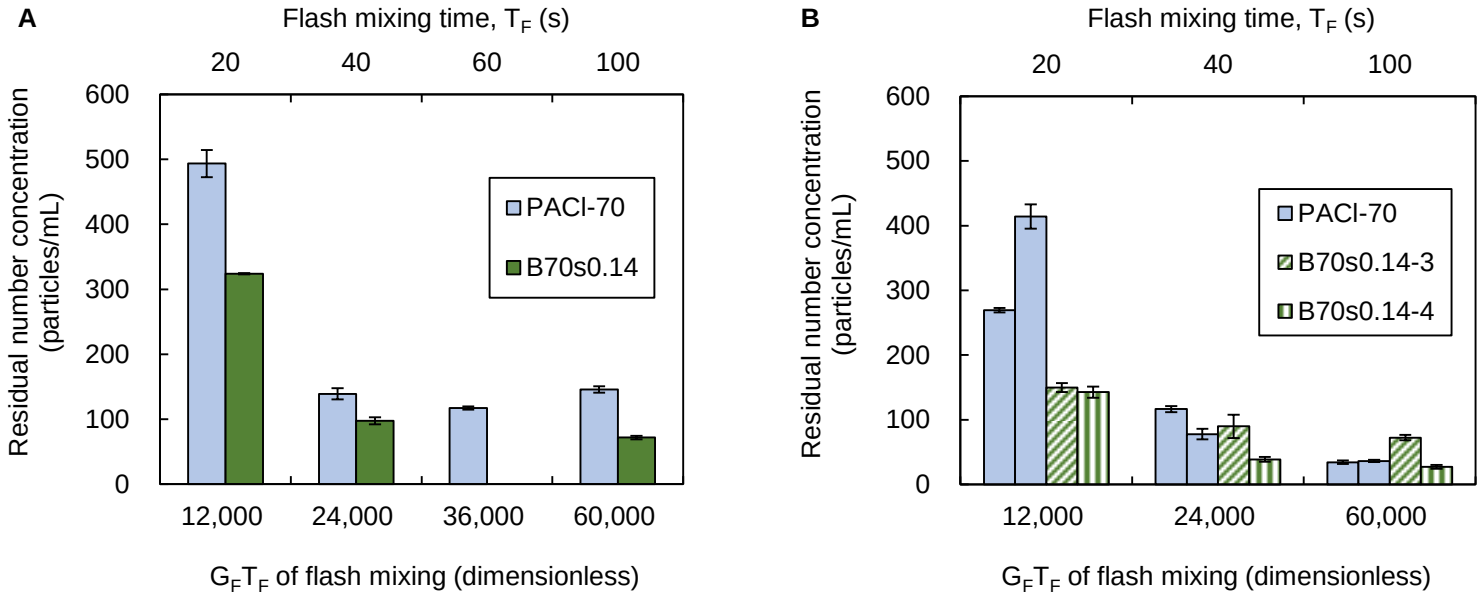

Fig. 3-36. Effect of flash mixing time on the particle number concentration of residual carbon. $SPAC_2$ was used. Initial $SPAC_2$ concentration was 10 mg/L. G_F value was fixed at 600 s^{-1}. G_ST_S of slow mixing was 15,100. Details of the mixing conditions are shown in Table 3-2. Error bars indicate standard deviations of measurements. (A) Filtered tap water supplemented with $SPAC_2$ was used as raw water; PACl-70 and B70s0.14-2 were used as coagulant. (B) River water (turbidity 2.5 NTU and TOC 0.6 mg/L) supplemented with $SPAC_2$ was used as raw water; PACl-70, B70s0.14-3, and B70s0.14-4 were used.

The PACls produced by $Al(OH)_3$-dissolution, including B70s0.14, which showed the high performance on the reduction of residual SPAC after CSF, contained Alc as the main component. However, the percentages of Ala, Alb, and Alc were almost the same as those of the Alc-type PACls prepared by base-titration (Fig. 3-37), which were not effective coagulants. This means that the Al species distribution determined by the ferron method is not informative in evaluating the ability for coagulation treatment targeting SPAC, in particular the ability of floc formation. Base-titration required a high temperature when adjusting the basicity and resulted in a high salt (Na and Cl) content in comparison to $Al(OH)_3$-dissolution. These differences were inferred to influence the ability of floc formation. Studies on PACl produced by $Al(OH)_3$-dissolution are scarcely seen, and further investigations are expected.

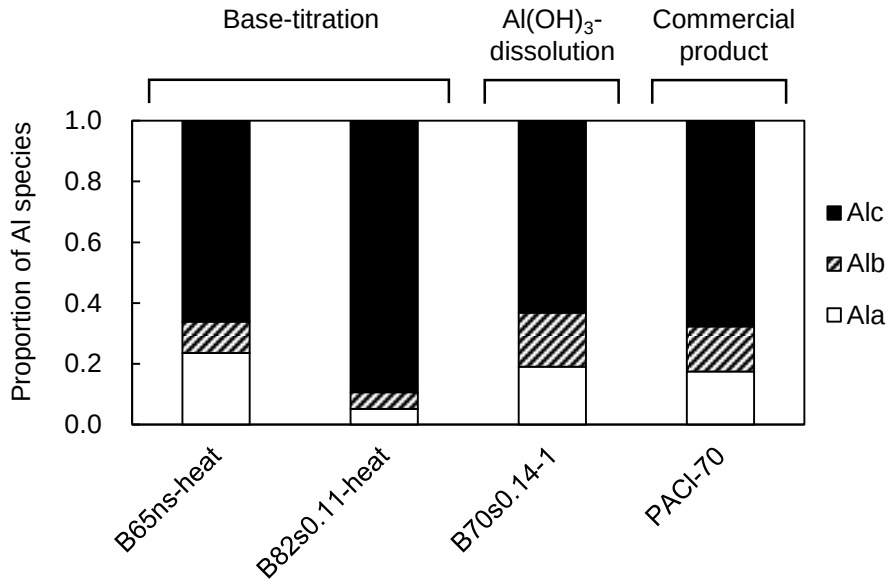

Fig. 3-37. Proportions of Al species in PACl coagulants made by base-titration, $Al(OH)_3$-dissolution, and commercial product.

3.4 Summary

The addition of SPAC in water treatment is a promising technology to remove organic contaminants, but efficient removal of the loaded SPAC is needed. In this study, key control points to attain the high log removal rates of SPAC and to reduce residual SPAC particles at trace concertation levels of 100 to 1000 particles/mL in treated water were examined, and their background mechanisms were discussed, focusing on the process points of coagulation-flocculation and coagulants in CSF. The following conclusions were obtained.

i. A sufficiently large G value in flash mixing for the first step of coagulation was clearly a dominant factor for minimizing residual carbon particle concentration in the treated water after the fourth step of sand filtration. Adequate mixing for coagulation would enable complete dispersion of coagulant thereby reducing the number of particles that were not charge-neutralized. Such particles would pass through the sand filter into the treated water.

ii. In a flow-through mode CSF process using SPAC, the residual carbon concentration in the sand filtrate was dramatically decreased with time during the initial 2 h of filtration due to filter ripening, and a filtrate quality of <200 particles/mL was achieved. The size distribution of the residual carbon particles in the sand filtrate was not changed during the filter-ripening period, suggesting an increase in the efficiency of particle attachment rather than transport to the sand surface during this

period. Therefore, charge-destabilization rather than particle size is likely key for minimizing residual particles.

iii. Commercially available PACls were compared with each other: high-basicity PACl (basicity 70%) was more effective in removing residual carbon particles. It was because the high-basicity PACl had a high charge neutralizing capacity to destabilize many particles, though it formed flocs slowly. However, this superiority of high-basicity PACl was provided by the sufficient flash mixing. Without sufficient flash mixing, not only the removal rate decreased but also the high-basicity PACl became inferior to conventional-basicity PACl.

iv. High-basicity PACl with SO_4/Al=0.14 reduced residual carbon particles down to the minimum concentration. Such a high performance PACl coagulant was produced by using $Al(OH)_3$-dissolution, and the dominant Al species was Alc determined by the ferron method. In contrast, Alb and Alc type PACls produced by base-titration had a high positive charge capacity and were poor at forming floc particles due to lack of bridge-forming ability; this was true even if they were used at a large dosage or the optimal dosage in terms of charge neutralization.

3.5 References

Aguilar, M.I., Sáez, J., Lloréns, M., Soler, A. and Ortuño, J.F. (2003) Microscopic observation of particle reduction in slaughterhouse wastewater by coagulation–flocculation using ferric sulphate as coagulant and different coagulant aids. Water Research 37(9), 2233-2241.

Bratby, J. (2006) Coagulation and Flocculation in Water and Wastewater Treatment, IWA Publishing.

Carns, K.E. and Stinson, K.B. (1978) Controlling Organics: The East Bay Municipal Utility District Experience. Journal (American Water Works Association) 70(11), 637-644.

Crittenden, J.C., Trussell, R.R., Hand, D.W., Howe, K.J. and Tchobanoglous, G. (2012) MWH's Water Treatment Principles and Design, Third Edition, John Wiley & Sons, Inc.

Edzwald, J.K. (2011) WATER QUALITY & TREATMENT A Handbook on Drinking Water, American Water Works Association, American Society of Civil Engineers, McGraw-Hill.

Gao, B. and Yue, Q. (2005) Effect of SO4 2-/Al3+ ratio and OH-/Al3+ value on the characterization of coagulant poly-aluminum-chloride-sulfate (PACS) and its coagulation performance in water treatment. Chemosphere 61(4), 579-584.

Gao, B.Y., Chu, Y.B., Yue, Q.Y., Wang, B.J. and Wang, S.G. (2005) Characterization and coagulation of a polyaluminum chloride (PAC) coagulant with high Al13 content. J Environ Manage 76(2), 143-147.

Gifford, J.S., George, D.B. and Adams, V.D. (1989) Synergistic effects of potassium permanganate and PAC in direct filtration systems for THM precursor removal. Water Research 23(10), 1305-1312.

Hendricks, D. (2010) Fundamentals of water treatment unit processes: physical, chemical, and biological, CRC Press Inc., London.

Jia, He, F. and Liu (2004) Synthesis of Polyaluminum Chloride with a Membrane Reactor: Operating Parameter Effects and Reaction Pathways. Industrial & Engineering Chemistry Research 43(1), 12-17.

Kan, C., Huang, C. and Pan, J.R. (2002) Time requirement for rapid-mixing in coagulation. Colloids and Surfaces A: Physicochemical and Engineering Aspects 203(1), 1-9.

Kimura, M., Matsui, Y., Kondo, K., Ishikawa, T.B., Matsushita, T. and Shirasaki, N. (2013) Minimizing residual aluminum concentration in treated water by tailoring properties of polyaluminum coagulants. Water Research 47(6), 2075-2084.

Kobayashi, S., Matsui, Y., Nakazawa, Y., Shinno, K., Abe, T., Matsushita, T. and Shirasaki, N. (2019) Survey of Residual Concentration of Powdered Activated Carbon in Rapid Sand Filtration System - Using Automatic Carbon Particles Counting Method (in Japanese), Japan Water Works Association, Hakodate, Hokkaido, Japan.

Lin, J.-L., Pan, J.R. and Huang, C. (2013) Enhanced particle destabilization and aggregation by flash-mixing coagulation for drinking water treatment. Separation and Purification Technology 115, 145-151.

Lin, J.L., Chin, C.J., Huang, C., Pan, J.R. and Wang, D. (2008) Coagulation behavior of Al(13) aggregates. Water Res 42(16), 4281-4290.

Matsui, Y., Aizawa, T., Kanda, F., Nigorikawa, N., Mima, S. and Kawase, Y. (2007) Adsorptive removal of geosmin by ceramic membrane filtration with super-powdered activated carbon. Journal of Water Supply: Research and Technology-Aqua 56(6-7), 411-418.

Matsui, Y., Hasegawa, H., Ohno, K., Matsushita, T., Mima, S., Kawase, Y. and Aizawa, T. (2009) Effects of super-powdered activated carbon pretreatment on coagulation and trans-membrane pressure buildup during microfiltration. Water Research 43(20), 5160-5170.

Matsui, Y., Shirasaki, N., Yamaguchi, T., Kondo, K., Machida, K., Fukuura, T. and Matsushita, T. (2017) Characteristics and components of poly-aluminum chloride coagulants that enhance arsenate removal by coagulation: Detailed analysis of aluminum species. Water Res 118, 177-186.

Nakazawa, Y., Matsui, Y., Hanamura, Y., Shinno, K., Shirasaki, N. and Matsushita, T. (2018) Identifying, counting, and characterizing superfine activated-carbon particles remaining after coagulation, sedimentation, and sand filtration. Water Research 138, 160-168.

Pan, L., Nishimura, Y., Takaesu, H., Matsui, Y., Matsushita, T. and Shirasaki, N. (2017) Effects of decreasing activated carbon particle diameter from 30 μm to 140 nm on equilibrium adsorption capacity. Water Res 124, 425-434.

Parker, D.R. and Bertsch, P.M. (1992) Identification and quantification of the "Al13" tridecameric aluminum polycation using ferron. Environmental Science & Technology 26(5), 908-914.

Parthasarathy, N. and Buffle, J. (1985) Study of polymeric aluminium(III) hydroxide solutions for application in waste water treatment. Properties of the polymer and optimal conditions of preparation. Water Research 19(1), 25-36.

Sato, F. and Matsuda, S. (2009) Novel Basic Aluminum Chloride, its Manufacturing Method and its Application., Japan.

Shi, B., Li, G., Wang, D. and Tang, H. (2007) Separation of Al13 from polyaluminum chloride by sulfate precipitation and nitrate metathesis. Separation and Purification Technology 54(1), 88-95.

Wang, D., Sun, W., Xu, Y., Tang, H. and Gregory, J. (2004) Speciation stability of inorganic polymer flocculant–PACl. Colloids and Surfaces A: Physicochemical and Engineering Aspects 243(1), 1-10.

Wang, D., Tang, H. and Gregory, J. (2002) Relative Importance of Charge Neutralization and Precipitation on Coagulation of Kaolin with PACl: Effect of Sulfate Ion. Environmental Science & Technology 36(8), 1815-1820.

Wu, X., Ge, X., Wang, D. and Tang, H. (2007) Distinct coagulation mechanism and model between alum and high Al13-PACl. Colloids and Surfaces A: Physicochemical and Engineering Aspects 305(1), 89-96.

Yan, M., Wang, D., Ni, J., Qu, J., Chow, C.W. and Liu, H. (2008) Mechanism of natural organic matter removal by polyaluminum chloride: effect of coagulant particle size and hydrolysis kinetics. Water Research 42(13), 3361-3370.

Younker, J.M. and Walsh, M.E. (2016) Effect of adsorbent addition on floc formation and clarification. Water Research 98, 1-8.

Zhao, B., Wang, D., Li, T., Chow, C.W.K. and Huang, C. (2010) Influence of floc structure on coagulation–microfiltration performance: Effect of Al speciation characteristics of PACls. Separation and Purification Technology 72(1), 22-27.

Zhao, H., Peng, J., Lin, S. and Zhang, Y. (2009) Covalently Bound Organic Silicate Aluminum Hybrid Coagulants: Preparation, Characterization, and Coagulation Behavior. Environmental Science & Technology 43(6), 2041-2046.

4 BEHAVIOR OF SUPERFINE POWDERED ACTIVATED CARBON PARTICLES IN TREATMENT PROCESSES

4.1 Introduction

SPAC has attracted a large attention as an excellent adsorbent from researchers and plant operators (Amaral *et al.* 2016, Ando *et al.* 2010, Ando *et al.* 2011, Apul *et al.* 2017, Ateia *et al.* 2019, Bonvin *et al.* 2016, Decrey *et al.* 2020, Dunn and Knappe 2019, Jiang *et al.* 2015, Matsui *et al.* 2015, Matsui *et al.* 2013, Matsui *et al.* 2012, Murray *et al.* 2019, Partlan *et al.* 2020). Such a superfine adsorbent particles need an adequate removal treatment, when it is applied in practical use (American Society of Civil Engineers and American Water Works Association 1998, Bureau of Waterworks Tokyo Metropolitan Government 2014). In a case with using SPAC in CSF treatment, if coagulation and flocculation are performed well, there should be few residual carbon particles in the treated water. That is because proper coagulation and flocculation results in the formation of large floc particles with good settling properties and water with low turbidity after settling and filtration. However, the previous chapters have shown that although carbon particles in raw water are effectively charge neutralized by coagulation treatment, resulting in good floc formation, some carbon particles still persist in the sand filtrate and that these particles lack charge neutralization. This suggests that although the size and settleability of floc particles and the persistence of residual particles in sand filtrate are determined by the performance of the coagulation–flocculation process, they reflect the results of different aspects of the process and are not necessarily interrelated.

Accordingly, this chapter aims to disclose the behavior of carbon particles during the CSF process. Particles after coagulation are supposed to be classified into two groups: particles that can grow into floc particles and those that cannot grow into floc particles. The latter particles are determined by using the method established in Chapter 2, and are examined as a source of the residual particles remaining in finished water, taking account of a charge-state and a size of particles.

This chapter has been already published by Elsevier, and the information is described as follows:

Title: Stray particles as the source of residuals in sand filtrate: Behavior of superfine powdered activated carbon particles in water treatment processes

Author: Nakazawa, Y.; Abe, T.; Matsui, Y.; Shirasaki, N.; Matsushita, T.

Name of journal: Water Research

Year: 2021

Volume: 190

Pages: 116786

DOI: https://doi.org/10.1016/j.watres.2020.116786

4.2 Materials and methods

4.2.1 Coagulants and activated carbon particles

Two kinds of commercially available poly-aluminum chloride (PACl), provided by Taki Chemical Co., Ltd. (Hyogo, Japan), were used as coagulants: PACl-70 (basicity, 2.1; %basicity, 70%; sulfate ion, 2.2 wt%) and PACl-50 (basicity, 1.5; %basicity, 50%; sulfate ion, 2.9 wt%). The Al speciation (Ala, monomeric Al species; Alb, polymeric Al species; and Alc, colloidal species) distributions of the PACls were determined by the Ferron method (Wang *et al.* 2004), which uses the difference in reaction time with Ferron reagent (8-hydroxy-7-iodoquinoline-5-sulfonic acid; Fujifilm Wako Pure Chemical Corporation, Osaka, Japan) to distinguish between the different Al species. The procedure of Kimura *et al.* (2013) was applied, as described in Section 7.4.

SPAC was prepared in our laboratory by wet ball milling (Nikkato, Osaka, Japan) for 6 h followed by wet bead milling for 30 min (LMZ015; Ashizawa Finetech, Ltd., Chiba, Japan), as described in detail elsewhere (Pan *et al.* 2017). The concentrations and particle sizes of carbon particles in water samples obtained from the CSF experiment were determined by membrane filtration (nominal pore diameter, 0.1 μm; Φ25 mm; polytetrafluoroethylene; Merck KGaA) and microscopic image analysis (1000× magnification; VHX-2000; Keyence Corporation, Osaka, Japan), as described in detail in Section 2.2.3.

4.2.2 Flow-through reactor tests of coagulation–flocculation, sedimentation, and rapid sand filtration

A series of flow-through mode CSF tests were performed using a bench-scale CSF plant comprising five components: preparation unit, rapid mixing unit for coagulation, slow mixing unit for flocculation, sedimentation unit, and sand filter (Fig. 3-3 and Table 3-3). The rapid mixing unit constituted a single-chambered reactor or a 3-chambered-reactor with three equally-sized chambers; the two reactors had the same total hydraulic retention time (HRT) of 100 s. The slow mixing unit constituted a single-chambered reactor or a 4-chambered reactor, both with four mixing impellers and the same total HRT of 2400 s. Regardless of reactor configuration, rapid mixing for coagulation was conducted at a fixed mixing intensity (G value: velocity gradient) of 600 s^{-1} for 100 s, and slow mixing for flocculation was conducted at a fixed G value of 12.5 s^{-1} for 2400 s. Residence time distributions of the reactors were measured via a step tracer test using NaCl as the tracer and conductivity detection (Crittenden *et al.* 2012). To prevent the effects of wind and temperature-induced density current, the bench-scale CSF plant was installed in a constant-temperature room with no wind, and the water temperature was kept at the same as the room temperature.

Toyohira River water, collected at the Moiwa Water Purification Plant, Sapporo, Japan (hereafter ‘River water 1’), was used as the raw water. We also used dechlorinated Sapporo municipal water (Municipal waters 1–3 and 5–7; Table 4-2) was also used because only a limited volume of River water was available. Raw water was pumped into the first mixing chamber of the preparation unit, and SPAC was added in the second mixing chamber at a concentration of 2 mg/L (3–5 × 10^6 particles/mL), which is a typical dose when SPAC is used as an adsorbent (Matsui *et al.* 2007). After the addition of NaOH or HCl to adjust the pH to 7.0, a coagulant (PACl) was injected into the coagulation reactor at a dose of 1.5 mg-Al/L, unless otherwise noted; the dose was predetermined to bring the

settling turbidity down to less than 2 NTU. After coagulation–flocculation, the water flowed through a sedimentation reactor, which had a HRT of 65 min. After sedimentation, the supernatant flowed to a sand filter. Sand filtration was conducted at a rate of 90 or 150 m d^{-1} using a 4-cm diameter column filled with sand (effective diameter, 0.94 mm; uniformity, 1.24; Nihon Genryo Co., Ltd., Japan) to a depth of 50 cm.

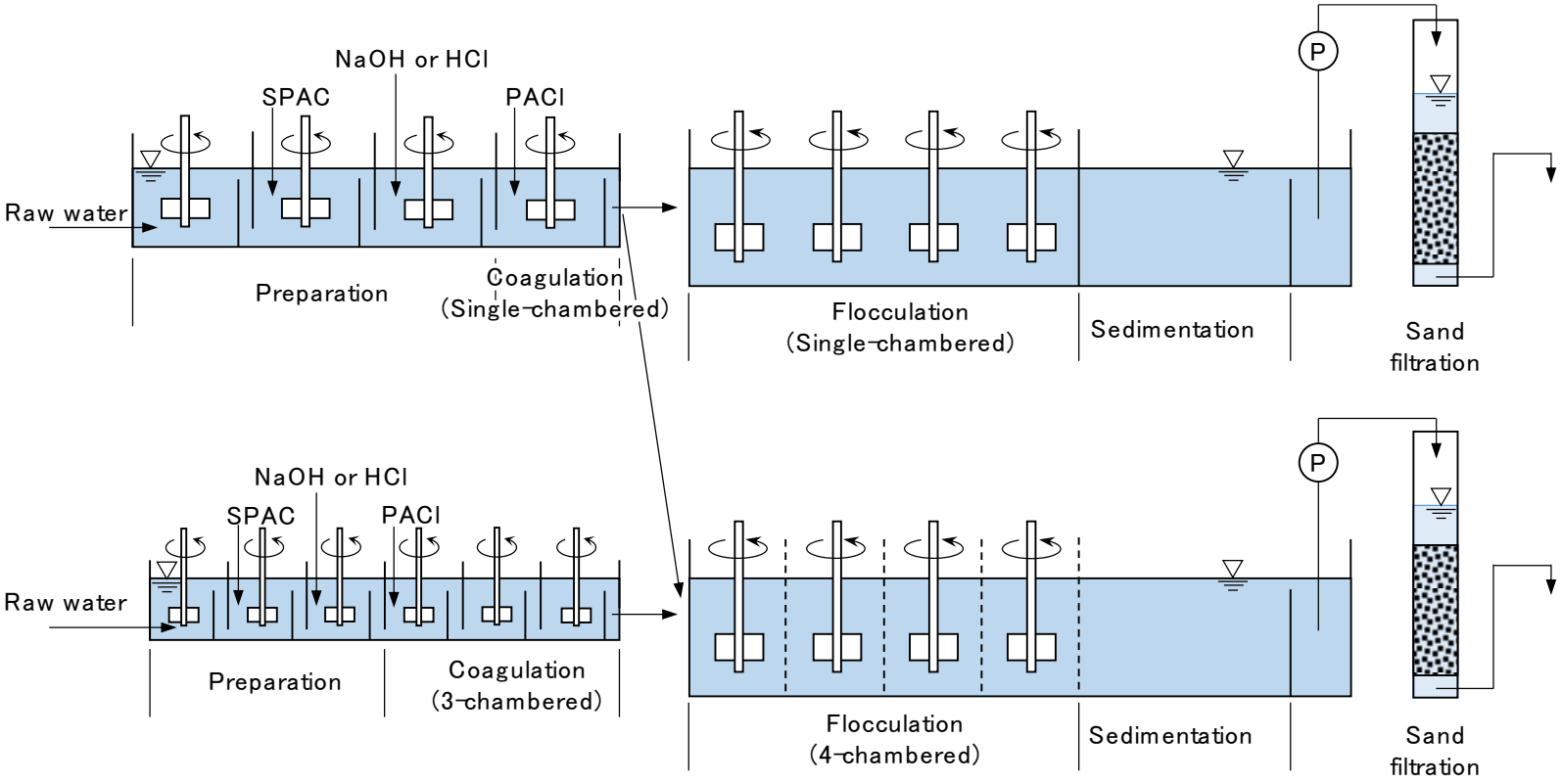

Fig. 4-1. Schematic diagram of the bench-scale CSF plant.

Table 4-1. Specifications of the bench-scale coagulation–flocculation, sedimentation, and rapid sand filtration plant.

Component	Type	Number of chambers	Length × width × height per chamber	Water depth	Volume per chamber	Hydraulic retention time per chamber	G value
			cm	cm	L	s	s^{-1}
Preparation unit	Connected to the single-chambered coagulation reactor	3	9.5 × 9.5 × 15	9.2	0.83	100	600
	Connected to the 3-chambered coagulation reactor	3	6.6 × 6.6 × 12	6.4	0.28	33	600
Coagulation reactor	Single-chambered reactor	1	9.5 × 9.5 × 15	9.2	0.83	100	600
	3-chambered reactor	3	6.6 × 6.6 × 12	6.4	0.28	33	600
Flocculation reactor	Single-chambered reactor	1	56 × 19 × 25	19	20	2400	12.5
	4-chambered reactor	4	14 × 19 × 25	19	5	600	12.5

Component	Length × width × height	Water depth	Volume	Hydraulic retention time	Overflow rate
	cm	cm	L	s	mm min^{-1}
Sedimentation reactor	88 × 19 × 25	19	32	3900	3.0

Component	Outer diameter of column	Inner diameter of column	The column to particle diameter ratio	Length of column	Effective diameter of sand	Uniformity coefficient of sand	Sand depth	Filtration rate
	cm	cm		cm	mm		cm	m d^{-1}
Sand filter	4	3.6	40	140 or 90	0.94	1.24	50	90 or 150

Table 4-2. Raw waters used in this chapter.

Raw water	Turbidity	Black particle concentration	DOC	Alkalinity	Na^+	K^+	Mg^{2+}	Ca^{2+}	Cl^-	NO_3^-	SO_4^{2-}	
	NTU	particles/mL	mg/L	mg/L as $CaCO_3$	mg/L	mg/L	mg/L	mg/L	mg/L	mg/L	mg/L	
River water 1	2.3	no data	0.8	16	12	2.1	1.8	10	21	1.5	20	Fig. 4-13, Fig. 4-14
River water 2	13	16	3.7	76	44	5.8	9.3	19	19	<0.14	6.1	Fig. 4-11
Municipal water 1	0.1	15	0.6	18	15	2.3	2.4	11	23	0.8	21	Fig. 4-11, Fig. 4-12
Municipal water 2	0.1	no data	0.5	20	17	2.6	2.1	10	24	1	19	Fig. 4-2 (PACl-70), Fig. 4-3 (PACl-70), Fig. 4-4 (PACl-70), Fig. 4-5 (PACl-70)
Municipal water 3	0.1	no data	0.6	20	18	2.6	1.6	11	28	0.8	19	Fig. 4-2 (PACl-50), Fig. 4-3 (PACl-50), Fig. 4-4 (PACl-50), Fig. 4-5 (PACl-50)
Municipal water 4	no data	no data	0.4	20	12	0.8	2.4	7	11	0.9	18	Fig. 4-6
Municipal water 5	0.1	no data	no data	16	13	1.7	1.8	9	23	0.9	18	Fig. 4-7, Fig. 4-8, Fig. 4-9, Fig. 4-10

4.2.3 Batch tests of coagulation–flocculation

Three series of batch tests were conducted to examine the removal of SPAC by coagulation–flocculation, measure the zeta potential of the carbon particles, and examine changes in the aluminum species distribution during coagulation–flocculation.

To examine SPAC coagulation–flocculation, 1 L of dechlorinated municipal drinking water (Municipal water 1; Table 4-2) or Wanigawa River water (Ibaraki, Japan; hereafter 'River water 2'; Table 4-2), was transferred to a rectangular beaker, supplemented with SPAC at a concentration of 2 mg/L, and used for the tests. After adding NaOH (0.05 N) to bring the pH to 7.0, one of the PACls (1.5 mg-Al/L) was injected, and the water was subjected to rapid mixing ($G = 600\ s^{-1}$) for coagulation; samples of the water were collected at predetermined times and used for analysis. In some tests, after the rapid mixing for 100 s, the water was subjected to slow mixing ($G = 12.5\ s^{-1}$) to flocculation.

To measure zeta potentials, raw water (Municipal water 4; Table 4-2) was treated as described above, but PACl doses of 1.5 and 2.0 mg-Al/L were used. At 100 s from the start of rapid mixing, a 55-mL sample of water was collected and used for the measurement of the zeta potential (Zetasizer Nano ZS; Malvern, United Kingdom) of the carbon particles; 10 mL was used immediately for the measurement of zeta potential, and the remaining 45 mL was used after being subjected to centrifugal separation (see Section 4.2.4).

To examine the changes in the aluminum species distributions, raw water (Municipal water 1) was treated as described above, but after adding NaOH to bring the pH to 7.0, one of the PACls was injected at a concentration of 270 mg-

Al/L. Rapid mixing ($G = 381\ s^{-1}$) was then conducted without SPAC. Immediately after sampling at predetermined times, the water was used for Ferron analyses with a glass cell (optical path length, 10 cm). The municipal water itself had little effect on the absorbance determined by Ferron analysis (blank test, data not shown).

4.2.4 Collection of stray particles by centrifugation

In the water samples collected during rapid and slow mixing processes in the flow-through reactor tests and batch tests, particles that had not settled after centrifugation were considered to be stray particles. The centrifuge procedure was as follows. Aliquots (45 mL) of a single water sample were dispensed into four 50-mL glass tubes. The tubes were centrifuged by using a centrifuge (CT6E; Eppendorf Himac Technologies Co., Ltd., Ibaraki, Japan) equipped with a swing rotor (T5SS; Eppendorf Himac Technologies Co., Ltd.). Centrifugation was carried out at 4800 rpm (3990g) for 10 min, halted, and then re-started for 20, 35, or 50 min (total time, 30, 45, and 60 min, respectively). The reason for the double centrifugation is discussed in Section 4.3.1. Thereafter, the concentrations of carbon particles in the centrifugal supernatant were determined by membrane filtration and microscopic image analysis (see also Section 7.5).

4.3 Results and Discussion

4.3.1 Stray particles as the source of the residual particles

As discussed in Section 3.3.4, less-charge-neutralized carbon particles with a size of 0.3–2 μm remained in the sand filtrate. I assumed that such particles were

particles that had not reacted with the coagulant during the coagulation–flocculation process (these particles was named ‘stray particles’) and then evaded being captured by the filter media. Based on this assumption, I next examined the relationship between residual carbon particle concentration and stray carbon particle concentration to see whether the stray carbon particle concentration could be used as an index of residual carbon particle concentration. In addition, the effect of coagulant dose on the stray carbon particle concentration and the residual carbon particle concentration in sand filtrate was examined. To do these, I determined the stray particle concentration in the centrifuged supernatant of water samples collected after coagulation treatment.

First, however, the conditions used for centrifugal separation was optimized. In test trials, it was found that preliminary centrifugation for 10 min was sufficient to allow large floc particles to settle. I also found that adhesion to the centrifuge tube wall could be minimized by conducting a second centrifugation after the preliminary centrifugation. In centrifugal separation, a brake is usually applied to stop the rotation of the centrifuge. However, it was found that small amounts of the particles were re-suspended by this braking operation. Therefore, the re-suspension of particles was minimized by waiting for the rotation to stop naturally. I also examined how total centrifugation time (the total time for both centrifugation stages) affected residual carbon particle concentration in the supernatant (Fig. 4-2). It was found that the residual carbon particle concentration after centrifugal separation markedly decreased when the centrifuge time was extended from 30 to 45 min, but that it did not further decrease when the time was extended to 60 min. I also found that the particle concentration after centrifugation for 45 min did not vary depending on coagulant dose (Fig. 4-2b), even though I found that the particle concentration in sand filtrate did vary (Fig. 4-3). Based on my findings, a centrifugal separation time of 30 min was used to determine stray particle concentrations in the subsequent experiments.

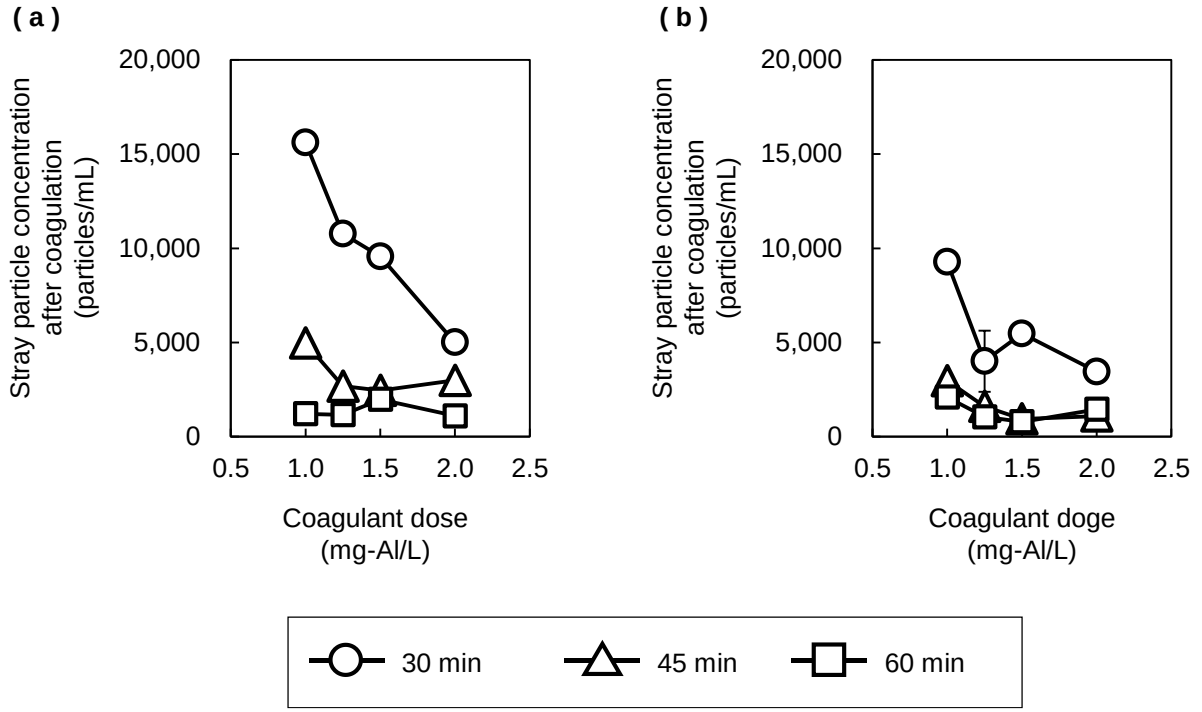

Fig. 4-2. Effect of coagulant dose on stray carbon particle concentration after coagulation with rapid mixing. PACl-50 (a) or PACl-70 (b) was used as the coagulant. Stray particles were collected from water sampled after coagulation by using a double-centrifugation method to remove floc particles. Total centrifugation times were 30 min (circles), 45 min (triangles), and 60 min (squares). Municipal water 2 (PACl-70) or Municipal water 3 (PACl-50) was used as the raw water. SPAC initial concentration, 2.0 mg/L. Coagulation, single-chambered reactor, G = 600 s^{-1}.

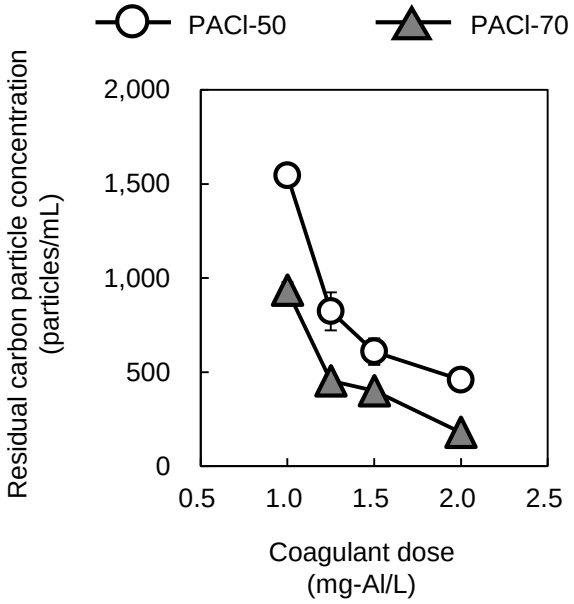

Fig. 4-3. Effect of coagulant dose on residual carbon particle concentration in sand filtrate. PACl-50 or PACl-70 was used as the coagulant at 1.0, 1.25, 1.5, or 2.0 mg-Al/L. Municipal water 2 (PACl-70) or Municipal water 3 (PACl-50) was used as the raw water. SPAC initial concentration, 2.0 mg/L. Coagulation, single-chambered reactor, G = 600 s^{-1}; flocculation, 4-chambered reactor, G = 12.5 s^{-1}; filtration rate, 90 m d^{-1}. The experimental conditions were the same as described in the caption to Fig. 4-5.

The stray carbon particles and the residual carbon particles were similarly smaller than the particles before the CSF treatment (Fig. 4-4). The concentrations were decreased with increasing PACl dosage (Fig. 4-5a). In addition, the stray particle concentration was found to be highly correlated with residual carbon particle concentration in the sand filtrate (R^2 = 0.89, square of Pearson's correlation coefficient). Thus, the stray particle concentration of the supernatant, which was determined after centrifugation for 30 min, was considered an index of the residual particle concentration in the sand filtrate. Furthermore, it was found that the concentration of stray particles decreased during coagulation with rapid mixing. After coagulation, the concentration of stray particles (maximum, 1.5 × 10^4 particles/mL, Fig. 4-5a) was less than 0.4% that of the initial suspension before coagulation (3–5 × 10^6 particles/mL). I also examined the correlation between the residual carbon particle concentration in the sand filtrate and the turbidity of settled water, which is conventionally used as an indicator of

treatment performance with respect to the removal of suspended matter, but I found a lower correlation (R^2 = 0.72) than that found for stray particle concentration (Fig. 4-5). Thus, stray particle concentration obtained by centrifugation was considered a better index of residual particle concentration than was the turbidity of water. It is important to note here that stray particle concentration was measured at an early stage of the CSF process (after coagulation), whereas turbidity was measured later in the process (after coagulation–flocculation and sedimentation). This suggests that the performance of the coagulation treatment, but not of the flocculation and sedimentation treatment, is the major determinant of the concentration of residual particles remaining after sand filtration. This is discussed further in Section 4.3.2.

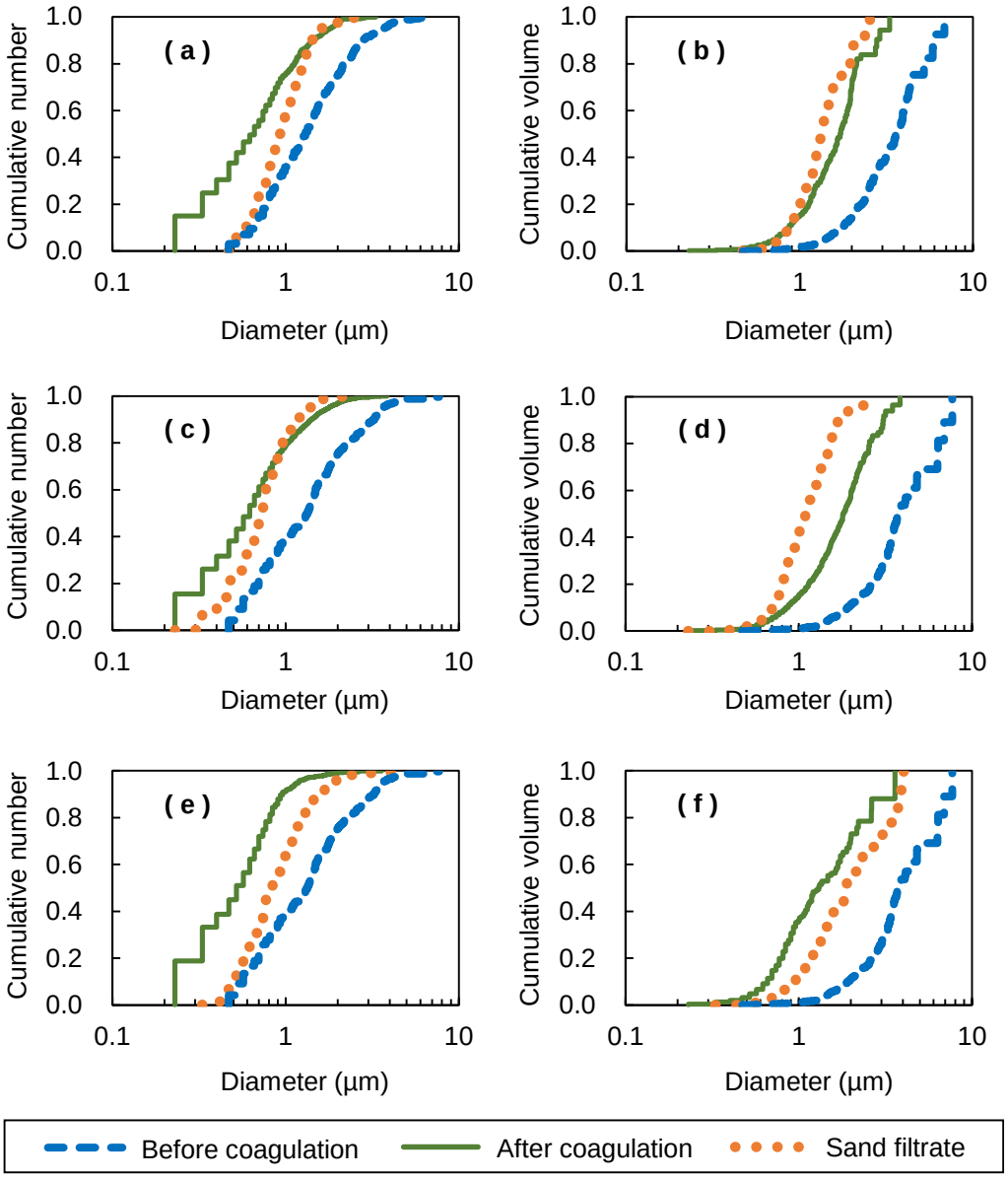

Fig. 4-4. Particle size distributions of carbon particles in water samples; cumlative number (a, c, e) or cumlative volume (b, d, f). Water samples were collected after coagulation, subjected to centrifugal separation treatment (see Section 4.2.4), and the supernatants were examined for particle size distribution. Water sampled before coagulation and sand filtrate were also examined. Particle sizes were determined by using membrane filtration and microscopic image analysis. Municipal water 2 (a, b) or Municipal water 3 (c, d, e, f) was used as the raw water. SPAC initial concentration, 2.0 mg/L. Coagulant, PACl-70 (a, b) or PACl-50 (c, d, e, f), 1.5 mg-Al/L (c, d) or 2.0 mg-Al/L (a, b, e, f). The experimental conditions were the same as described in the caption to Fig. 4-5.

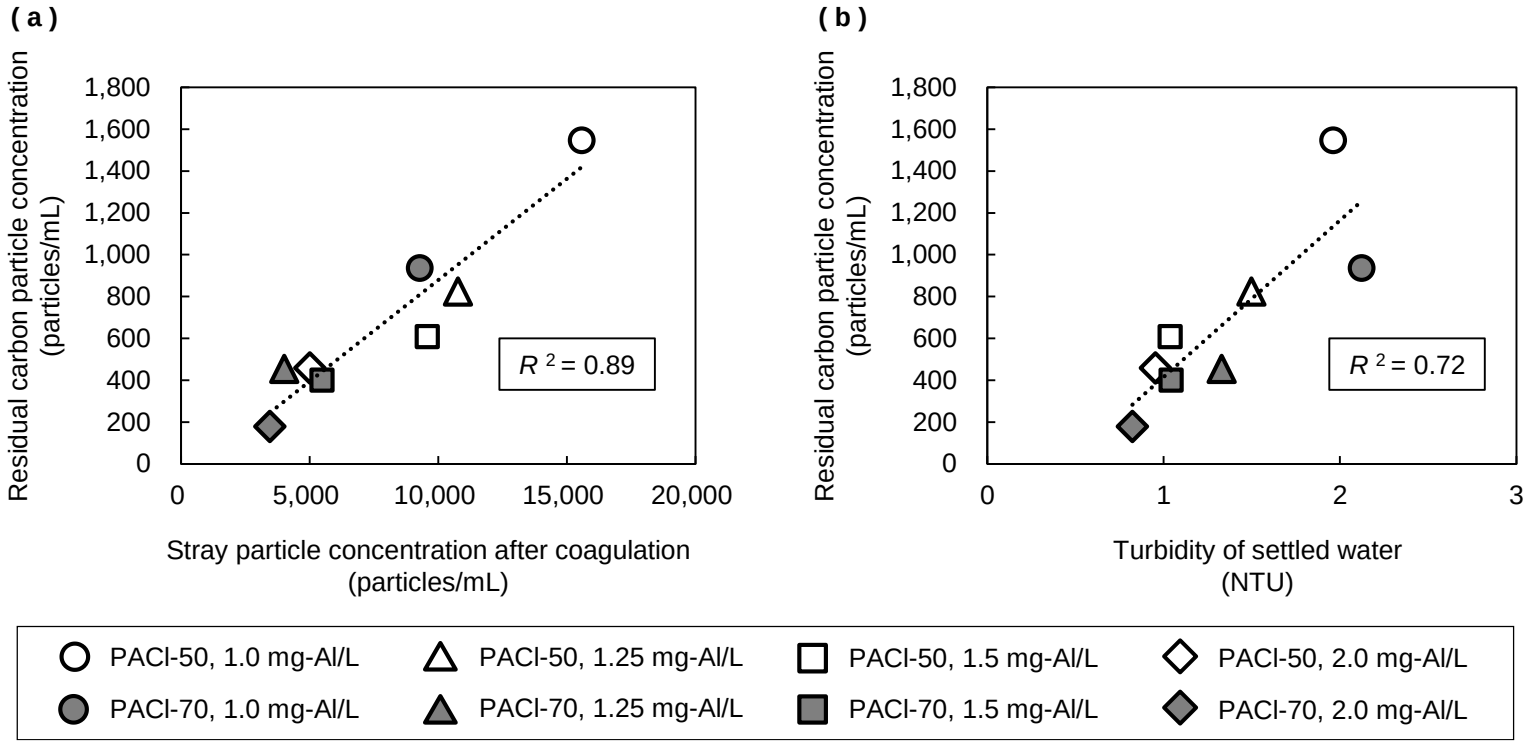

Fig. 4-5. Correlation between residual carbon particle concentration in sand filtrate and stray carbon particle concentration after coagulation with rapid mixing (a), and between residual carbon particle concentration of sand filtrate and turbidity of settled water (b). Municipal water 2 (PACl-70) or Municipal water 3 (PACl-50) was used as the raw water. SPAC initial concentration, 2.0 mg/L. Coagulant (PACl-50 or PACl-70), 1.0, 1.25, 1.5, or 2.0 mg-Al/L. Coagulation, single-chambered reactor, G = 600 s^{-1}; flocculation, 4-chambered reactor, G = 12.5 s^{-1}; filtration rate, 90 m d^{-1}.

Next, the zeta potentials of bulk particles and stray particles in water samples collected after coagulation was examined (Fig. 4-6). The bulk particles were charged-neutralized and had zero or only a slightly positive/negative charge. In contrast, the stray particles, which were only a portion of these particles, had a negative charge. This finding that the stray particles had less charge neutralization was similar to the previous researches. Ding *et al.* (2016) report that meso-particles (20 nm–0.5 μm) remained with less charge-neutralization in comparison with the larger floc particles when surface water was treated by coagulation. Yu *et al.* (2015) report that the zeta potential of the remaining flocs became more negative after sedimentation process. A similar phenomenon was also observed for the residual carbon particles in the sand filtrate, which had less charge neutralization compared with the bulk particles sampled after coagulation (see also Chapter 2), although the zeta potentials of the stray particles showed that they had a less-negative charge than did the residual carbon particles. This is thought to be because most of the stray particles with less-negative charges are preferentially removed by the sand filter, as will be discussed in Section 4.3.4.

Together, these findings further support the idea that stray carbon particles are the main source of the residual carbon particles in sand filtrate. This suggests that coagulation–flocculation treatments should be optimized not only to decrease settling turbidity via the formation of large-size floc particles but also to reduce the number of stray particles.

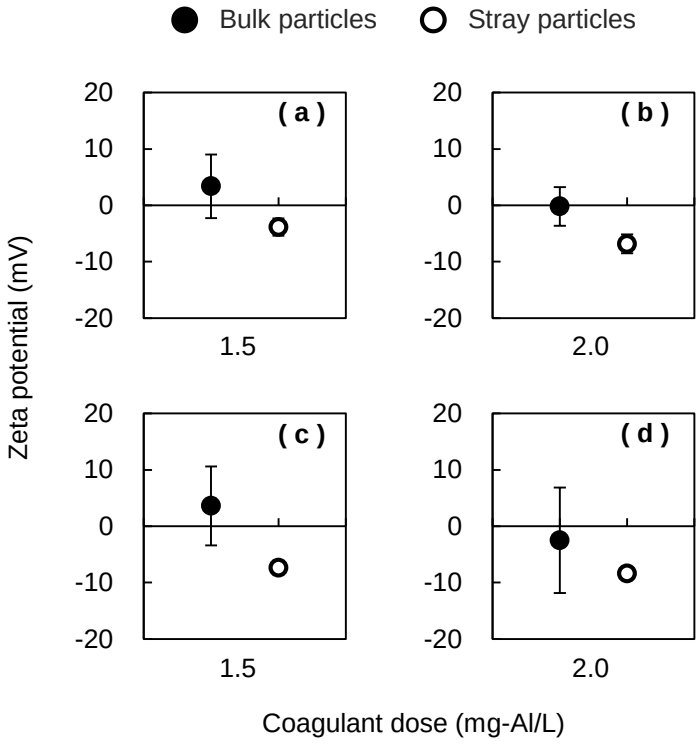

Fig. 4-6. Comparison of the zeta potentials of bulk particles and stray carbon particles after coagulation. Water samples were collected after coagulation with rapid mixing. The zeta potentials of bulk particles were determined for each sample without further processing. The zeta potentials of the stray particles were determined after the samples were subjected to centrifugal separation. Municipal water 4 was used as the raw water. SPAC initial concentration, 2.0 mg/L; coagulant, PACl-70 (a, b) or PACl-50 (c, d), 1.5 or 2.0 mg-Al/L. This was a batch-type coagulation test using a 1-L rectangular beaker and a mixing velocity of G = 600 s^{-1}. The error bars represent standard deviations of measurements.

4.3.2 Effect of mixing reactor configuration on the concentrations of stray particles and residual particles

The effect of coagulation reactor (rapid mixing unit) configuration on residual carbon particle concentration in sand filtrate was examined in Section 3.3.5. Although the single-chambered reactor and the 3-chambered reactor had the same mixing intensity (G value) and HRT, a lower residual carbon particle concentration was obtained with the 3-chambered reactor than with the single-chamber reactor (Fig. 3-23, Fig. 3-24, and Fig. 3-23a). The same trend was observed for stray particle concentrations in water sampled at the end of flocculation: use of the single-chambered coagulation reactor resulted in a higher stray particle concentration (Fig. 3-23b). Thus, when a large proportion of the

residence time distribution included short residence times, which was observed in the distribution for the single-chambered reactor (Fig. 3-21 and Fig. 3-22), the stray particle concentration was increased, which subsequently increased the residual carbon particle concentration in the sand filtrate.

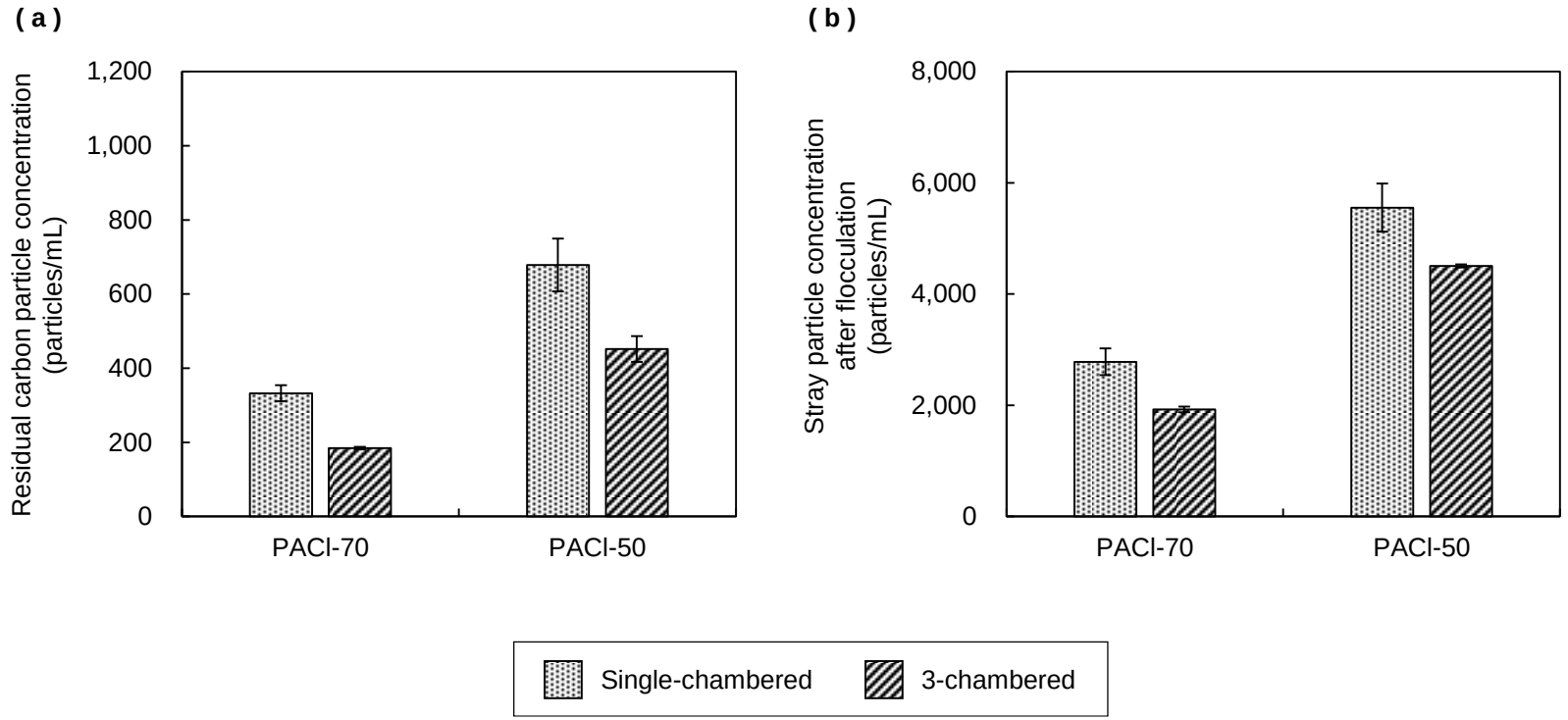

Fig. 4-7. Effect of rapid mixing reactor configuration (a single-chambered or 3-chambered coagulation reactor) on (a) residual particle concentration in sand filtrate and (b) stray particle concentration in water sampled after flocculation. Both reactors used the same mixing intensity ($G = 600\ s^{-1}$) and same total HRT (100 s), and were followed by a 4-chambered flocculation reactor ($G = 12.5\ s^{-1}$) and a sand filter. Municipal water 5 was used as the raw water. SPAC initial concentration, 2.0 mg/L; coagulant (PACl-50 or PACl-70), 1.5 mg-Al/L; filtration rate, 90 m d^{-1}.

Additionally, the effect of flocculation reactor (slow mixing unit) configuration on residual carbon particle concentration in sand filtrate (Fig. 3-25, Fig. 3-26, and Fig. 3-25a) was examined (see also Section 3.3.5). The 4-chambered reactor resulted in a lower residual particle concentration in the sand filtrate than the single-chambered reactor when PACl-50 was used as the coagulant. The same trend was observed for stray particle concentration in water sampled at the end of flocculation treatment (Fig. 3-25b). However, when PAC-70 was used, this trend was not observed, because flocculation with slow mixing did not reduce the stray particle concentration, as discussed in the next section.

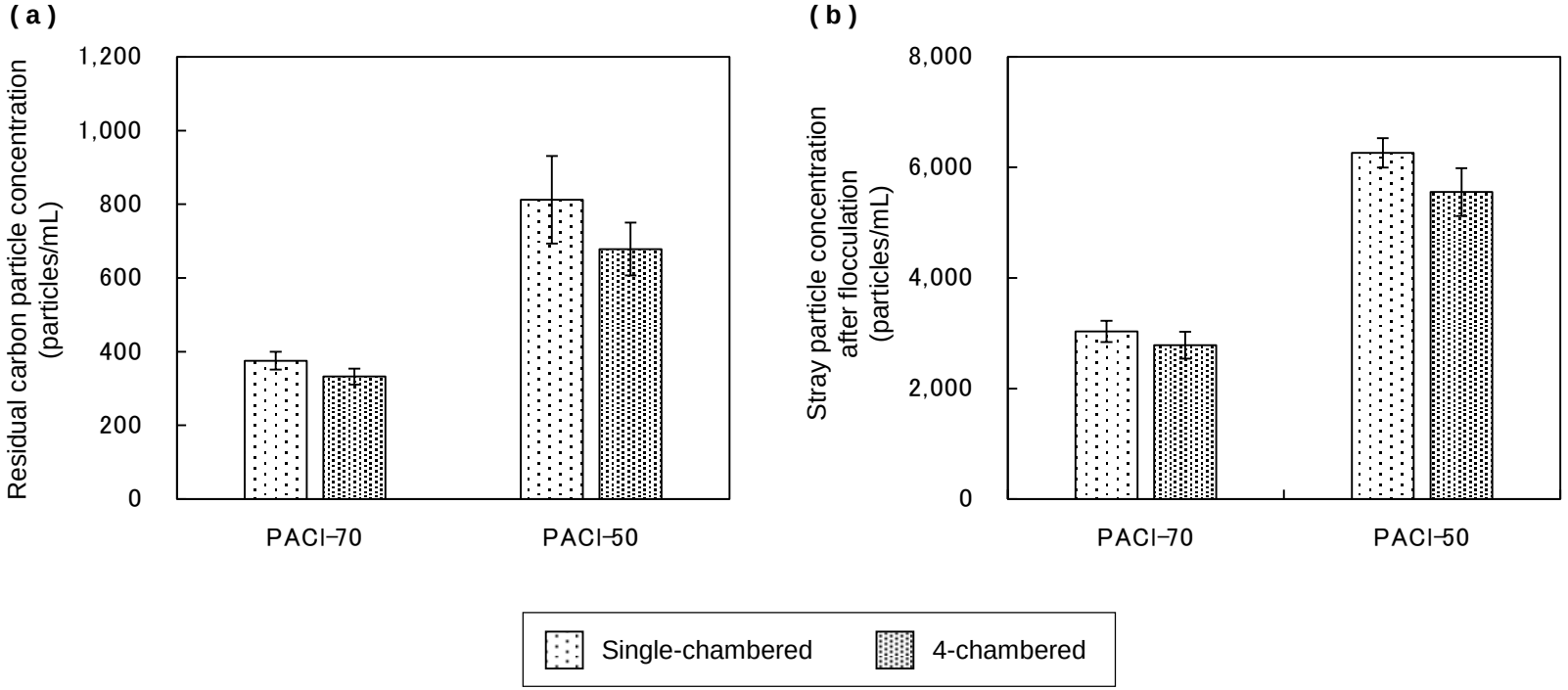

Fig. 4-8. Effect of slow mixing reactor configuration (a single-chambered or 4-chambered flocculation reactor) on (a) residual particle concentration in sand filtrate and (b) stray carbon particle concentration in water sampled after flocculation. Both reactors used the same mixing intensity (G = 12.5 s^{-1}) and same total HRT (2400 s) and were preceded by a single-chambered coagulation reactor (G = 600 s^{-1}). The experimental conditions were the same as described in the caption to Fig. 3-23.

When the residual carbon particle concentration in sand filtrate was plotted against the stray particle concentration in water sampled after flocculation treatment (slow mixing), a strong positive correlation was observed ($R^2 = 0.96$, Fig. 4-9a). This supports my finding that stray particle concentration can be used as an index of residual particle concentration in sand filtrate, and that such particles are the origin of the residual carbon particles. The correlation between the residual carbon particle concentration in sand filtrate and the stray particle concentration in water collected after coagulation treatment (rapid mixing) was also examined, but a correlation was lower ($R^2 = 0.70$; Fig. 4-9b). I concluded that this was because the stray particle concentration was changed slightly during the flocculation process after PACl-50 coagulation, as discussed in the next section. Similarly, the correlation between the residual carbon particle concentration in sand filtrate and the turbidity of settled water sampled after sedimentation was examined. The turbidity of settled water was not correlated with residual carbon particle concentration in sand filtrate ($R^2 = 0.15$; Fig. 4-9c), although the turbidity of settled water was found to also be influenced by the residence time distribution of the coagulation and flocculation reactors (Fig. 3-27). I concluded that turbidity was not an index of the residual carbon particle concentration in the sand filtrate.

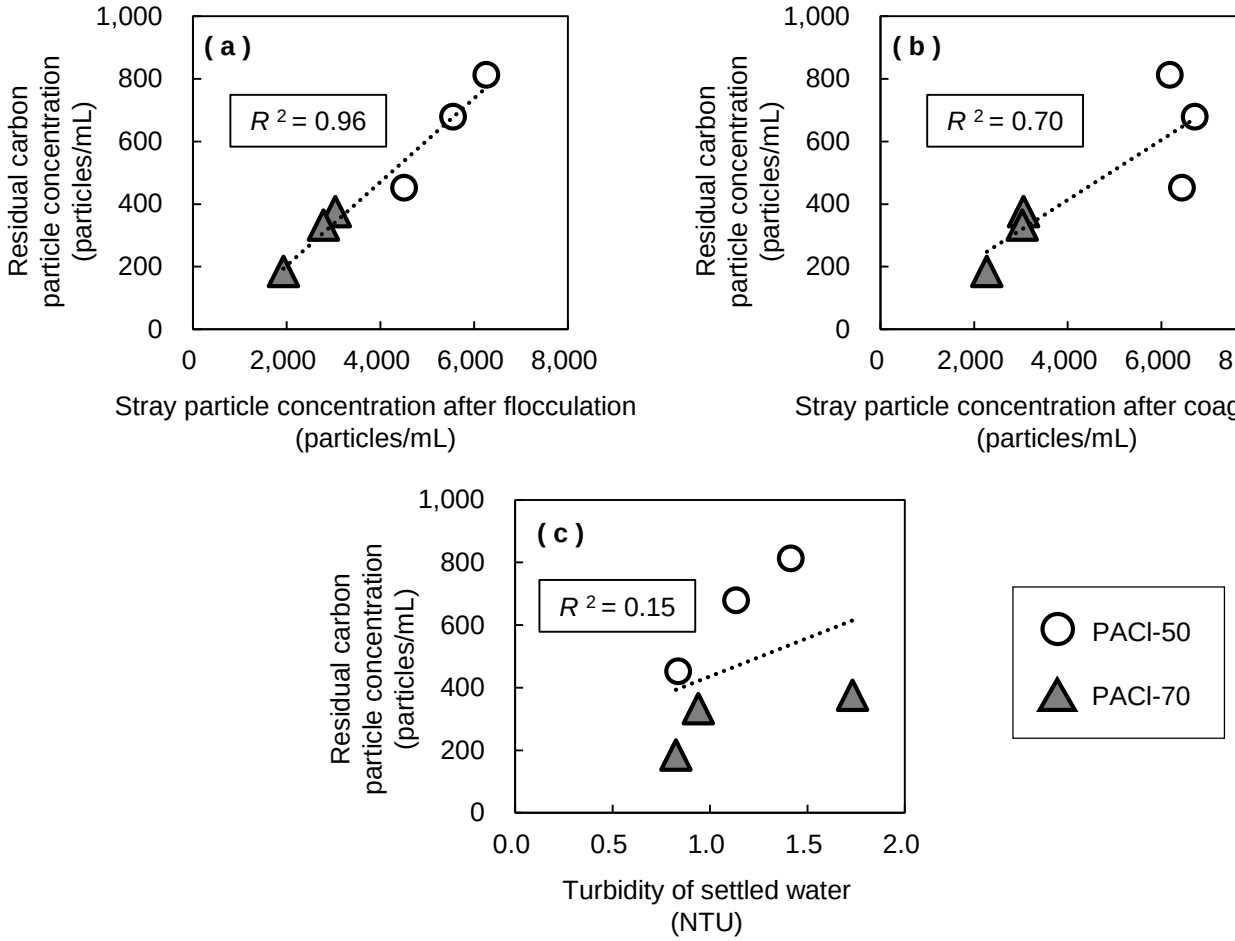

Fig. 4-9. Correlations between residual carbon particle concentration in sand filtrate and stray particle concentration in water sampled after flocculation with slow mixing (a), stray particle concentration in water after coagulation with rapid mixing (b), and turbidity of settled water (c). The experimental conditions were the same as described in the captions to Fig. 3-23, Fig. 3-25, and Fig. 3-27, respectively.

4.3.3 Effect of PACl type on stray particle concentration after coagulation and flocculation

The stray particle concentration was markedly decreased during coagulation treatment but left unchanged or slightly decreased by flocculation treatment (Fig. 4-10). More specifically, stray particle concentration was decreased by flocculation treatment with a 4-chambered-reactor slow-mixing when PACl-50, but not clearly PACl-70, was used as the coagulant. To further examine why the behavior of the stray particles during the flocculation treatment differed depending on the coagulant used, a series of batch experiments was conducted. As shown in Fig. 4-11, the stray carbon particles behaved differently during coagulation and flocculation depending on which coagulant was used. When PACl-70 was used, the stray particle concentration was high during the initial 20 s of rapid mixing for coagulation and was markedly decreased at 100 s of rapid mixing. During the subsequent slow mixing for flocculation, the concentration remained unchanged. This trend was also held for raw water with high NOM (natural organic matter) concentration (DOC: 3.8 mg/L), though stray particle concentrations were generally high due to the consumption of coagulant by NOM (DOC after SPAC dose was 3.7 mg/L and DOC after SPAC and coagulant doses was 2.5 mg/L) (Bratby 2006). In contrast, when PACl-50 was used, the stray particle concentration was lower at 20 s of rapid mixing compared with that when PACl-70 was used, and it then gradually decreased until the end of slow mixing.

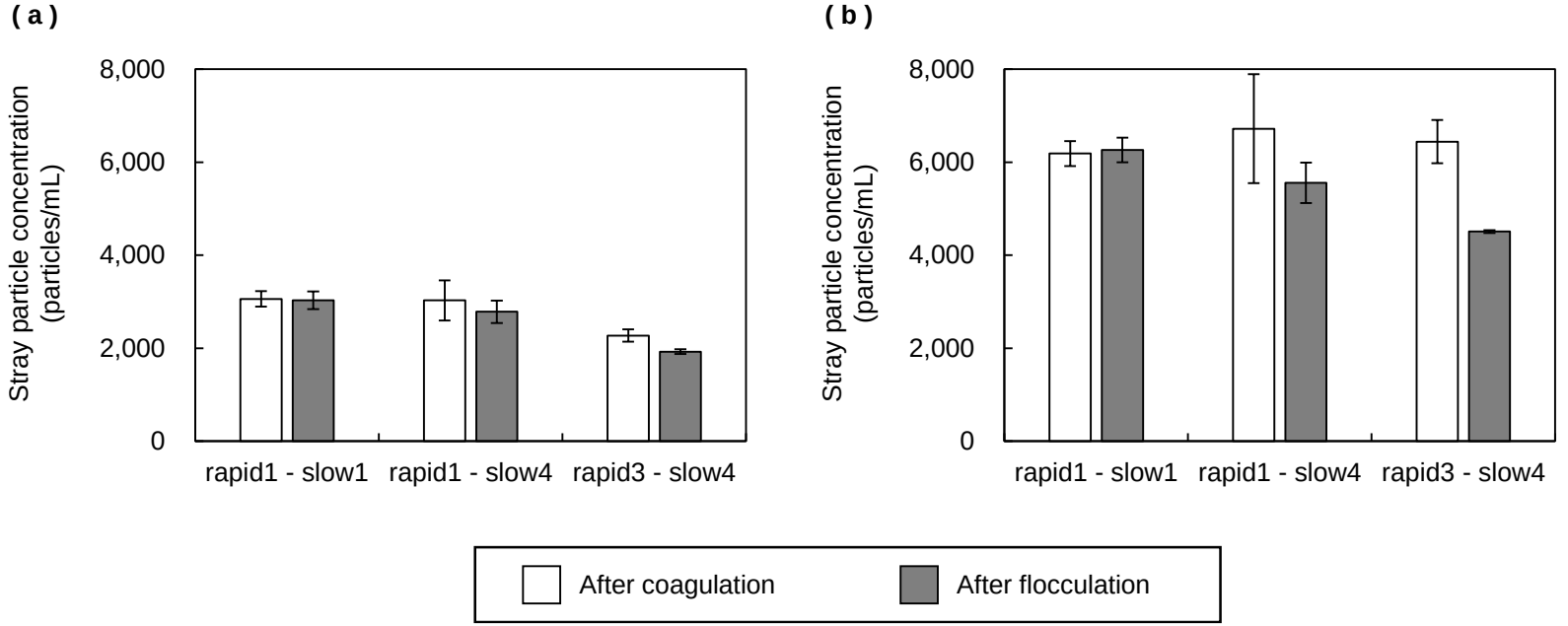

Fig. 4-10. Change in stray particle concentration after coagulation and flocculation. On the horizontal axis, the numbers after “rapid” and “slow” indicate the number of chambers in the coagulation and flocculation reactors, respectively. Coagulation was conducted with rapid mixing (G = 600 s^{-1}, 100 s). Flocculation was conducted with slow mixing (G = 12.5 s^{-1}, 2400 s). SPAC initial concentration, 2 mg/L. PACl-70 (a) or PACl-50 (b) was used as the coagulant. The experimental conditions were the same as described in the caption to Fig. 3-23 and Fig. 3-25.

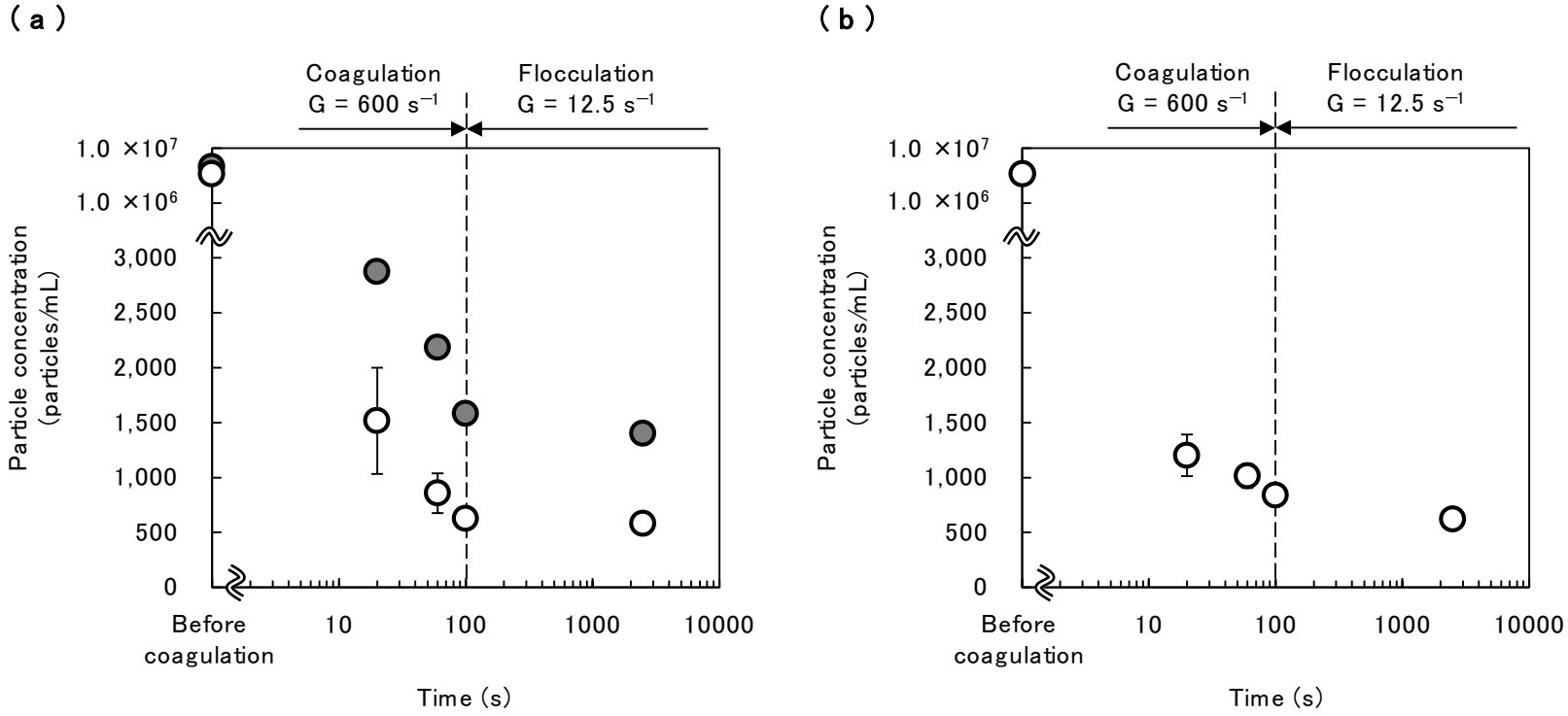

Fig. 4-11. Change of particle concentration against mixing time during coagulation and flocculation. Batch experiments were conducted using a 1-L rectangular beaker, Municipal water 1 (white plots) or River water 2 (grey plots) as the raw water, and PACl-70 (a) or PACl-50 (b) at 1.5 mg-Al/L as the coagulant. SPAC initial concentration, 2.0 mg/L. Water samples were collected during coagulation and flocculation treatments and then subjected to centrifugal separation treatment (see Section 4.2.4). Centrifugal supernatants were examined for carbon particle concentration. Water sampled before coagulation was also examined. Two runs were conducted for Municipal water 1, and one run for River water 2. Error bars represent the standard deviations for experiments, but some of them are hidden behind the symbols.

The relationship between the behavior of the stray carbon particles and the distributions of the aluminum species derived from the coagulants was also examined. Fig. 4-12 shows the changes in the Al species distributions for PACl-70 and PACl-50 during rapid mixing (G = 381 s^{-1}) and flocculation with slow mixing (G = 8 s^{-1}). The stock solution of PACl-50 contained 42% Ala, 23% Alb, and 35% Alc. When PACl-50 was added to water and hydrolyzed, almost no Ala remained at 20 s from the beginning of rapid mixing, and the amount of Alb increased to become the dominant species. Alb remained the dominant species until the second half of the slow mixing. In contrast, the stock solution of PACl-70 contained 25% Ala, 14% Alb, and Alc, 61%. When PACl-70 was added to water and hydrolyzed, as for PACl-50, almost no Ala remained at 20 s from the beginning of rapid mixing. However, unlike for PACl-50, Alc remained the dominant species throughout the rapid and slow mixing processes.

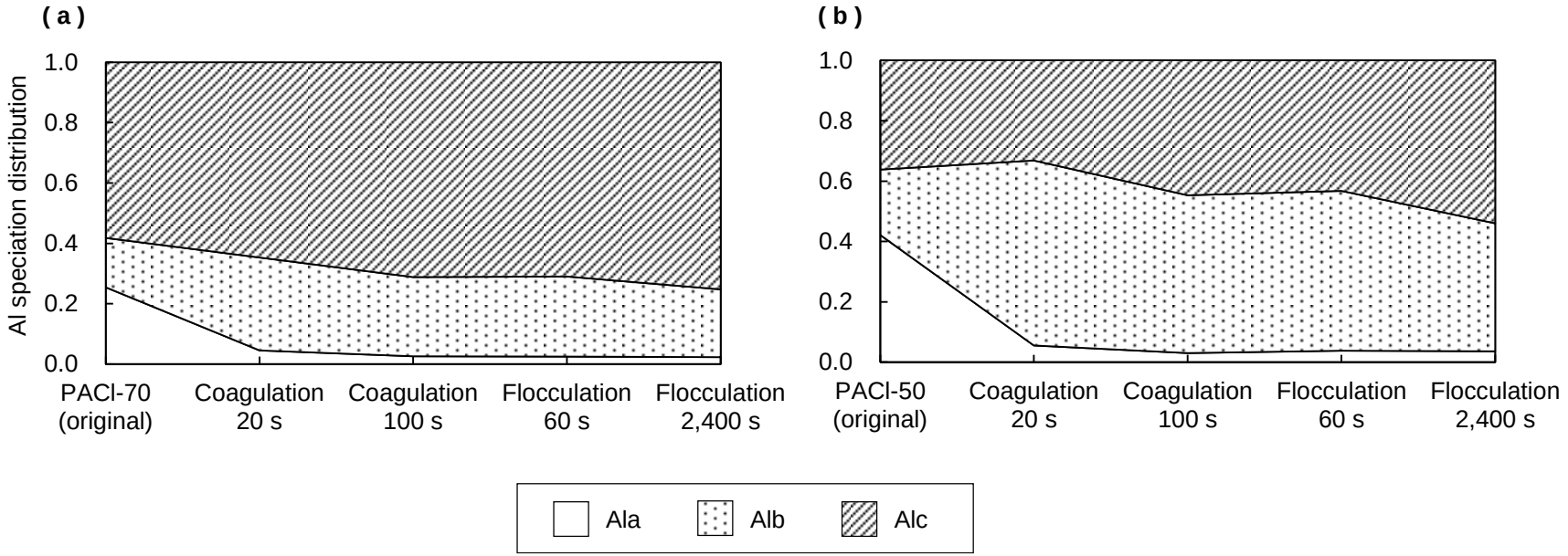

Fig. 4-12. Change in Al species distribution of PACl by coagulation and flocculation. PACl-70 (a) and PACl-50 (b) were hydrolyzed at 270 mg-Al/L in Municipal water 1 without carbon particles. Batch-type coagulation tests were conducted using a 1-L rectangular beaker. “original” means the Al speciation distribution of the PACl stock solution. “Coagulation” refers to coagulation with rapid mixing ($G = 381\ s^{-1}$); “Flocculation” refers to flocculation with slow mixing ($G = 8\ s^{-1}$). Ala, Alb, and Alc are monomeric, polymeric, and colloidal species, respectively.

Considering that PACl-70 markedly decreased the concentration of stray particles within several tens of seconds from the beginning of rapid mixing, unlike PACl-50, the present data suggest that the reactive hydrolysis product formed from Alc contributed to the rapid decrease of stray particles after only a short period of mixing. However, the stray particle concentration was not decreased further after rapid mixing, probably because the reactive hydrolysis product was fast-acting but unstable, which could easily transform into unreactive products, although the unreactive product was still categorized as Alc. When using PACl-70, rapid dispersion of the short-lived reactive hydrolysis product formed from Alc may be key for reducing the number of stray particles. This interpretation is consistent with my finding that PACl-70 needs more rapid, intense mixing to reduce the concentration of residual particles after CSF compared with that needed by PACl-50 (see also Chapter 3).

In contrast to PACl-70, PACl-50 decreased stray particles less during rapid mixing because of lower Alc content. PACl-50 contained more Ala and Alb, the latter of which is reported to be effective for charge neutralization but have poor floc-forming ability (Yan *et al.* 2008). During slow mixing, the concentration of Alb decreased measurably by 15%, and the concentration of Alc increased in response. Therefore, this newly formed reactive Alc might contribute to the slight decrease of stray particles observed during slow mixing when PACl-50 was used. Therefore, it is expected that the stray particle concentration will be reduced even during slow mixing for flocculation if multiple stages of slow mixing are used. However, the formation of reactive Alc from Alb in slow mixing is slow, and then the decrease of stray particles is only slight.

4.3.4 Fate and removal of stray particles by sand filtration

As shown in Fig. 4-5 and Fig. 4-9, the concentrations of stray particles in water sampled after coagulation and flocculation were much higher than the residual particle concentrations in the sand filtrate. Furthermore, it was found that stray particles are able to pass through the flocculation and sedimentation processes with only a slight decrease in their concentration (Fig. 4-13). Assuming that the source of the residual particles in the sand filtrate was stray particles (see the discussion in Section 4.3.1), most, but not all, of them are removed by sand filtration.

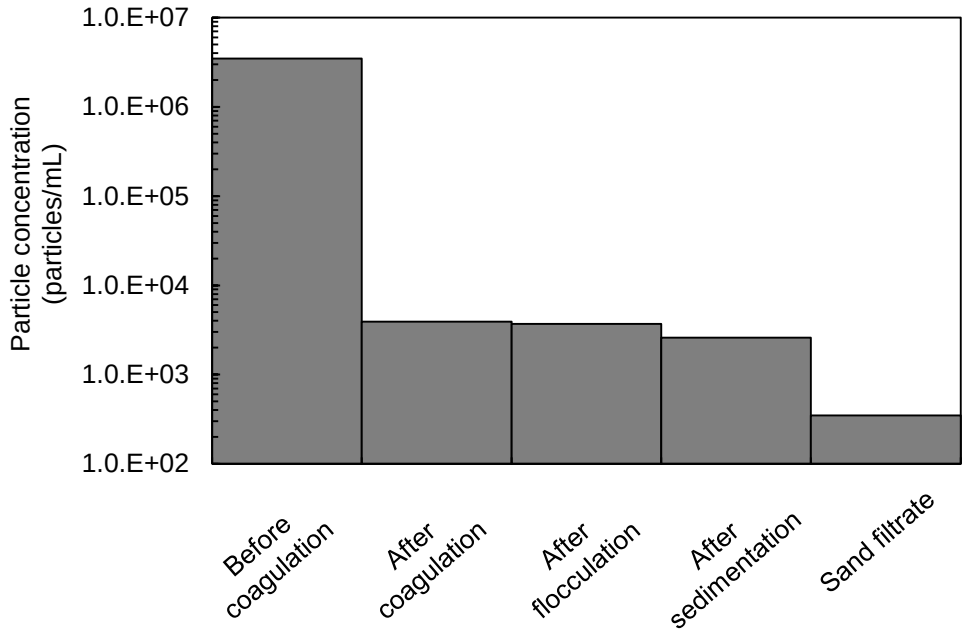

Fig. 4-13. Change in carbon particle concentration during the CSF process. Water samples were collected after coagulation, after flocculation, and after sedimentation, subjected to centrifugal separation treatment (see Section 4.2.4), and the supernatants were examined for carbon particle concentration. Water sampled before coagulation and sand filtrate were also examined. River water was used as the raw water. Coagulant (PACl-70) dose, 2.25 mg-Al/L. The experimental conditions were the same as described in the caption to Fig. 3-18.

When the removal rate of particles by particle size using the stray particle concentration in water sampled after sedimentation and the residual carbon particle concentrations in sand filtrate was calculated, it was found that the

removal rate of stray particles was in the range of 60%–90% for particles with a diameter of 0.3 to 2.0 μm (Fig. 4-14). There are many models that can be used to estimate the removal rate of fine particles by sand filtration. I used three representative models [RT model (Rajagopalan and Tien 1976), TE model (Tufenkji and Elimelech 2004), and Yao model (Yao *et al.* 1971)] presented by Crittenden et al. (2012) to estimate the removal rate of particles with a size of 0.3 to 2 μm, which included both the stray particles and the residual particles in sand filtrate. The modeled removal rates, 15%–55% for the particles with sizes of 0.3–2 μm (Fig. 4-15), were much lower than the experimentally observed values of 60%–90%. Since the theoretical models assume a filtration media of spherical particles of uniform size, which is quite different from actual filters, it is not surprising that the experimental and calculated removal rates did not agree. Nevertheless, these findings suggest that a removal rate >60% would be achieved for particles with a diameter of 0.3 to 2 μm. This suggests that some of the particles categorized as stray particles were easily removed by sand filtration. I imagine that such particles might be actually larger in size than the size of the particles observed under the microscope because the aluminum, which attaches to the particles and neutralizes their charge, is transparent and does not appear in microphotographs. As already discussed in Section 4.3.1, zeta potential measurement revealed that the stray particles had less negative-charge than did the residual carbon particles in sand filtrate, which indicates that most of the stray particles were more charge-neutralized by the attachment of a larger amount of aluminum. This suggests that the true size of stray particles is likely to be larger than the apparent grain size observed under the microscope. Therefore, the removal efficiency of such particles would be higher than expected according to apparent particle size and filtration theory. In addition, I imagine that among the stray particles there are particles with much-less charge-neutralization and that these much-less-charge-neutralized, stray particles are able to easily pass through the sand filter and reach the filtrate. Thus, in future studies it will be important to

evaluate not only particle size diversity but also charge diversity rather than rely only on average values. Such examinations will allow us to more efficiently control the carbon particle residual after CSF treatment.

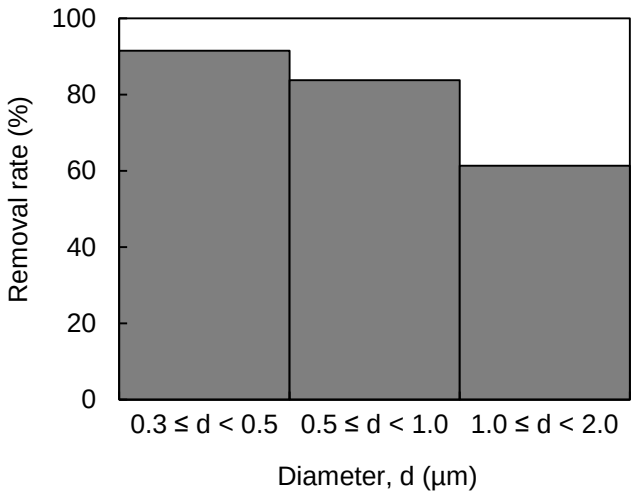

Fig. 4-14. Removal rate of carbon particles in three size classes by sand filtration. Removal rate was calculated between the stray particle concentration in water sampled after sedimentation and the residual carbon particle concentration in sand filtrate. River water was used as the raw water. Coagulant (PACl-70) dose, 2.25 mg-Al/L. The experimental conditions were the same as described in the caption to Fig. 3-18.

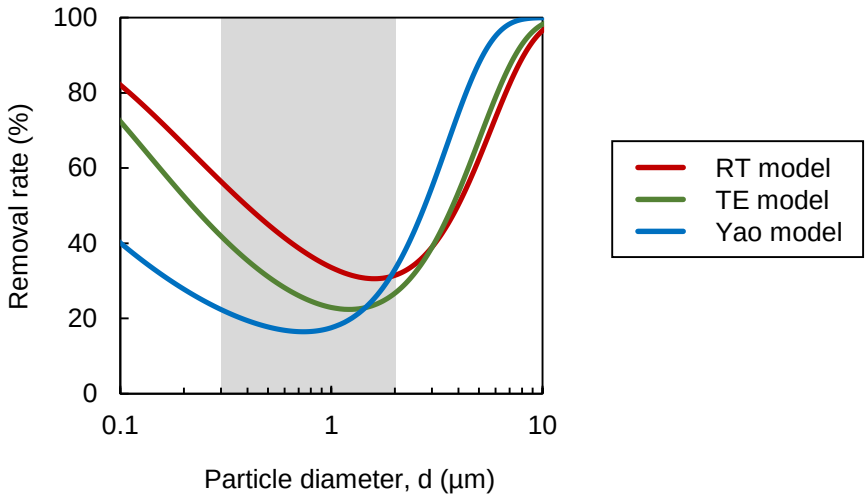

Fig. 4-15. Theoretical rates of particle removal by sand filtration, as determined by three different models. Removal rates were calculated by using the three models [RT model (Rajagopalan and Tien 1976), TE model (Tufenkji and Elimelech 2004), and Yao model (Yao et al. 1971)] and the following parameters: collector diameter (effective diameter of sand), d_c = 0.94 mm; filtration rate, v = 3.75 m/h; temperature, T = 20 °C; particle density, ρ_P = 1,330 kg/m^3; depth of filter, L = 0.5 m; bed porosity, ε = 0.40; and Hamaker constant, Ha = 1.73 × 10^{-20}, geometric mean of Ha values of activated carbon (Chen and Huang 2017) and quartz (Adamczyk 2017). In the figure, the grey band (particle diameter, 0.3–2 μm) shows the particle

size range for the stray particles and residual carbon particles in sand filtrates in the present study.

4.4 Summary

Summary of this chapter is described as follows:

i. Stray carbon particles, which were determined as the particles remaining in the centrifugal supernatant of the water sampled after rapid mixing for coagulation and slow mixing for flocculation, were less charge-neutralized than the bulk particles. The concentration of stray particles dropped markedly during rapid mixing process, and then it was unchanged or only slightly decreased during slow mixing and sedimentation processes. The concentrations of stray carbon particles in water sampled after rapid/slow mixing processes for coagulation/flocculation were well correlated with the residual carbon particle concentrations in sand filtrate, but the turbidity of water entering the sand filter water was not.

ii. Among the bulk particles, stray particles, which account for less than 0.4% of the bulk particles, could be a major source of residual particles in sand filtrate due to their lower charge neutralization. Therefore, a goal of the coagulation treatment process should be to reduce the stray particle concentration.

iii. Optimizing reactor configurations and the type and dose of coagulant were effective for reducing stray particle and residual carbon particle concentrations in sand filtrate. PACl-70 performed better with a multi-chambered reactor than with a single-chambered reactor for coagulation

with rapid mixing. In contrast, PACl-50 performed better with a multi-chambered reactor than with a single-chambered reactor for both coagulation with rapid mixing and flocculation with slow mixing. The performance requirements of the reactors for coagulation and flocculation were related to the predominant aluminum species in the coagulant: Alc of PACl-70 is fast-acting, whereas Ala of PACl-50 is slow-acting.

4.5 References

Adamczyk, Z. (2017) Particles at Interfaces, Interactions, Deposition, Structure, Academic Press.

Amaral, P., Partlan, E., Li, M., Lapolli, F., Mefford, O.T., Karanfil, T. and Ladner, D.A. (2016) Superfine powdered activated carbon (S-PAC) coatings on microfiltration membranes: Effects of milling time on contaminant removal and flux. Water Research 100, 429-438.

American Society of Civil Engineers and American Water Works Association, U. (1998) Water Treatment Plant Design, McGraw-Hill.

Ando, N., Matsui, Y., Kurotobi, R., Nakano, Y., Matsushita, T. and Ohno, K. (2010) Comparison of natural organic matter adsorption capacities of super-powdered activated carbon and powdered activated Carbon. Water Res 44(14), 4127-4136.

Ando, N., Matsui, Y., Matsushita, T. and Ohno, K. (2011) Direct observation of solid-phase adsorbate concentration profile in powdered activated carbon particle to elucidate mechanism of high adsorption capacity on super-powdered activated carbon. Water Research 45(2), 761-767.

Apul, O.G., Hoogesteijn von Reitzenstein, N., Schoepf, J., Ladner, D., Hristovski, K.D. and Westerhoff, P. (2017) Superfine powdered activated carbon incorporated into electrospun polystyrene fibers preserve adsorption capacity. Science of The Total Environment 592, 458-464.

Ateia, M., Erdem, C.U., Ersan, M.S., Ceccato, M. and Karanfil, T. (2019) Selective removal of bromide and iodide from natural waters using a novel AgCl-SPAC composite at environmentally relevant conditions. Water Research 156, 168-178.

Bonvin, F., Jost, L., Randin, L., Bonvin, E. and Kohn, T. (2016) Super-fine powdered activated carbon (SPAC) for efficient removal of micropollutants from wastewater treatment plant effluent. Water Research 90, 90-99.

Bratby, J. (2006) Coagulation and Flocculation in Water and Wastewater Treatment, IWA Publishing.

Bureau of Waterworks Tokyo Metropolitan Government, T. (2014) Personal communication.

Chen, C. and Huang, W. (2017) Aggregation kinetics of nanosized activated carbons in aquatic environments. Chemical Engineering Journal 313, 882-889.

Crittenden, J.C., Trussell, R.R., Hand, D.W., Howe, K.J. and Tchobanoglous, G. (2012) MWH's Water Treatment Principles and Design, Third Edition, John Wiley & Sons, Inc.

Decrey, L., Bonvin, F., Bonvin, C., Bonvin, E. and Kohn, T. (2020) Removal of trace organic contaminants from wastewater by superfine powdered activated carbon (SPAC) is neither affected by SPAC dispersal nor coagulation. Water Research 185, 116302.

Ding, Q., Yamamura, H., Murata, N., Aoki, N., Yonekawa, H., Hafuka, A. and Watanabe, Y. (2016) Characteristics of meso-particles formed in coagulation process causing irreversible membrane fouling in the coagulation-microfiltration water treatment. Water Research 101, 127-136.

Dunn, S.E. and Knappe, D.R.U. (2019) DBP Precursor and Micropollutant Removal by Powdered Activated Carbon.

Jiang, W., Xiao, F., Wang, D.S., Wang, Z.C. and Cai, Y.H. (2015) Removal of emerging contaminants by pre-mixed PACl and carbonaceous materials. RSC Advances 5(45), 35461-35468.

Kimura, M., Matsui, Y., Kondo, K., Ishikawa, T.B., Matsushita, T. and Shirasaki, N. (2013) Minimizing residual aluminum concentration in treated water by tailoring properties of polyaluminum coagulants. Water Research 47(6), 2075-2084.

Matsui, Y., Aizawa, T., Kanda, F., Nigorikawa, N., Mima, S. and Kawase, Y. (2007) Adsorptive removal of geosmin by ceramic membrane filtration with super-powdered activated carbon. Journal of Water Supply: Research and Technology-Aqua 56(6-7), 411-418.

Matsui, Y., Nakao, S., Sakamoto, A., Taniguchi, T., Pan, L., Matsushita, T. and Shirasaki, N. (2015) Adsorption capacities of activated carbons for geosmin and 2-methylisoborneol vary with activated carbon particle size: Effects of adsorbent and adsorbate characteristics. Water Res 85, 95-102.

Matsui, Y., Nakao, S., Taniguchi, T. and Matsushita, T. (2013) Geosmin and 2-methylisoborneol removal using superfine powdered activated carbon: shell adsorption and branched-pore kinetic model analysis and optimal particle size. Water Research 47(8), 2873-2880.

Matsui, Y., Yoshida, T., Nakao, S., Knappe, D.R. and Matsushita, T. (2012) Characteristics of competitive adsorption between 2-methylisoborneol and natural organic matter on superfine and conventionally sized powdered activated carbons. Water Res 46(15), 4741-4749.

Murray, C.C., Vatankhah, H., McDonough, C.A., Nickerson, A., Hedtke, T.T., Cath, T.Y., Higgins, C.P. and Bellona, C.L. (2019) Removal of per- and polyfluoroalkyl substances using super-fine powder activated carbon and ceramic membrane filtration. Journal of Hazardous Materials 366, 160-168.

Pan, L., Takagi, Y., Matsui, Y., Matsushita, T. and Shirasaki, N. (2017) Micro-milling of spent granular activated carbon for its possible reuse as an adsorbent: Remaining capacity and characteristics. Water Research 114, 50-58.

Partlan, E., Ren, Y., Apul, O.G., Ladner, D.A. and Karanfil, T. (2020) Adsorption kinetics of synthetic organic contaminants onto superfine powdered activated carbon. Chemosphere 253, 126628.

Rajagopalan, R. and Tien, C. (1976) Trajectory analysis of deep-bed filtration with the sphere-in-cell porous media model. AIChE Journal 22(3), 523-533.

Tufenkji, N. and Elimelech, M. (2004) Correlation Equation for Predicting Single-Collector Efficiency in Physicochemical Filtration in Saturated Porous Media. Environmental Science & Technology 38(2), 529-536.

Wang, D., Sun, W., Xu, Y., Tang, H. and Gregory, J. (2004) Speciation stability of inorganic polymer flocculant–PACl. Colloids and Surfaces A: Physicochemical and Engineering Aspects 243(1), 1-10.

Yan, M., Wang, D., Ni, J., Qu, J., Chow, C.W. and Liu, H. (2008) Mechanism of natural organic matter removal by polyaluminum chloride: effect of coagulant particle size and hydrolysis kinetics. Water Research 42(13), 3361-3370.

Yao, K.-M., Habibian, M.T. and O'Melia, C.R. (1971) Water and waste water filtration. Concepts and applications. Environmental Science & Technology 5(11), 1105-1112.

Yu, W.-z., Qu, J.-h. and Gregory, J. (2015) Pre-coagulation on the submerged membrane fouling in nano-scale: Effect of sedimentation process. Chemical Engineering Journal 262, 676-682.

5 ACTIVATED CARBON, VIRGIN/DECAYED MICRO PLASTICS, VIRUS, AND KAOLINITE/MONTMORILLONITE CLAY PARTICLES IN TREATMENT PROCESS

5.1 Introduction

In drinking water treatment employing a CSF process, many kinds of particles including micro plastics (MPs) should be adequately removed as well as AC particles.

MPs have drawn attention throughout the world, since it have been revealed that MPs have widely been distributing in the ocean, freshwater, the air, and soil (Dris *et al.* 2016, Freeman *et al.* 2020, Iqbal *et al.* 2020, Iwasaki *et al.* 2017, Koelmans *et al.* 2019, Rodrigues *et al.* 2018, Wang *et al.* 2021, Wong *et al.* 2020, Wu *et al.* 2019, Zhou *et al.* 2020). MPs with a size of <10 μm have been reported their toxicity on human health (Kögel *et al.* 2020, Revel *et al.* 2018), and so their fate in drinking water treatment processes should be well understood (WHO 2019).

Quite recently, the effects of treatment conditions on the treatability of MP in water treatment have been investigated by using waters spiked MP (Ma *et al.* 2019, Rajala *et al.* 2020, Skaf *et al.* 2020, Wang *et al.* 2020b, Zhou *et al.* 2021). Zhang *et al.* (2020) use fluorescent particles at a concentration similar to that observed in practice (1800−9500 particles/L) and report the removal rate of 86.9−99.9% by a media filter. Moreover, it has been reported that industrially produced MP has been physically/photochemically weathered after being emitted

to environment (Sun *et al.* 2020), and the weathered MP (called as secondary MP) (WHO 2019) has been changed in hydrophobicity and chemical composition (Lin *et al.* 2020, Naik *et al.* 2020, Wang *et al.* 2020a, Zhu *et al.* 2020a, Zhu *et al.* 2020b). The changes related to weathering on MP might affect its removal efficiency in water treatment.

The primary objective of CSF treatment is to reduce turbidity by removing suspended particles, fundamentally clay particles, and the turbidity reduction is well examined (Edzwald 2011). CSF has proven effective in removing such clay particles even with smaller size and higher concentrations than those of micro plastics (WHO 2019). However, the behavior of particulate matter as particles in CSF and its residual at the low concentration level found for micro plastics in filtered water are not enough discussed. Turbidity measurement does not fundamentally have enough sensitivity for evaluating trace concentrations of particles and their high removal rates (log reduction) (Cho *et al.* 2020). On the other hand, the removals of viruses with the particle sizes ranging from 30 to 100 nm by CSF are studied by quantifying their number concentration in real-time polymerase chain reaction (PCR), and the removals at 0.8−2.5 log levels are reported (Shirasaki *et al.* 2018).

Accordingly, this chapter aims to reveal the fates and removals of MPs, clay, activated carbon, and virus particles during CSF. We applied counting methods for identifying and quantifying these particles including clay particles at very low concentration levels, which enabled comparative discussion for all particles with the same accuracy on the removal rate evaluation.

5.2 Materials and methods

5.2.1 Target particles

5.2.1.1 Activated carbon

Conventionally sized PAC (hereafter just called PAC) and superfine PAC (SPAC) were used as target PACs. The PAC was a commercially available wood-based PAC (Taiko W; Futamura Chemical Co., Ltd., Nagoya, Japan). SPAC was prepared in our laboratory from the PAC by wet-mode ball milling (Nikkato, Osaka, Japan) followed by wet-mode bead mill (LMZ015; Ashizawa Finetech, Ltd., Chiba, Japan). Detailed preparation procedure is illustrated elsewhere (Pan *et al.* 2017).

5.2.1.2 *MPs*

Three types of commercially available sphere MPs were used as removal targets. NYLON 12 (SP-500; d50=4.9 μm; 1.02 g cm^{-3}; hereafter 'PA') was provided by Toray Industries, Inc. (Tokyo, Japan). Polysilicone-21 (KMP-600; d50=4.8 μm; 0.99 g cm^{-3}; hereafter 'PSi') was provided by Shin-Etsu Chemical Co., Ltd. (Tokyo, Japan). Polyethylene (LE-1080; d50=6 μm; 0.92 g cm^{-3}; hereafter 'PE') was provided by Sumitomo Seika Chemicals Company, Limited. (Osaka, Japan).

MPs were prepared as suspensions before using for experiments, as follows. First, each MP was added in separate pure water (Milli-Q water; Milli-Q Advantage A10 System; Merck KGaA, Darmstadt, Germany) at 100 mg/L

respectively. To sufficiently disperse the MP in the water, the MP suspension was exposed to ultrasonic (FU-180C, Tokyo Garasu Kikai Co., Ltd., Tokyo, Japan) at 360 W for 24 h, and then stored at 4 °C before use. Immediately before use for batch tests of CSF, the MP suspension was diluted with Milli-Q water to be at 23.2 μg/L and then exposed to ultrasonic (CPX8800h-J, Yamato Scientific Co., Ltd., Tokyo, Japan) at 280 W for 30 min. Immediately before use for measurement of particle size and zeta potential, the MP suspension was exposed to ultrasonic as the same way except dilution.

Photochemically weathering was simulated by using PA, as follows. First, PA suspension was prepared with PA adding in Milli-Q water contained with a clear glass bottle at 50 mg/L and then exposed to ultrasonic (FU-180C, Tokyo Garasu Kikai Co., Ltd., Tokyo, Japan) at 360 W for 24 h. After that, the bottle containing the PA suspension was kept by the window with periodic turnover, exposing to the sun (Sapporo, Japan) daytime for 68 days from August 18 2020 to October 24 2020. Here, the photochemically weathered PA is denoted as PA-photo.

Physically weathering was simulated by using PA, as follows. First, PA (10 g) was transferred into a closed-chamber ball mill including 5- and 10-mm-diameter Al_2O_3 balls for the disintegrating media, and the PA was rubbed at 94 rpm for 24 h. Here, the physically weathered PA is denoted as PA-physic.

The particle size distribution of MP was determined by using a laser light diffraction and scattering method (Microtrac MT3300EXII; MicrotracBEL Corp., Osaka, Japan) after adding a dispersant (Triton X-100; Kanto Chemical Co., Inc., Tokyo, Japan; final concentration, 0.08% w/v) and exposing ultrasonication at 150 W for 1 min. The zeta potential of MP was determined by using Zetasizer Nano ZS (Malvern, United Kingdom).

5.2.1.3 *Virus*

F-specific RNA bacteriophage MS2 (NBRC 102619, National Institute of Technology and Evaluation Biological Research Center, Kisarazu, Japan) and pepper mild mottle virus (PMMoV pepIwateHachiman1 strain, MAFF 104099, National Institute of Agrobiological Sciences Genebank, Tsukuba, Japan) were used as removal target viruses after propagated in the Escherichia coli bacterial hosts (NBRC 13965) and Nicotiana benthamiana, respectively and purified. The concentrations were quantified by real-time polymerase chain reaction (PCR).

Detailed procedures of propagation, purification and quantification of the viruses were described elsewhere (Shirasaki *et al.* 2016, Shirasaki et al. 2018).

5.2.1.4 *Clay*

Commercially available kaolin (FUJIFILM Wako Pure Chemical Corporation, Osaka, Japan) and montmorillonite (Sigma-Aldrich Co. LLC., St. Louis, MO, USA) were used as removal target clay. These were respectively added to Milli-Q water at 10 g L^{-1} to prepare stock suspensions.

5.2.2 Coagulant

A commercially available poly-aluminum chloride [PACl; the basicity of 1.5 (basicity of 50%), sulfate ion 2.9 wt%], provided by Taki Chemical Co., Ltd. (Hyogo, Japan), were used as coagulant.

5.2.3 Batch tests of coagulation-flocculation, sedimentation, and rapid sand filtration

Toyohira river water taken at Moiwa Water Purification Plant (Sapporo, Japan) was filtered by a membrane (pore diameter 0.2 mm; PTFE; Toyo Roshi Kaisha, Ltd., Tokyo, Japan) to remove suspended matters, and then supplemented with PAC (10 mg/L, 7−8 NTU, 4.0×10^6 particles/mL), SPAC (2.0 mg/L, 7−8 NTU, 5.1×10^6 particles/mL), MP (1.0 μg/L, 11 particles/mL), virus (10^7 copies/mL), and/or clay particles (10 mg/L, 7−8 NTU, 8.7×10^5 particles/mL, for kaolin; 10 mg/L, 1.8 NTU, 2.2×10^4 particles/mL, for montmorillonite) to prepare a raw water (see also Table 5-1) for batch tests of coagulation-flocculation, sedimentation, and rapid sand filtration. The batch test was conducted in a rectangular beaker containing 11-L raw water. The dosage of the coagulant PACl was predetermined at 3.0 mg-Al/L so that visible floc particles were formed and turbidity of sedimentation supernatant was < 0.2 NTU. The coagulant PACl was injected to the raw water after adding NaOH or HCl to make the coagulation pH 7.0. Rapid mixing for coagulation was conducted at the G value of 600 s^{-1} for 100 s, which was followed by slow mixing for flocculation at the G value of 12.5 s^{-1} for 2,400 s. After the slow mixing, the water was kept at rest for 60 min as sedimentation. Thereafter, 10 L of the supernatant from the settled water was transferred to another beaker. A portion of the supernatant was also subjected for centrifugal pretreatment (see Section 5.2.4) or acid-sonic pretreatment (see Section 5.2.5) before determining concentration of AC, MP and clay particles (see Section 5.2.6). Virus concentration was directly determined with none of these pretreatments. The remaining supernatant was pumped to a sand filter (effective diameter and uniformity of sand grains; 0.94 mm and 1.24, sand depth 50 cm, column inner diameter 3.6 cm). Sand filtration was performed at the down-flow direction with a rate of 90 m d^{-1}, and sand filtrates were collected from 0 to 50 min, and from 50 to 100 min to determine concentrations of each particles and

turbidity. After each filtration run, the sand filter was backwashed with tap water, then washed forward with Milli-Q water. Additionally, after each test, instruments contacted to virus were exposed to chlorine and washed with Milli-Q water to prevent virus contamination for the next run.

Table 5-1. Raw waters used in this chapter.

Raw water	Particle type	Concentration
1	SPAC	2 mg/L
	Kaolin	10 mg/L
	PA	1 μg/L
2	SPAC	2 mg/L
	Kaolin	10 mg/L
	PA-photo	1 μg/L
3	SPAC	2 mg/L
	Montmorillonite	10 mg/L
	PA	1 μg/L
4	SPAC	2 mg/L
	Kaolin	10 mg/L
	PE	1 μg/L
	PMMoV	10^7 copies/mL
	MS2	10^7 copies/mL
5	PAC	10 mg/L
	Kaolin	10 mg/L
	PA	1 μg/L
6	SPAC	2 mg/L
	Kaolin	10 mg/L
	PSi	1 μg/L
7	PAC	10 mg/L
	Kaolin	10 mg/L
	PSi	1 μg/L

5.2.4 Centrifugal pretreatment

Aliquots (45 mL) of a water sample collected after sedimentation treatment were dispensed into four 50-mL glass tubes. The tubes were centrifuged by using a centrifuge (CT6E; Koki Holdings Co., Ltd., Tokyo, Japan) equipped with a swing rotor (T5SS; Koki Holdings Co., Ltd.). Centrifugation was carried out at

4800 rpm (3990*g*) for 10 min, halted, and then re-started for 10 min. Thereafter, the concentrations of particles in the centrifugal supernatant were determined by membrane filtration and microscopic image analysis (see Section 5.2.6).

5.2.5 Acid-sonic pretreatment

The sample collected after sedimentation treatment was transferred to a glass bottle, and added with HCl to bring the pH < 3.0. The resultant water was exposed ultrasonic (CPX8800h-J, Yamato Scientific co., ltd., Tokyo, Japan) with 280 W for 1 h to disperse particles suspended in the water. Thereafter, the concentrations of particles in the sonicated water were determined by membrane filtration and microscopic image analysis (see Section 5.2.6).

5.2.6 Measurement of particle concentration and particle size distribution

AC, MP and clay particles in a water sample were captured on a white membrane filter (nominal pore diameter, 0.1 μm; Φ25 mm; polytetrafluoroethylene; Merck KGaA, Darmstadt, Germany) and a black membrane filter (nominal pore diameter, 0.45 μm; Φ25 mm; mixed cellulose esters; Merck KGaA) by filtrating. The filter was dried at room temperature.

AC particles were detected on the color digital photomicrographs taken for the surface of a white membrane filter by a digital microscope (VHX-2000; Keyence Corporation, Osaka, Japan) at 1000× magnification by using the image analysis software associated with the microscope, and then their particle number concentration and particle size were calculated. MP particles were detected on the color digital photomicrographs taken for the surface of a white membrane filter at 500× magnification and quantified. Clay particles were detected for a back membrane filter at 1000× magnification and quantified.

Virgin MP particles (sphere) and clay particles (non-sphere) in the same photomicrographs were detected separately based on their shape. However, PA-physic particles were mostly non-spherical, but a CSF test using the mixture of PA-physic and clay particles was not conducted.

5.2.7 Other analysis of particles

Zeta potentials of AC, MP and clay particles with change in pH were determined as follows. Toyohira river water (Sapporo) was supplemented with PAC (10 mg/L), SPAC (2.0 mg/L), MP (1.0 mg/L), or clay particles (10 mg/L) to prepare a raw water. The water was added NaOH or HCl to adjust the pH 1.5−11.5 and measured for the zeta potential (Zetasizer Nano ZS; Malvern, United Kingdom). FTIR analysis was conducted by using an FTIR spectrophotometer (IR-7500S, Shimadzu, Kyoto, Japan) at a resolution of 4 cm^{-1} (Ninomiya et al. 2020) for KBr pellets containing PA or PA-photo particles at 0.25 wt%. PA, PA-photo, and PA-physic particles were collected on a membrane filter (nominal pore diameter, 0.45 μm; Φ25 mm; mixed cellulose esters; Merck KGaA) and subsequently the MP particles on the filter were observed using a field-emission scanning electron microscope (JSM-7400F, JEOL Ltd., Tokyo, Japan).

5.2.8 Sampling sand filtrates in full-scale water purification plants

Sampling sand filtrates were conducted at 14 full-scale water treatment plants, which applied the CSF process (Table 5-2), when PAC was used for the water treatment. The samples were quantified for residual black-particle concentrations by using membrane filtration and microscopic image analysis described in Section 5.2.6.

Table 5-2. Full-scale water treatment plants where sand filtrates were collected.

	City	Sampling date	Raw water		PAC			Coagulant			Coagulation	Sedimentation	Filtration		
			Turbidity	DOC	Material	D50	Dosage	Type	Basicity	Dosage	pH	Time	Rate	Anthracite	Sand
			NTU	mg/L		μm	mg-dry/L		%	mg-Al/L		min	m/d	cm	cm
1	Kurume	2018/8/20	4	1.2	Wood	19	5	PACl	67–75	1.2	7.3	374	72	30	40
2	Ebina	2018/8/21	2	0.6	Wood	33	3	PACl	52.8	1.0	6.8	164	67	25	45
3	Sendai	2018/8/22	2	1.2	Coconutshell	17	1	PACl	no data	1.5	6.9	85	71	no data	60
4	Hatinohe	2018/8/28	5	1.2	Wood	22	4	PACl	59.2	1.3	7.1	240	69	10	60
5	Sakurai	2018/8/27	7	2.2	Wood	21	14	PACl	52.2	1.2	7.0	105	120	0	70
6	Matsudo	2018/8/28	8	1.5	Wood	21	15	PACl	51	2.1	6.9	170	120	0	65
7	Inzai	2018/8/24	9	2.2	Wood	22	30	PACl	49	2.9	7.0	240	120	0	80
8	Niigata	2018/8/27	5	1.3	Wood	23	10	PACl	53.1	1.4	7.0	342	120	3	60
9	Sapporo	2018/9/5	14	1.4	Wood	19	10	PACl	51–55	2.1	6.9	169	83	0	65
10	Yokohama	2018/11/8	2	0.5	no data	5.4	1	PACl	54.7	1.1	7.3	209	no data	no data	60
11	Hamura	2018/7/27	no data	0.1	Wood	21	25	PACl	54	1.1	7.2	47	81	7	53
12	Hamura	2018/8/30	no data	no data	Wood	21	3	PACl	54	1.4	no data	47	no data	7	53
13	Naka	2018/8/27	4	2.5	Wood	17	15	PACl	51.5	1.3	7.0	139	54	0	60
14	Naka	2018/8/28	18	2.8	Wood	17	60	PACl	51.5	2.6	7.1	156	47	0	60

5.3 Results and Discussion

5.3.1 Residual carbon particles in full-scale CSF plants

Fig. 5-1 shows the number concentrations of residual black particles remaining in sand filtrates in the 14 full-scale water purification plants, which treated the water by applying PAC followed by a CSF process. The residual concentrations were plotted against the PAC dosages, but there was no correlation (Fig. 5-1). This is reasonable because plant configurations and operations were not the same. There was a weak correlation between the residual black particle concentrations and turbidities of settled waters (Fig. 5-2). The residual black particle concentrations in sand filtrates were in the range from 40 to 200 particles/mL. Turbidities of the sand filtrates were not different from those observed in the plant operation without PAC addition in the plants (data not shown). Actually, no correlation was also observed between the turbidities of sand filtrates and the particle number concentrations in sand filtrates. This is reasonable because the hypothetical turbidity originating from the black particles were estimated to be 4.7×10^{-6}–6.7×10^{-5} NTU (see also Chapter 2), which was much smaller than the observed turbidity and therefore the observed turbidity should not be related to the black particles. No customer complaints about black particles were reported on the waters supplied from these plants, and in that sense we could not identify the concentration level which could induce customer complaints. However, the 200 particles/mL was the highest experimentally observed concentration without costumer complaint, and we regarded this level as a rough indication of practical treatment level for carbon particles in the following SPAC

experiments under the circumstance that there is no clear treatment goal was set for remaining carbon particles when PAC and SPAC are applied.

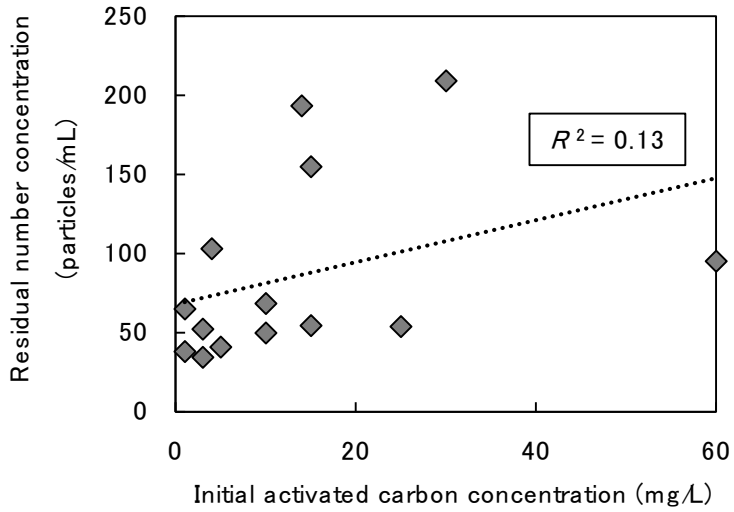

Fig. 5-1. The residual carbon particle concentration in finished water vs. the initial activated carbon concentration. These data were obtained from the total number of the 14 full-scale water purification plants employing the CSF process.

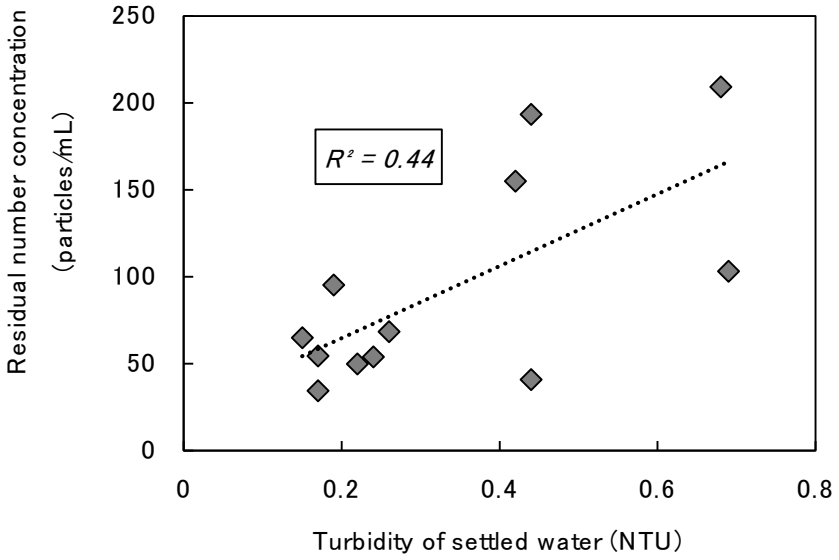

Fig. 5-2. Correlation between the residual black particle concentrations and turbidities of settled waters. These data were obtained from the total number of the 14 full-scale water purification plants employing the CSF process.

5.3.2 Fate of particles during CSF process

Removal rates of particles treated by CSF process are shown in Fig. 5-3. Removal rates were differed between particle types. AC particles (PAC and SPAC) had the highest removal rate (4−5 log), this trends had been also observed in the former chapters. Viruses (PMMoV and MS2) had the second highest removal rate (3−4 log), which was ~1 log higher than that reported by Shirasaki et al. (2018). This is probably because viruses were induced to be taken into floc particles with presence of other AC and clay particles which could be nuclei of coagulation. MPs (PA, PSi, and PE) and clay particles (kaolin and montmorillonite) had the lowest removal rate (~3 log).

Change in particle/virus concentrations during each steps of CSF process was shown in Fig. 5-4 and Fig. 5-5, respectively. Concentrations of bulk AC (PAC and SPAC) particles were 2 log decreased by coagulation-flocculation and sedimentation, and concentrations of stray particles were further 2 log smaller. This means that fine floc particles in bulk of settled water taking in large amount of AC particles, and then such AC particles in bulk flocs were separated by sand filter at high removal rate (2.5 log). In the same way, concentrations of clay particles (kaolin and montmorillonite) were 2 log decreased by coagulation-flocculation and sedimentation, however most of remaining particles in settled water were forming as stray particles and they little removed by sand filter. Behaviors of MPs (PA and PE) were similar with that of clay particles. Clay particles and MPs had relatively more in stray particles in settled water. Considering the discussion described in Chapter 4, clay particles and MPs need stronger treatment to let stray particles be taken into flocs. Particles had high negative charge around pH 7.0 (Fig. 5-6). Initial particle concentration was consisting mostly of AC particles (Fig. 5-4), so coagulant was probably consumed by AC particles mainly to neutralize their high negative charge at pH 7.0 (Fig.

5-6). In this context, kaolin particle concentration in initial suspension was close to PAC concentration, but its high negative charge at pH 7.0 as similar as that of PAC might need higher efficiency in charge neutralization to be taken into flocs.

Viruses (PMMoV and MS2) were not removed by adsorption by PAC, but were largely (~3 log) by coagulation-flocculation and sedimentation. MS2 was removed by sand filter (~1 log), but PMMoV was not. Difference of removal rate among particle type was revealed, however the effect of characteristics of particles on the difference need further study.

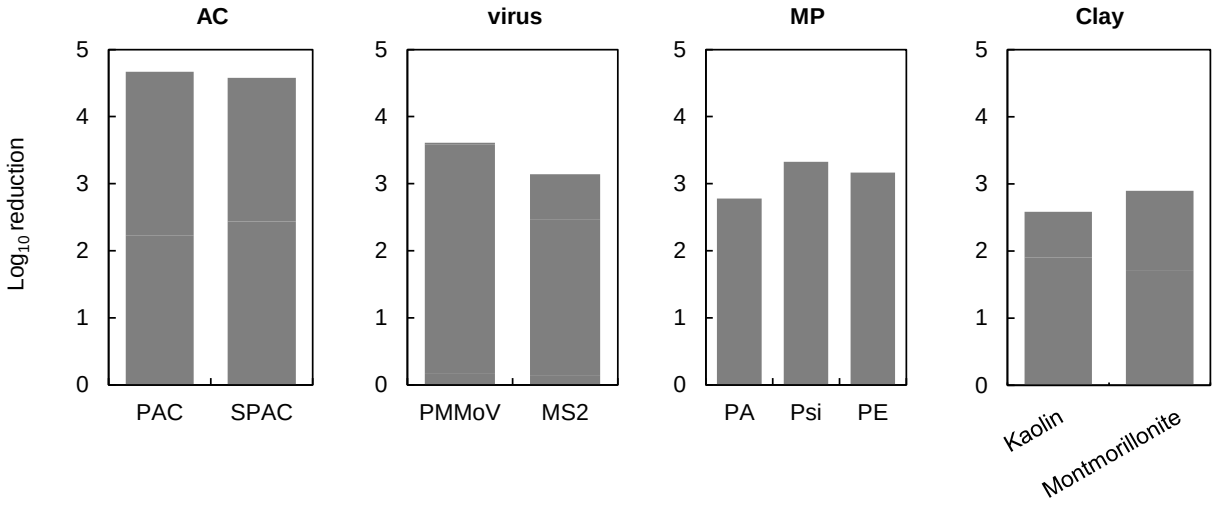

Fig. 5-3. Comparison of removal rates between particles. Removal rate was calculated as common logarithm of initial concentration divided by final concentration. Toyohira river water taken at Moiwa Water Purification Plant (Sapporo, Japan) was filtered by a membrane (pore diameter 0.2 mm; PTFE; Toyo Roshi Kaisha, Ltd., Tokyo, Japan) and used as raw water. Initial concentrations of PAC, SPAC, viruses, MP, and clay particles were 10 mg/L, 2.0 mg/L, 10^7 copies/mL, 1.0 µg/L, and 10 mg/L, respectively. Coagulant, PACl, 3 mg-Al/L. Coagulation, G = 600 s^{-1}; flocculation, G = 12.5 s^{-1}; filtration rate, 90 m d^{-1}.

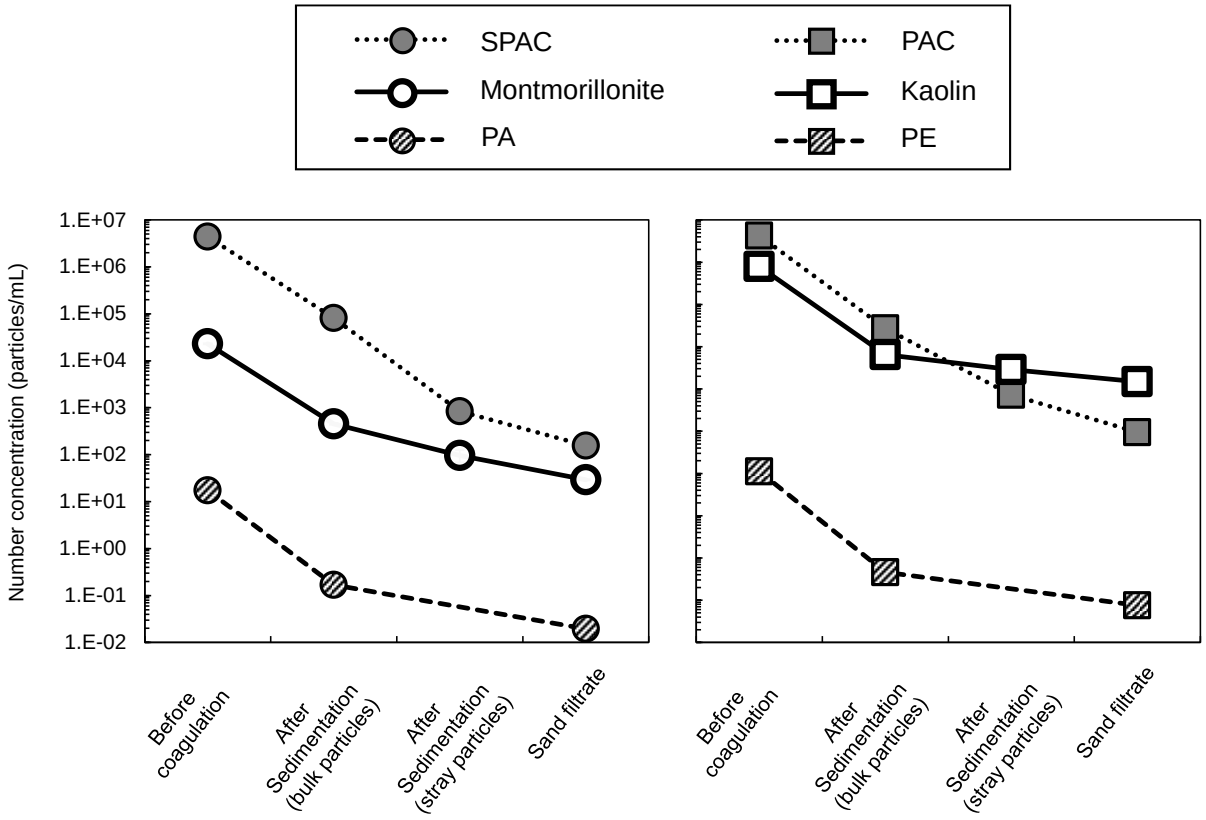

Fig. 5-4. Fate of particles during coagulation-flocculation, sedimentation, and sand filtration. Concentrations of bulk particles and stray particles in waters sampled after sedimentation were determined after the acid-sonic pretreatment or the centrifugal pretreatment, respectively. The experimental conditions were the same as described in the caption to Fig. 5-3.

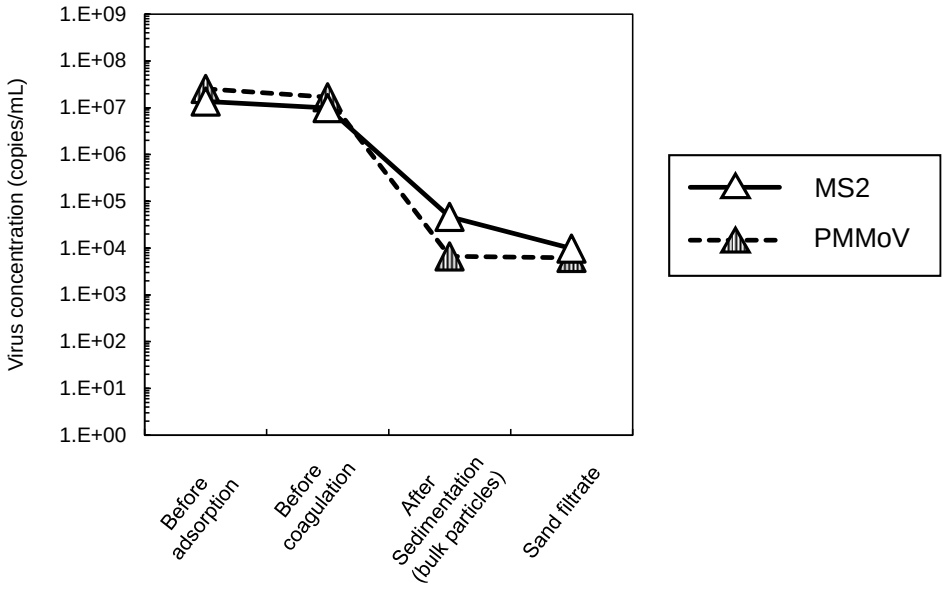

Fig. 5-5. Fate of viruses during coagulation-flocculation, sedimentation, and sand filtration. Concentrations of viruses in waters sampled after sedimentation were determined without any pretreatment. The experimental conditions were the same as described in the caption to Fig. 5-3.

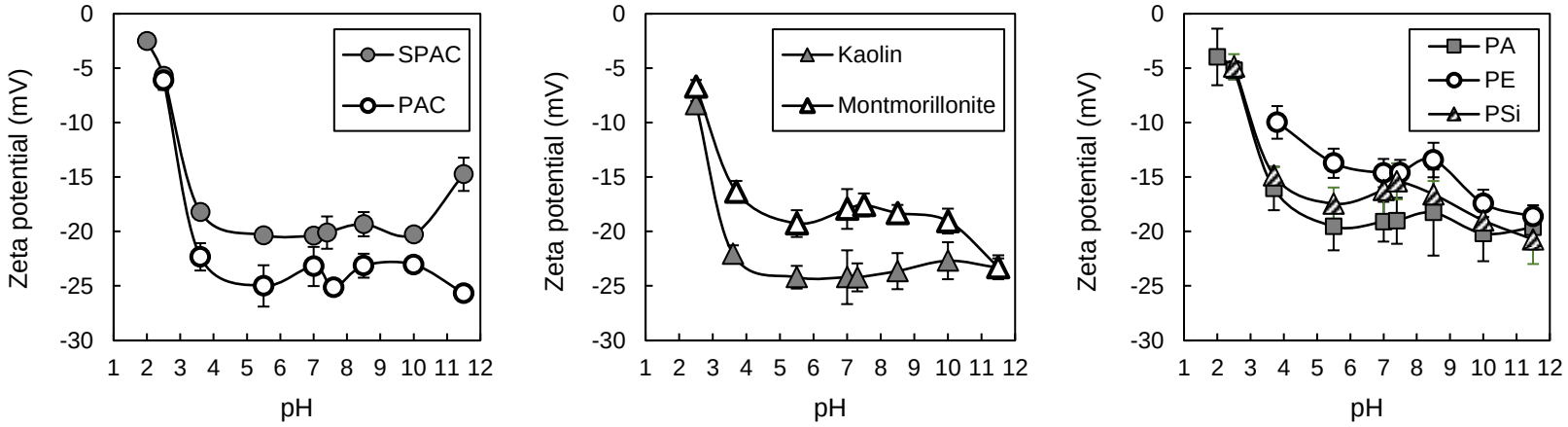

Fig. 5-6. Zeta potential of particles vs. pH of solution. HCl or NaOH was used to adjust pH. Concentrations of PAC, SPAC, MP, and clay particles were 10 mg/L, 2.0 mg/L, 1.0 mg/L, and 10 mg/L, respectively.

5.3.3 Effect of MP weathering on treatment performance in CSF process

It have been reported that MP is physically/photochemically weathered after being emitted to environment (Sun et al. 2020), and the effect of its weathering on drinking water treatment performance should be revealed (WHO 2019). Taking this into account, the effect of photochemically weathering by sun light on behavior of MP in CSF process was investigated (Fig. 5-7). PA-photo, which were exposed to sun for 68 days (861 MJ/m^2), had lower removal rate in CSF process than that of raw PA. This is probably because MP got more hydrophilicity by surface aging as being exposed to UV of sun light (Lin et al. 2020), and then efficiency in catchment by sand filter decreased. However, no difference was observed in FTIR (Fig. 5-8), zeta potential (Fig. 5-9), and shape (Fig. 5-10). Effect of weathering on removal performance of MP was suggested, however the effect of weathering on the physical property and the relationship between them need further study.

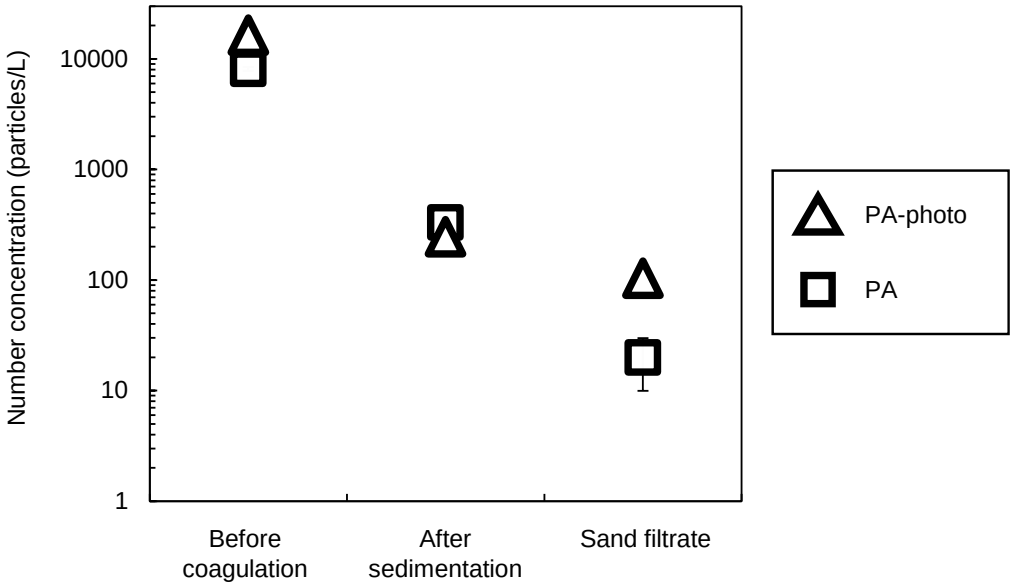

Fig. 5-7. Effect of weathering on fates of MP particles during coagulation-flocculation, sedimentation, and sand filtration. Concentrations of particles in waters sampled after sedimentation were determined after the acid-sonic pretreatment. The experimental conditions were the same as described in the caption to Fig. 5-3.

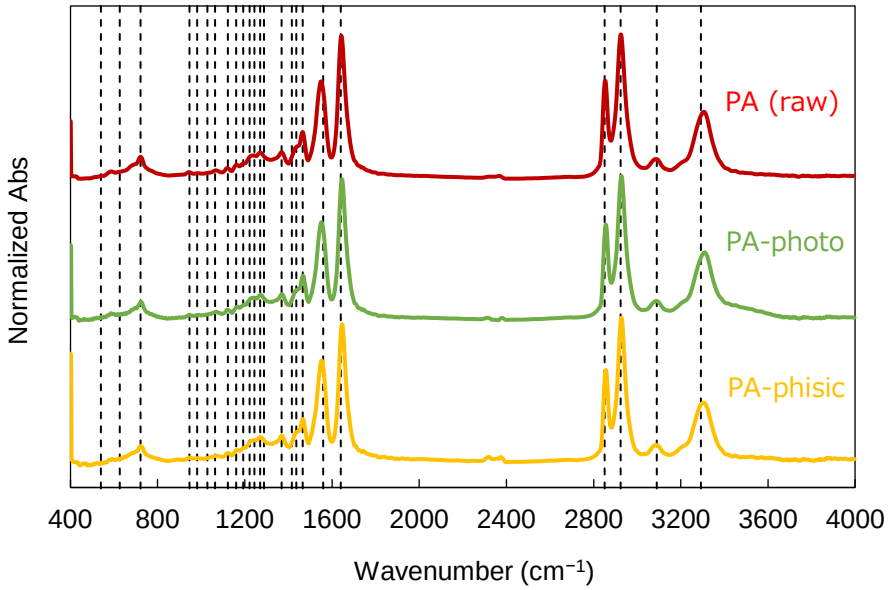

Fig. 5-8. Effect of weathering on FTIR of MP particles. Black broken lines denote peaks which appear with PA (Rhee and White 2002).

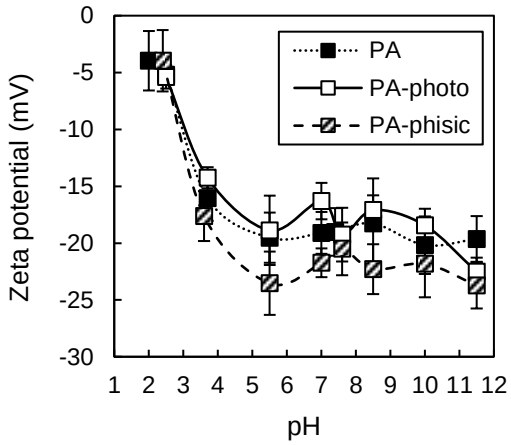

Fig. 5-9. Effect of weathering on zeta potential of MP particles.

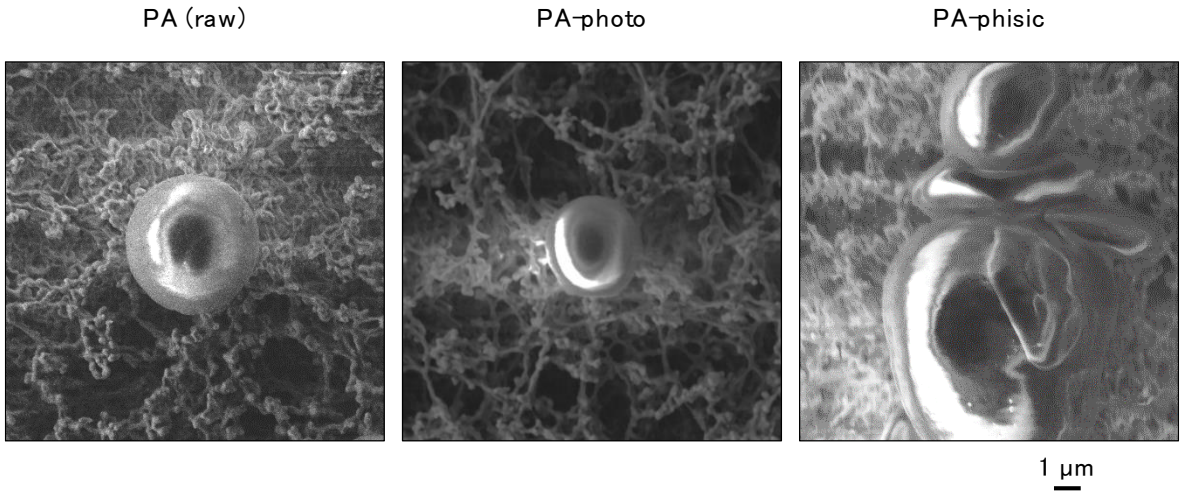

Fig. 5-10. Effect of weathering on surface condition and shape of MP particles.

5.4 Summary

Summary of this chapter is described as follows:

i. Removal rates of particles in CSF process were differed between particle types. AC particles (PAC and SPAC) had the highest removal rate (4−5 log), and viruses (PMMoV and MS2) had the second highest removal rate (3−4 log). MPs (PA, PSi, and PE) and clay particles (kaolin and montmorillonite) had the lowest removal rate (~3 log).

ii. AC particles, clay particles, and MPs had high negative charge at pH 7.0, and so particles which had the larger concentration consumed the more coagulant and efficiently decreased stray particles after coagulation-flocculation and sedimentation.

iii. Photochemically weathering of MP decreased MP removal efficiency mainly in sand filtration. The reduction of removal efficiency was probably caused by getting hydrophilicity, however, no difference of MP with/without photochemically weathering was observed in FTIR, zeta potential, and shape.

5.5 References

Cho, K., An, B.M., So, S., Chae, A. and Song, K.G. (2020) Simultaneous control of algal micropollutants based on ball-milled powdered activated carbon in combination with permanganate oxidation and coagulation. Water Research 185, 116263.

Dris, R., Gasperi, J., Saad, M., Mirande, C. and Tassin, B. (2016) Synthetic fibers in atmospheric fallout: A source of microplastics in the environment? Marine Pollution Bulletin 104(1), 290-293.

Edzwald, J.K. (2011) WATER QUALITY & TREATMENT A Handbook on Drinking Water, American Water Works Association, American Society of Civil Engineers, McGraw-Hill.

Freeman, S., Booth, A.M., Sabbah, I., Tiller, R., Dierking, J., Klun, K., Rotter, A., Ben-David, E., Javidpour, J. and Angel, D.L. (2020) Between source and sea: The role of wastewater treatment in reducing marine microplastics. Journal of Environmental Management 266, 110642.

Iqbal, S., Xu, J., Allen, S.D., Khan, S., Nadir, S., Arif, M.S. and Yasmeen, T. (2020) Unraveling consequences of soil micro- and nano-plastic pollution on soil-plant system: Implications for nitrogen (N) cycling and soil microbial activity. Chemosphere 260, 127578.

Iwasaki, S., Isobe, A., Kako, S.i., Uchida, K. and Tokai, T. (2017) Fate of microplastics and mesoplastics carried by surface currents and wind waves: A numerical model approach in the Sea of Japan. Marine Pollution Bulletin 121(1), 85-96.

Kögel, T., Bjorøy, Ø., Toto, B., Bienfait, A.M. and Sanden, M. (2020) Micro- and nanoplastic toxicity on aquatic life: Determining factors. Science of The Total Environment 709, 136050.

Koelmans, A.A., Mohamed Nor, N.H., Hermsen, E., Kooi, M., Mintenig, S.M. and De France, J. (2019) Microplastics in freshwaters and drinking water: Critical review and assessment of data quality. Water Research 155, 410-422.

Lin, J., Yan, D., Fu, J., Chen, Y. and Ou, H. (2020) Ultraviolet-C and vacuum ultraviolet inducing surface degradation of microplastics. Water Research 186, 116360.

Ma, B., Xue, W., Hu, C., Liu, H., Qu, J. and Li, L. (2019) Characteristics of microplastic removal via coagulation and ultrafiltration during drinking water treatment. Chemical Engineering Journal 359, 159-167.

Naik, R.A., Rowles, L.S., Hossain, A.I., Yen, M., Aldossary, R.M., Apul, O.G., Conkle, J. and Saleh, N.B. (2020) Microplastic particle versus fiber generation during photo-transformation in simulated seawater. Science of The Total Environment 736, 139690.

Pan, L., Takagi, Y., Matsui, Y., Matsushita, T. and Shirasaki, N. (2017) Micro-milling of spent granular activated carbon for its possible reuse as an adsorbent: Remaining capacity and characteristics. Water Research 114, 50-58.

Rajala, K., Grönfors, O., Hesampour, M. and Mikola, A. (2020) Removal of microplastics from secondary wastewater treatment plant effluent by coagulation/flocculation with iron, aluminum and polyamine-based chemicals. Water Research 183, 116045.

Revel, M., Châtel, A. and Mouneyrac, C. (2018) Micro(nano)plastics: A threat to human health? Current Opinion in Environmental Science & Health 1, 17-23.

Rhee, S. and White, J.L. (2002) Crystal structure and morphology of biaxially oriented polyamide 12 films. Journal of Polymer Science Part B: Polymer Physics 40(12), 1189-1200.

Rodrigues, M.O., Abrantes, N., Gonçalves, F.J.M., Nogueira, H., Marques, J.C. and Gonçalves, A.M.M. (2018) Spatial and temporal distribution of microplastics in water and sediments of a freshwater system (Antuã River, Portugal). Science of The Total Environment 633, 1549-1559.

Shirasaki, N., Matsushita, T., Matsui, Y., Marubayashi, T. and Murai, K. (2016) Investigation of enteric adenovirus and poliovirus removal by coagulation processes and suitability of bacteriophages MS2 and φX174 as surrogates for those viruses. Science of The Total Environment 563-564, 29-39.

Shirasaki, N., Matsushita, T., Matsui, Y. and Yamashita, R. (2018) Evaluation of the suitability of a plant virus, pepper mild mottle virus, as a surrogate of human enteric viruses for assessment of the efficacy of coagulation–rapid sand filtration to remove those viruses. Water Research 129, 460-469.

Skaf, D.W., Punzi, V.L., Rolle, J.T. and Kleinberg, K.A. (2020) Removal of micron-sized microplastic particles from simulated drinking water via alum coagulation. Chemical Engineering Journal 386, 123807.

Sun, Y., Yuan, J., Zhou, T., Zhao, Y., Yu, F. and Ma, J. (2020) Laboratory simulation of microplastics weathering and its adsorption behaviors in an aqueous environment: A systematic review. Environmental Pollution 265, 114864.

Wang, C., Xian, Z., Jin, X., Liang, S., Chen, Z., Pan, B., Wu, B., Ok, Y.S. and Gu, C. (2020a) Photo-aging of polyvinyl chloride microplastic in the presence of natural organic acids. Water Research 183, 116082.

Wang, Y., Wang, X., Li, Y., Li, J., Liu, Y., Xia, S. and Zhao, J. (2021) Effects of exposure of polyethylene microplastics to air, water and soil on their adsorption behaviors for copper and tetracycline. Chemical Engineering Journal 404, 126412.

Wang, Z., Sedighi, M. and Lea-Langton, A. (2020b) Filtration of microplastic spheres by biochar: removal efficiency and immobilisation mechanisms. Water Research 184, 116165.

WHO (2019) Microplastics in drinking-water.

Wong, J.K.H., Lee, K.K., Tang, K.H.D. and Yap, P.-S. (2020) Microplastics in the freshwater and terrestrial environments: Prevalence, fates, impacts and sustainable solutions. Science of The Total Environment 719, 137512.

Wu, P., Huang, J., Zheng, Y., Yang, Y., Zhang, Y., He, F., Chen, H., Quan, G., Yan, J., Li, T. and Gao, B. (2019) Environmental occurrences, fate, and impacts of microplastics. Ecotoxicology and Environmental Safety 184, 109612.

Zhang, Y., Diehl, A., Lewandowski, A., Gopalakrishnan, K. and Baker, T. (2020) Removal efficiency of micro- and nanoplastics (180 nm–125 μm) during drinking water treatment. Science of The Total Environment 720, 137383.

Zhou, G., Wang, Q., Li, J., Li, Q., Xu, H., Ye, Q., Wang, Y., Shu, S. and Zhang, J. (2021) Removal of polystyrene and polyethylene microplastics using PAC and FeCl3 coagulation: Performance and mechanism. Science of The Total Environment 752, 141837.

Zhou, Y., Wang, J., Zou, M., Jia, Z., Zhou, S. and Li, Y. (2020) Microplastics in soils: A review of methods, occurrence, fate, transport, ecological and environmental risks. Science of The Total Environment 748, 141368.

Zhu, K., Jia, H., Sun, Y., Dai, Y., Zhang, C., Guo, X., Wang, T. and Zhu, L. (2020a) Long-term phototransformation of microplastics under simulated sunlight irradiation in aquatic environments: Roles of reactive oxygen species. Water Research 173, 115564.

Zhu, L., Zhao, S., Bittar, T.B., Stubbins, A. and Li, D. (2020b) Photochemical dissolution of buoyant microplastics to dissolved organic carbon: Rates and microbial impacts. Journal of Hazardous Materials 383, 121065.

6 SUMMARY AND CONCLUSION

6.1 Summary

In this study, I set the objectives to reveal a fate and characteristics of fine carbon particles passing through water purification process composed of coagulation-flocculation, sedimentation, and sand filtration, and to find optimal coagulation conditions achieving efficiently removal of them. According to the objectives, I have conducted experiments and discussion, dividing into four chapters. The fruits of respective chapters were summarized as follows.

In Chapter 1, the background and the challenges for application of SPAC to conventional water purification process composed of coagulation-flocculation, sedimentation, and sand filtration was described. SPAC has attracted considerable attention from researchers and water treatment plant operators, and been expected to apply to the water treatment process. Plant operators employing adsorption treatment with activated carbon have paid attention mainly to efficient removal of target contaminants, and also to a leakage of fine carbon particles into water distribution system causing claims from consumers. In this context, SPAC particles in finished water after the water treatment process should be controlled at low concentration not causing problems. However, conventional detection methods could not evaluate a trace concentration of these fine carbon particles. Thus, a detection and determination method for a trace carbon particles were needed and treatment efficiency for them in the water treatment process should be evaluated.

In Chapter 2, I developed a method to detect and measure the number of a trace carbon particles and analyzed characteristics of residual carbon particles remaining in sand filtrate. The method used membrane filtration, digital microscopy, and image analysis. By using this method, carbon particles with diameters > 0.2 μm at a concentration as low as 0.1 μg/L could be identified. Additionally, this method enabled determining the residual carbon particles, which lied below the limit of turbidity detection, in sand filtrates. The residual concentration of SPAC was similar to that of PAC when the SPAC was used at 25% of the PAC mass concentration, a percentage that resulted in comparable adsorption of dissolved organic contaminants by SPAC and PAC. This result suggests that when SPAC is used instead of PAC in the CSF process, no more increasing residual particles occurs. The residual carbon concentrations were 100–200 particles/mL when 7.5 mg/L SPAC and 30 mg/L PAC were treated. Reductions of approximately 5-log in terms of particle number concentrations were attained via CSF. Residual carbon particles in sand filtrate were smaller in size than the carbon particles before treatment. The small carbon particles remaining after CSF treatment had a more negative charge than the carbon particles after coagulation treatment. The tendency of smaller particles to appear in the sand filtrate was therefore related to their lower destabilization rate during the coagulation process as well as their lower collision rates in the flocculation and filtration processes.

In Chapter 3, key control points to attain the high log removal rates of SPAC and to reduce residual SPAC particles at trace concentration levels in treated water were examined, and their background mechanisms were discussed, focusing on the process points of coagulation-flocculation and coagulants in CSF. It was clearly found that a sufficiently large G value in flash mixing for the first step of coagulation was a dominant factor for minimizing residual carbon particles in the treated water after the fourth step of sand filtration. Adequate mixing for

coagulation would enable complete dispersion of coagulant thereby reducing the number of particles that were not charge-neutralized. In a flow-through CSF process using SPAC, the residual carbon concentration in the sand filtrate was dramatically decreased with time during the initial 2 h of filtration due to filter ripening, and a filtrate quality of <200 particles/mL was achieved. The size distribution of the residual carbon particles in the sand filtrate was not changed during the filter-ripening period, suggesting an increase in the efficiency of particle attachment rather than transport to the sand surface during this period. Therefore, charge-destabilization rather than particle size is likely key for minimizing residual particles. Commercially available PACls (high-basicity PACl, basicity 70%; conventional-basicity PACl, basicity 50%) were compared with each other, and high-basicity PACl was more effective in removing residual carbon particles. It was because the high-basicity PACl had a high charge neutralizing capacity to destabilize many particles, though it formed flocs slowly. However, this superiority of high-basicity PACl was provided by the sufficient flash mixing. Additionally, I produced a lot of lab-made PACls and compared each other in terms of removal performance for carbon particles. Among them, high-basicity PACl with SO_4/Al=0.14 reduced residual carbon particles down to the minimum concentration. Such a high performance PACl coagulant was produced by using $Al(OH)_3$-dissolution, and the dominant Al species was Alc determined by the ferron method. In contrast, Alb and Alc type PACls produced by base-titration had a high positive charge capacity and were poor at forming floc particles due to lack of bridge-forming ability.

In Chapter 4, fate of fine carbon particles in CSF treatment process was examined and the source of residual carbon particles in sand filtrate was discussed. Stray carbon particles, which were determined as the particles remaining in the centrifugal supernatant of the water sampled after coagulation with rapid mixing and flocculation with slow mixing, were less charge-neutralized than the bulk

particles. The concentration of stray particles dropped markedly during coagulation, and then it was unchanged or only slightly decreased during flocculation and sedimentation. The concentrations of stray carbon particles in water sampled after coagulation/flocculation were well correlated with the residual carbon particle concentrations in sand filtrate, but the turbidity of water entering the sand filter water was not. Among the bulk particles, stray particles, which account for less than 0.4% of the bulk particles, could be a major source of residual particles in sand filtrate due to their lower charge neutralization. Therefore, a goal of the coagulation treatment process should be to reduce the stray particle concentration. Optimizing reactor configurations and the type and dose of coagulant were effective for reducing stray particle and residual carbon particle concentrations in sand filtrate. high-basicity PACl performed better with a multi-chambered reactor than with a single-chambered reactor for coagulation with rapid mixing. In contrast, conventional-basicity PACl performed better with a multi-chambered reactor than with a single-chambered reactor for both coagulation with rapid mixing and flocculation with slow mixing. The performance requirements of the coagulation and flocculation reactors were related to the predominant aluminum species in the coagulant: Alc of high-basicity PACl is fast-acting, whereas Ala of conventional-basicity PACl is slow-acting.

In Chapter 5, fates and removals of MPs, clay, activated carbon, and virus particles during CSF were examined. Removal rates of these particles in CSF process were differed from each particle types. AC particles (PAC and SPAC) had the highest removal rate (4−5 log), and viruses (PMMoV and MS2) had the second highest removal rate (3−4 log). MPs (PA, PSi, and PE) and clay particles (kaolin and montmorillonite) had the lowest removal rate (~3 log). AC particles, clay particles, and MPs had high negative charge at pH 7.0, and so particles which had the larger concentration consumed the more coagulant and efficiently

decreased stray particles after coagulation-flocculation and sedimentation. Additionally, effect of weathering MP on their removal rate was examined. Photochemically weathering decreased MP removal efficiency mainly in sand filtration. The reduction of removal efficiency was probably caused by MP getting hydrophilicity, however, no difference of MP with/without photochemically weathering was observed in FTIR, zeta potential, and shape.

6.2 Conclusion

It can be concluded that SPAC application to conventional drinking water treatment process (CSF) is now available with sufficient coagulation condition. In a practical adsorption treatment, SPAC can reduce its dosage down to ≤1/4 of PAC mass concentration. With this in mind, SPAC and PAC at practical initial concentration were treated by CSF, and the residual particle concentrations were the same level. This denotes that no more increasing of residual particles are brought by SPAC application in CSF compared to already applied PAC. Especially, two key coagulation conditions for reducing residual carbon particles were revealed: using high-basicity PACl coagulant containing high sulfate ion concentration and providing sufficiently large flash mixing immediately after the addition of PACl into raw water. These conditions allow particles efficiently to be charge-neutralized and to grow into floc particles and be removed, and then induce the residual particles reduction. This study might contribute to expand diversity of SPAC application in water treatment, and consequently contribute to offering security/safety drinking water.

7 APPENDIX

7.1 Calculation of G (velocity gradient) value

The mean velocity gradient G (s^{-1}) is defined as a function of P, μ, and V as follows.

$$G = \sqrt{\frac{P}{\mu V}} \qquad (1)$$

where P is power consumed by the agitating impeller in a mixing vessel (W), μ is the viscosity of water (Pa s), and V (m^3) is the volume of the water in the mixing vessel.

Power consumption is given by the product of force acting on an impeller blade and its moving velocity. Velocity and force acting on the blade of the impeller varies radially such that the tip of the blade moves fastest (tip speed) and the force acting on the tip is strongest, but the root end of the blade moves slowest and its force is smallest. Therefore, power consumed by a rotating impeller blade is given by:

$$P_B = \int v\, p dA \qquad (2)$$

$$p = \frac{1}{2}\rho_w C_d v^2 \qquad (3)$$

where, P_B is the power required to move a blade (W), v is the velocity of the moving blade (m/s), p is the pressure acting vertically on the blade (Pa), A is the area of blade (m^2), ρ_w is the density of fluid (kg/m^3), and C_d is drag coefficient (dimensionless).

For a flat rectangular blade shown in Fig. 7-1,

$$v = 2\pi(1 - K_r)xN_s \qquad (4)$$

$$dA = hdx \qquad (5)$$

where, K_r is corotation coefficient (dimensionless), x is the radial distance from the impeller center (m), N_s is rotational speed (rps), and h is the height of a impeller blade (m).

By substituting equations (3), (4) and (5) into (2):

$$P_B = \int_{r_1}^{r_2} \frac{1}{2}\rho_w C_d [2\pi(1 - K_r)xN_s]^3 hdx$$
$$= \rho_w C_d [\pi(1 - K_r)N_s]^3 h({r_2}^4 - {r_1}^4) \qquad (6)$$

The total power input to the mixing tank having multiple impeller blades is given by:

$$P = nP_B = n\rho_w C_d [\pi(1 - K_r)N_s]^3 h({r_2}^4 - {r_1}^4) \qquad (7)$$

where, n is the number of impeller blades in a mixer.

Substituting Eq. (10) into Eq. (1) gives,

$$G = \sqrt{\frac{n\rho_w C_d \pi^3 (1 - K_r)^3 {N_s}^3 h({r_2}^4 - {r_1}^4)}{\mu V}}. \qquad (8)$$

The values used for the calculation of G values by equation (8) were summarized in Table 7-1.

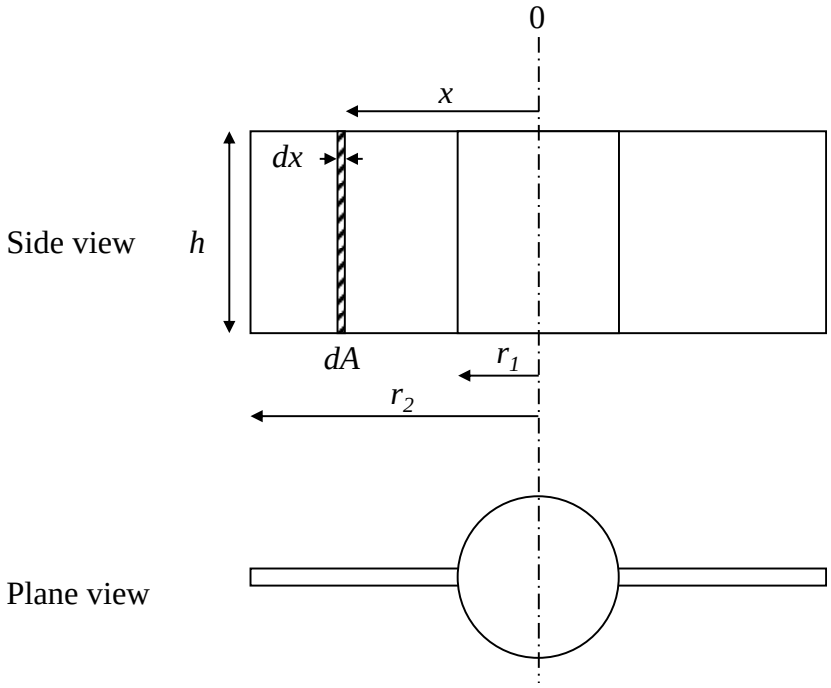

Fig. 7-1. Schematic diagram of mixing blade for the calculation of G value.

Table 7-1. Parameter values used for G value calculation.

Parameter symbol	**Unit**	**Value**
V	m^3	0.004
μ	Pa s	1.005×10^{-3}
h	m	0.035
r_1	m	0.014
r_2	m	0.05
ρ_w	kg m^{-3}	9.982×10^2
C_d	dimensionless	1.5
K_r	dimensionless	0
n	dimensionless	4
N_S	rps	from 0.22 to 3.28

7.2 Preparation of coagulants by base-titration

The 10 poly-aluminum chlorides (PACls) were produced by base-titration. These PACls are designated by the following rules: the number after "B" represents "% basicity", "s" indicates "sulfated", "ns" indicates "non-sulfate", "heat" indicates "heated", the number after "s" represents "mole ratio of sulfate ion to aluminum: SO_4/Al", and the number after the hyphen indicates serial number. $AlCl_3 \cdot 6H_2O$, $Al_2(SO_4)_3 \cdot 14\sim18H_2O$, and Na_2CO_3 were provided by FUJIFILM Wako Pure Chemical Corporation (Osaka, Japan), and NaOH was by Kanto Chemical Co., Inc. (Tokyo, Japan).

B65ns was prepared as follows: an $AlCl_3$ solution (0.5 M as Al, 80 mL) in a 500 mL Erlenmeyer flask was titrated with NaOH (0.24 M, 320 mL) by means of a peristaltic pump at a rate of 4 mL/min. During the titration, a combined hot plate/magnetic stirrer was used to agitate the solution in the flask and maintain the temperature at 85–90 °C. B80ns-1 was prepared with the same materials and procedure for B65ns, except that the concentrations of $AlCl_3$ solution and NaOH were 0.25 M as Al and 0.15 M. The same materials and procedure were used to prepare B80ns-2, except that the concentration of $AlCl_3$ solution was 0.3 M. B82s0.11 was prepared as follows: an Al solution (0.49 M as Al, SO_4/Al=0.11 in mole ratio, 80 mL) was prepared with $AlCl_3$ and $Al_2(SO_4)_3$ in a 500 mL Erlenmeyer flask and titrated with NaOH (0.3 M, 320 mL) as the same procedure described above.

B65ns-heat was prepared by heating B65ns at 121 °C for 5 h with an autoclave (MLS-3781; PHC Holdings Corporation, Tokyo, Japan). B80ns-2-heat was prepared by heating B80ns-2 at 120 °C for 20 min with the same autoclave.

B82s0.11-heat was prepared by heating B82s0.11 at 90~95 °C for 72 h with a combined hot plate/magnetic stirrer.

B79s0.10-1 was prepared by adding a Na_2CO_3 solution and an $Al_2(SO_4)_3$ solution into B65ns at ambient temperature until the basicity became 79% (calculation of the basicity is described in Section 3.2.2) and SO_4/Al became 0.10. B79s0.10-2-heat was prepared by adding a Na_2CO_3 solution and an $Al_2(SO_4)_3$ solution into B65ns-heat at ambient temperature. B88s0.10 was also prepared by adding a Na_2CO_3 solution and an $Al_2(SO_4)_3$ solution into B80ns-2 at ambient temperature.

7.3 Jar-tests using the coagulants made by base-titration

Filtered tap water was obtained by the method described in the Section 3.2.3 except that its alkalinity was not adjusted. The water was supplemented with an SPAC slurry (median diameter is described in Table 3-6) at concentration 10 mg/L to make raw water for the experiment consisting of coagulation-flocculation and sedimentation (jar test). Jar-tests were conducted in a 1-L rectangular beaker. After a predetermined volume of HCl or NaOH (0.1 N) was added to order to achieve the coagulation pH at 7.0, the coagulant (PACl) was injected into the beaker to a final concentration between 0 and 1.5 mg-Al/L (see also Table 3-6). Then, the water was mixed rapidly and slowly. The mixing speed (G value) and times (T value) of the flash and slow mixing were varied depending on each experiment (see also Table 3-6). The water was then left at rest for 1 h. A supernatant of 50 mL was sampled and determined for turbidity (2100Q portable turbidimeter; Hach Company, Loveland, CO, USA).

7.4 Ferron method for aluminum speciation in poly-aluminum chloride

In the Ferron method, Ala denotes aluminum species that react with Ferron within 30 s, which are mainly monomeric Al species. Alb denotes Al species that react with Ferron from 30 s to 120 min, which are mainly polymeric Al species. Alc denotes Al species that do not react with Ferron, which are mainly colloidal Al species. The Ferron analyses of the poly-aluminum chlorides (PACls) were conducted immediately after diluting each PACl with pure water (Milli-Q water; Milli-Q Advantage A10 System; Merck KGaA, Darmstadt, Germany) to 0.27 g-Al/L (0.01 mol-Al/L). Absorbance at 366 nm was measured using a glass cell that had a 10-cm optical path length. Dilution is reported to have little effect on the Ferron assay for PACl (Kimura *et al.* 2013).

7.5 Membrane filtration and microscopic image analysis to determine carbon particle concentration and particle size

The concentrations and particle sizes of carbon particles were determined by membrane filtration and microscopic image analysis. Carbon particles in water samples were captured on a membrane filter (nominal pore diameter, 0.1 μm; Φ25 mm; polytetrafluoroethylene; Merck KGaA). After the filter was left to dry naturally at room temperature, color digital photomicrographs of the filter surface were recorded under a digital microscope (VHX-2000; Keyence Corporation, Osaka, Japan) at 1000× magnification. The number of observation zones (9, 10, or 18 per filter; microscope view area, 247 μm × 330 μm) were predetermined depending on particle concentration (see also Section 2.2.3). Finally, the

photomicrographs were analyzed by using the image analysis software associated with the microscope and the particle concentration, and the sizes calculated were represented by the surface-equivalent sphere diameter. The analytical procedures are described in detail in Section 2.2.3.

7.6 Flow-through coagulation–flocculation, sedimentation, and sand filtration experiment

The plant comprised five components: preparation unit, coagulation reactor (rapid mixing), flocculation reactor (slow mixing), sedimentation reactor, and sand filter (Fig. 3-3 and Table 4-1). Coagulation was conducted using a single-chambered reactor or a 3-chambered-reactor with three equally-sized chambers; the two reactors had the same total hydraulic retention time (HRT) of 100 s. Flocculation was conducted using a single-chambered reactor or a 4-chambered reactor, both with four mixing impellers and the same total HRT of 2400 s. Regardless of reactor configuration, coagulation was conducted with rapid mixing at a fixed mixing intensity (G value: velocity gradient) of 600 s^{-1} for 100 s, and flocculation was conducted with slow mixing at a fixed G value of 12.5 s^{-1} for 2400 s. Residence time distributions of the reactors were measured by tracer test using NaCl as the tracer and conductivity detection (Crittenden *et al.* 2012). All chemicals and raw water were fed into the plant via peristaltic pumps at constant flow rates.

Toyohira River water, collected at Moiwa Water Purification Plant, Sapporo, Japan (hereafter ‘River water’) was used as the raw water. Dechlorinated Sapporo municipal water (Municipal waters 1–3 and 5) was also used because only a limited volume of River water was available (Table 4-2). The raw waters

were stored in a tank (130 or 500 L) and then pumped into the first mixing chamber of the preparation unit at 0.5 L/min. SPAC was added to the second mixing chamber of the preparation unit at a concentration of 2 mg/L, which is a typical dose when SPAC is used as an adsorbent (Nakayama *et al.* 2020).

After the addition of NaOH (0.05 N) or HCl (0.05 N) to adjust the final coagulation pH to 7.0 in the third chamber of the preparation unit, coagulant (PACl) was injected into the coagulation reactor; when the 3-chambered reactor was used for coagulation, the coagulant was injected into the first chamber. The coagulant dose was 1.5 mg-Al/L, unless otherwise noted, and it was predetermined to bring the settling turbidity to less than 1.0 NTU. Samples of water were collected from the outlet of the coagulation reactor and from the outlet of the flocculation reactor for the determination of non-coagulated carbon particle concentration, as described in Sections 4.2.4 and 7.5, respectively.

After flocculation, the water flowed through a sedimentation unit, which had a HRT of 60 min, and a portion of the supernatant was sampled for the determination of turbidity (2100Q portable turbidimeter; Hach Company, Loveland, CO, USA). In some cases, a portion of supernatant was sampled for the determination of stray carbon particle concentration.

After sedimentation, the supernatant was transferred to a sand filter. Sand filtration was conducted at a rate of 90 or 150 m d^{-1} in the down-flow direction using a 4-cm diameter column filled with sand (effective diameter, 0.94 mm; uniformity, 1.24; Nihon Genryo Co., Ltd., Japan) to a depth of 50 cm. After the start of filtration, sand filtrates were collected from 0 to 25, from 35 to 60, from 85 to 110, from 165 to 190, from 285 to 310, and from 405 to 430 min, representing filtration times of 12.5, 47.5, 97.5, 178, 298, and 418 min, respectively, and used to determine turbidity and carbon particle concentration.

After each filtration run, the sand filter was backwashed with municipal water and then washed forward with Milli-Q water before the next filtration run.

7.7 Reference

Crittenden, J.C., Trussell, R.R., Hand, D.W., Howe, K.J. and Tchobanoglous, G. (2012) MWH's Water Treatment Principles and Design, Third Edition, John Wiley & Sons, Inc.

Kimura, M., Matsui, Y., Kondo, K., Ishikawa, T.B., Matsushita, T. and Shirasaki, N. (2013) Minimizing residual aluminum concentration in treated water by tailoring properties of polyaluminum coagulants. Water Research 47(6), 2075-2084.

Nakayama, A., Sakamoto, A., Matsushita, T., Matsui, Y. and Shirasaki, N. (2020) Effects of pre, post, and simultaneous loading of natural organic matter on 2-methylisoborneol adsorption on superfine powdered activated carbon: Reversibility and external pore-blocking. Water Research 182, 115992.